Old plants, new tricks: machine learning and the conifer fossil record

Matilda Jane Munro Brown

BSc(Hons)

School of Natural Sciences | College of Science and Engineering

Submitted in fulfilment of the requirements for the Degree of Doctor of Philosophy

University of Tasmania

March 2022

Declaration of Originality

This thesis contains no material which has been accepted for a degree or diploma by the University of Tasmania or any other institution, and to the best of my knowledge and belief, this thesis contains no material previously published or written by another person, except where due acknowledgement is made in the text of this thesis.

Signed: .....Date: 1/11/2021

Matilda Jane Munro Brown

Authority of Access

Signed: .....Date: 1/11/2021

Matilda Jane Munro Brown

Statement regarding Published Work

The publishers of the papers comprising Chapters 2 and 3 hold the copyright for that content and access to the material should be sought from the respective journals/publishers. The remaining nonpublished content of the thesis may be made available for loan and limited copying and communication in accordance with the Statement of Access and the Copyright Act 1968. Due to the inclusion of published material there is unavoidable repetition of material between chapters in this thesis.

Signed: .....Date: 1/11/2021

Matilda Jane Munro Brown

Statement of Co-Authorship

The following people and institutions contributed to the publication of work undertaken as part of this thesis:
Candidate. Matilda J.M. Brown; School of Natural Sciences, University of Tasmania, Hobart, Australia
Author 2. Gregory J. Jordan; School of Natural Sciences, University of Tasmania, Hobart, Australia
Author 3. Timothy J. Brodribb; School of Natural Sciences, University of Tasmania, Hobart, Australia
Author 4. Barbara R. Holland; School of Natural Sciences, University of Tasmania, Hobart, Australia

Contribution of work by co-authors for each paper:
Paper 1: Located in Chapter 2
Brown, M.J.M., Holland, B.R., Jordan, G.J. (2020). HYPEROVERLAP: Detecting biological overlap in n-dimensional space. Methods in Ecology and Evolution. 11: 513– 523. https://doi.org/10.1111/2041-210X.13363
Author contributions:
Conceived and developed R package: Candidate
Wrote the manuscript: Candidate, Author 1, Author 3

Paper 2: Located in Chapter 3
Brown, M.J.M., Brodribb, T.J., Jordan, G.J. (2021). No-analogue associations in the fossil record of southern conifers reveal conservatism in precipitation, but not temperature axes. Global Ecology and Biogeography. 30(12), 2455-2466). https://doi.org/10.1111/geb.13398
Author contributions:
Conceived and designed the study: Candidate, Author 2
Collated the data: Candidate, Author 2
Analysed the data: Candidate
Wrote the manuscript: Candidate, Author 2, Author 3

We, the undersigned, endorse the above stated contribution of work undertaken for each of the published (or submitted) peer-reviewed manuscripts contributing to this thesis:
Signed:

Matilda JM Brown	Prof Gregory Jordan	A/Prof Julianne O'Reilly-Wapstra
Candidate	Primary Supervisor	Head of School
School of Natural Sciences	School of Natural Sciences	School of Natural Sciences
University of Tasmania	University of Tasmania	University of Tasmania

Date: 1/11/2021

Acknowledgements

First, to Greg Jordan (aka Gregolas aka Greggles) – I cannot thank you enough for your mentorship, knowledge, support, philosophical discussions and fun over the past five years. It has been an honour and a privilege to be your student. I promise to continue to hassle you into the future (albeit remotely for a while).

This thesis would not have been possible without Tim Brodribb and Barbara Holland, who complete the ‘dream team’ of supervision. Your perspectives, wisdom and humour have been invaluable and I am sincerely grateful to have had such a team in my corner.

To the ‘rats’ of Room 237 – Kate Johnson, Rose Brinkhoff, Vanessa Tonet, Ibrahim Bourbia, Freya Richardson, Hans Ammitzboll and Deborah Corso – y’all have been the best officemates I could have asked for. I hope that we can continue to eat snacks and do quizzes forever.

I am deeply grateful to everyone at UTAS for creating a wonderful, welcoming department to work in. In particular, thank you to the school administration staff - Cath Bresnehan, Jodi Noble, Morgan Green, Clancy Carver and many others – for dealing with any and all issues that have cropped up over the course of my scholarship.

To my family, thank you for your endless support and interest in my research (even if your eyes sometimes glaze over when I explain what I am doing). Particular thanks to Mum for proofreading my last chapter on short notice.

Finally, to Brenton – words cannot express how grateful I am for everything that you do. You have picked me up from the ground (both literally and metaphorically) so many times I’ve lost count. To paraphrase Annabel Crabb – thank you for being my wife.

This research was supported by an Australian Government Research Training Program (RTP) Scholarship, and by a Westpac Scholars Trust Future Leaders Scholarship.

Table of Contents

List of Tables

List of Figures

Abstract

The palaeobotanical record contains a wealth of information on the evolution and ecology of species, as well as the palaeoenvironment. However, accessing and analysing this information can be challenging. It is not possible to study the ecology of fossils directly, but there are two main inferential approaches to palaeoecology: nearest living relative (NLR) techniques, and physiognomic methods.

In NLR techniques, the taxonomic identity of the fossil is key – once the nearest living relatives of a fossil have been identified, we can study the ecology of living species in order to make inferences about the fossil species. However, there are instances where the nearest living relatives of co-occurring fossils are climatically incompatible, which suggests that some extant taxa inhabit different climates to their fossilised relatives. To date, no study has quantitatively analysed this phenomenon in fossils older than the Quaternary (the last 2.6 million years), possibly because of a lack of suitable methodologies.

Alternatively, physiognomic methods seek to extract environmental signal that is encoded in the fossil morphology. This approach has been widely used for macroscopic leaf traits, but comparatively less for epidermal characters (in particular, the shape and arrangement of epidermal cells). The epidermis is the interface between the plant and its environment and is responsible for many functions, including gas exchange and mediation of transpiration (via stomata), so there is good reason to believe that there will be links between epidermal traits and environment. However, the calibration of epidermal physiognomic proxies has been hampered by the non-feasibility of undertaking large multivariate studies where each character is extremely time-consuming and laborious to measure, as well as the complex relationships between genetic and plastic variation.

In this dissertation, I explore how we can use novel computational techniques (including machine learning) to glean new insights from the fossil record, with a focus on southern conifers (Podocarpaceae, Araucariaceae, Callitroideae).

I present two new computational methods (with accompanying R packages) and their palaeoecological applications.

In the first chapter, I provide an overview of some of the analytical challenges in palaeoecology and why machine learning techniques are well-suited to solve these problems. I also provide a short review of existing machine learning approaches in palaeoecology.

In the second chapter, I present ‘hyperoverlap’, an R package that uses a novel application of a machine learning classifier to evaluate multi-dimensional overlap between point clouds (e.g. occurrence records in climate space). This chapter is published.

In the third chapter, I use ‘hyperoverlap’ to quantitatively examine the fossil record of southern conifers and to identify no-analogue associations (those pairs of fossils for which the nearest living relatives inhabit disparate climatic conditions). By quantitatively analysing the climatic overlap in fossil communities, I found that there is significant lability in the thermal niches of southern conifers, but extreme stability in the precipitation niche, implying that future changes to rainfall regime may pose more of a threat to southern conifers than thermal shifts. This chapter is under review, after revision.

In the fourth chapter, I present ‘epidermalmorph’, an R package that automates the extraction of leaf epidermal traits from images. As well as trait measurement, this package includes tools for pre-processing, estimations of trait reliability (for any study system) and optimising sampling effort.

In the fifth chapter, I use ‘epidermalmorph’ to assess the degree of climatic adaptation in the epidermal cells of Podocarpaceae. I found some evidence for adaptive significance of stomatal index and cell wall undulation, but there were no viable proxies for either tree height or climatic conditions, suggesting that the functional variability in Podocarpaceae leaves is more likely to be plastic, rather than hard-coded.

In the final chapter, I summarise this thesis, discuss the challenges and limitations to applying sophisticated computational techniques to the palaeobotanical record and suggest potential avenues for future research.

Chapter 1 : Introduction

The palaeobotanical record is an invaluable source of information about the past, but accessing and interpreting this information is not always straightforward. Almost all macrofossils are mere fragments of the plants that produce them, so identification of fossil plants often relies on different characters to those used to identify extant species. Palaeobotany is unavoidably haphazard in sampling and fossil data are sparse and biased, making quantitative analyses challenging (Spicer, 1988). It is also not possible to directly measure the ecology of fossils, so we must use information from the fossils themselves to try to make inferences about the paleoenvironment (Wolfe, 1993).

There are two main approaches to estimating palaeoenvironmental conditions from fossils. We can use the ecology of the nearest living relatives (NLRs) of fossils as a proxy (Mosbrugger & Utescher, 1997), under the assumption that the climatic tolerances of fossil species were similar to those of their extant counterparts. We can use the morphological/anatomical traits of the fossil in concert with known trait-climate relationships (physiognomic methods, Wolf, 1990; Yang *et al.*, 2011), using the assumption that links between traits and climatic conditions in modern species can be applied to fossils. In this thesis, I explore the use of novel computational techniques to glean new insights from the palaeobotanical record from both these perspectives, with a focus on southern semisphere conifers.

Fossil record of the southern conifers

The ‘southern conifers’ are a group of conifer lineages that are now mostly confined to the southern hemisphere: Podocarpaceae, Araucariaceae, Callitroideae (Cupressaceae) and *Austrotaxus* (Taxaceae). They have an exceptionally rich and well-documented fossil record (see Hill & Brodribb, 1999; Wilf, 2012; Macphail *et al.*, 2013; Andruchow-Colombo *et al.*, 2019) that extends into the Northern Hemisphere and as far back as the Jurassic (Stockey, 1982). The fossil record of southern conifers demonstrates extraordinary morphological stability – Eocene fossils of *Papuacedrus prechilensis* are indistinguishable from modern *Papuacedrus* foliage (Wilf *et al.*, 2009) – and it is often assumed that this stability extends to ecology (Jin *et al.*, 2021; Sundaram & Leslie, 2021).

For many taxa (e.g. *Microcachrys, Dacrycarpus, Lagarostrobos, Halocarpus)*, fossils are much more widespread than the extant species (Brodribb & Hill, 2004; Pole, 2007; Carpenter *et al.*, 2011), which has been interpreted as evidence for a widespread decline in range and diversity, particularly in the Neogene and Quaternary (Brodribb & Hill, 2004; Truswell & MacPhail, 2009). This decline coincides with a period of global cooling and drying (Westerhold *et al.*, 2020), so it is often assumed that changes in climate are responsible (Hill, 1995; Kooyman *et al.*, 2013). However, it is unclear whether temperature or precipitation are more likely to have affected southern conifers.

No-analogue fossils

A curious aspect of the southern conifers is that their fossil record contains 'no-analogue associations' – that is, the nearest living relatives of these fossil species inhabit dissimilar environmental conditions (Jordan, 1997b). One example of a no-analogue pair is the co-occurrence of *Acmopyle* and *Microcachrys*, which, according to fossil evidence, co-existed at Lake Cethana, Tasmania approximately 35 million years ago (Carpenter *et al.*, 1994). Today, *Acmopyle* is restricted to the tropical lowlands of Fiji and New Caledonia, while *Microcachrys* is restricted to the cold and open mountaintops of Tasmania (neither species is part of the extant community at Lake Cethana, Farjon & Filer, 2013). These kinds of anomalies have been noted for many southern conifers at several fossil sites (Jordan, 1997b; Macphail, 2007) but have not yet been quantitatively analysed beyond the site level (see Jordan, 1997). No-analogue associations challenge the key assumption for NLR approaches - that the ecology of the living taxon is the same as that of the fossil. They also seem at odds with the ideas that conifers are slow to evolve (Buschiazzo *et al.*, 2012) and are ecologically conservative (Jin *et al.*, 2021), as some no-analogue pairs are relatively recent (e.g. Jordan 1997). No-analogue associations thus merit further study, but quantifying them requires creative analytical approaches that can utilise sparse, multivariate data.

Machine learning and the palaeobotanical record

Machine learning is an integral aspect of many modern statistical methods, from linear regression through to highly sophisticated neural networks and

image processing. At the core of machine learning is the idea of a 'performance metric' – this can be the proportion of correctly classified instances, the prediction error or some other, more complex metric – that is optimised by the machine (Jordan & Mitchell, 2015). Machine learning is typically associated with either classification or regression – given a set of training data with known classes (or values, in the case of regression), the aim is to construct a model that will accurately predict the class (or value) of future data. However, machine learning is not limited to purely predictive applications – unsupervised machine learning (where training data are unlabelled, e.g. clustering analyses) can expose patterns in datasets, and interrogation of predictive models can reveal new palaeobotanical insights (Wilf *et al.*, 2016). Here, I provide a brief overview of some of the ways that fossil data has been analysed from three main perspectives: nearest living relative methods, physiognomic methods, and image processing. Although image processing typically forms part of a broader analytical workflow, it requires specialised approaches so I have considered it separately. I particularly focus on how machine learning has been employed in these three types of analyses.

Nearest living relative methods

Nearest living relative (NLR) methods assume that the climatic requirements of a fossil were similar to those of its NLRs (Mosbrugger & Utescher, 1997). Thus, by examining the NLRs of an entire fossil flora, the most parsimonious estimated palaeoclimate is the set of environmental conditions that would allow the greatest number of species to coexist (Jordan, 1997c; Mosbrugger

& Utescher, 1997). In practice, this usually involves using occurrence data to quantify the ecological range of each NLR, and then measuring the overlap between NLRs, often using machine learning algorithms (Broennimann *et al.*, 2012). The overlap between NLRs can be analysed in single climatic dimensions (e.g. Jordan 1997) or multi-dimensional space (Broennimann *et al.* 2012) and recent studies have incorporated more complex environmental niche models (ENMs) into the NLR approach (Harris *et al.*, 2014). Still more methods use probability density functions (estimated via another class of machine learning algorithm) to estimate palaeoclimate from extant occurrences (e.g. CREST, Chevalier *et al.*, 2014; Sniderman *et al.*, 2016; CrACLE, Harbert & Baryiames, 2020), although these have not yet been as widely adopted as the coexistence approach of Mosbrugger and Utescher (1997). It should be noted that in all of these methods, no-analogue fossils are generally treated as outliers and either ignored or removed.

Physiognomy

Unlike NLR approaches, physiognomic methods do not rely upon the taxonomic identity of a fossil – instead, these methods rely on relationships between climate and traits that can be measured from the fossil directly. The key assumptions for these methods are that plants inhabiting a particular environment will converge on the optimum morphology for that environment (Peppe *et al.*, 2018), and that relationships between traits and climate have remained constant over deep time (Spicer *et al.*, 2020). Like NLR methods, physiognomic methods can be univariate or multivariate, and frequently use

machine learning algorithms. One of the most frequently used is the Climate-Leaf Multivariate Analysis Program (CLAMP, Wolf, 1990; Wolfe, 1993; Yang *et al.*, 2011; Spicer *et al.*, 2020), which uses canonical correspondence analysis to predict the values of up to ten environmental variables from a set of 31 leaf traits. More recently, Wei *et al.* (2021) compared different machine learning algorithms for palaeoclimatic estimation based on digital leaf physiognomy (e.g. DiLP, Huff *et al.*, 2003; Royer *et al.*, 2005; Peppe *et al.*, 2011; Li *et al.*, 2016) and found that boosted trees and support vector machines performed significantly better than multilinear regression, highlighting the value of using more complex methods for this type of data.

Physiognomic methods are fundamentally limited by our understanding of trait-climate relationships, and are further clouded by the uncertain effect of phylogeny on these traits (Little *et al.*, 2010). One major criticism of physiognomic methods is that the mechanistic basis of many physiognomic proxies is unknown, which adds significant uncertainty to palaeoclimatic reconstructions based on these traits (Jordan, 1997a, 2011; Peppe *et al.*, 2018) Another is that many trait-climate relationships are based on either very broad or very narrow taxonomic systems, (e.g. the single extant species of *Gingko*; Jordan 2011). It is unclear how far back in time these physiognomic links can be extrapolated, and to what extant they are system-specific – the widely utilised relationship between leaf margin shape and temperature is significantly different between Southern and Northern Hemisphere floras (Kennedy *et al.*, 2014), highlighting the need to carefully consider how physiognomic methods are calibrated.

Physiognomic methods that use macroscopic leaf traits (e.g. CLAMP, DiLP) are largely inapplicable to conifers, where the gross leaf morphology is strongly constrained by phylogenetic history (Farjon, 2010). However, the physiognomic approach can be applied to micromorphological traits, where there is significantly higher variation within clades (e.g. Stark Schilling & Mill, 2011).

The plant cuticle retains an imprint of the epidermal cells that can be preserved for hundreds of millions of years (Blomenkemper *et al.*, 2021). The epidermis forms the interface between the plant and its environment and is multifunctional (see Vőfély *et al.*, 2019)), so it is not surprising that there are several documented links between epidermal morphology and climate (e.g. Rahim & Fordham, 1991; Beerling *et al.*, 1998; Aasamaa *et al.*, 2001; Torre *et al.*, 2003; Thomas *et al.*, 2004; Deccetti *et al.*, 2008; Haworth *et al.*, 2010; Dunn *et al.*, 2015b; Okanume *et al.*, 2017; Bidhendi *et al.*, 2019). While some of these relationships have been used for physiognomic palaeoclimatic reconstructions (e.g. stomatal density, stomatal index and physiological models derived from these Beerling *et al.*, 1998; McElwain *et al.*, 2016; Steinthorsdottir *et al.*, 2016; McElwain, 2018; Purcell *et al.*, 2018; Li *et al.*, 2019; Porter *et al.*, 2019), these studies have been largely univariate, and are complicated by the apparent clade specificity of many of the trait-climate relationships (Dunn *et al.*, 2015a). It is likely that the dearth of multivariate physiognomic methods for epidermal traits is because of the labour-intensive nature of measuring epidermal traits from microscope images.

Image analysis

In the context of data science, an image is a large matrix, where each pixel is an observation. Each pixel has coordinates (x and y values) and one or more variables to represent the colour (Fig. 1.1). The colour value of a pixel can be represented in a myriad of ways, including grayscale (a single value between 0 and 255) and RGB colour (a value each for red, green and blue, ranging from 0 to 255; depicted in Fig. 1.1). Additionally, pixels are spatially autocorrelated – the value of a given pixel is not independent of its neighbours. This data structure (large sample size, spatial non-independence) makes machine learning an ideal tool for image analysis. Typically, machine learning for images is either classification ('what kind of cell is in this picture?') or segmentation ('which parts of this picture are stomata?'). In palaeobotanical studies, there has been a substantial amount of work done on using machine learning to automate the identification of fossil pollen from images (Holt *et al.*, 2011; Johnsrud *et al.*, 2013; Khanzhina *et al.*, 2018), grass phytoliths from 3D models (Gallaher *et al.*, 2020) and vegetative remains from images of cleared leaves (Wilf *et al.*, 2016). Although machine learning is typically associated with a 'black-box' predictive result, careful interrogation of the algorithms can reveal new descriptive insights – Wilf *et al.* (2016) found that the angle between second-order veins can be used to identify which family the sample belongs to.

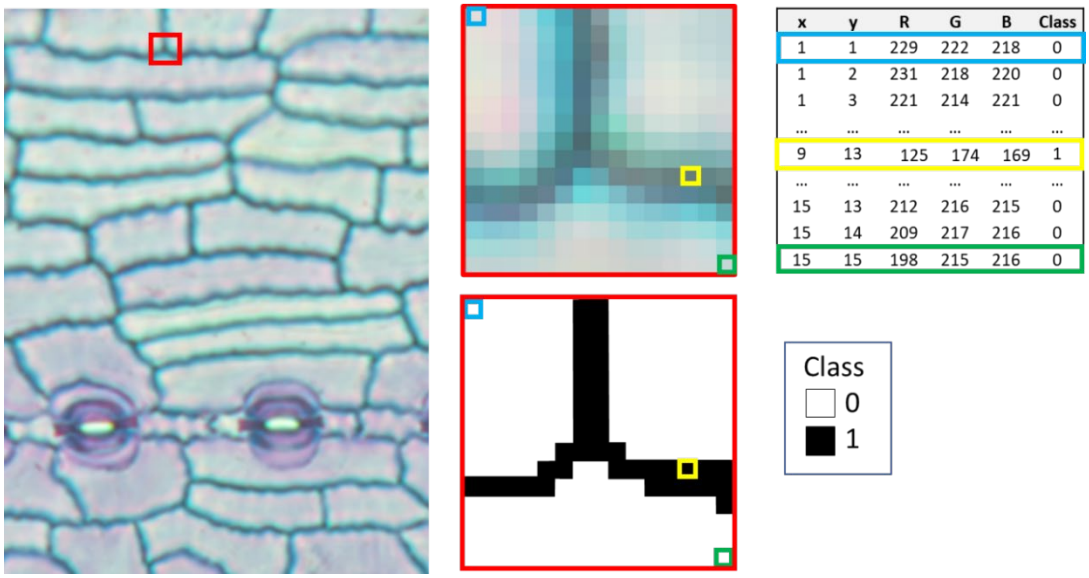

Figure 1.1. Example of how an image can be represented as data. The cuticle of *Podocarpus coriaceus*, showing the outlines of epidermal cells (a), enlargement of part of this image (red square) showing individual pixels (b), the same region showing the classification of each pixel (c), and these data in matrix form (d), where the coordinates of each pixel are given by *x* and *y*, the colour by *R, G* and *B* (red, green and blue values) and the classification by *Class*.

Thesis structure and aims

The aim of this thesis was to explore novel applications of machine learning to the fossil record of southern conifers with a focus on identifying possible explanations for no-analogue pairs. Given the two typical approaches to studying the fossil record (NLR methods and physiognomy), I centred this thesis around two main questions:

1. *What can no-analogue pairs tell us about the past, present and future ecology of the southern conifers?*

2. *Is it possible to identify changes in the bioclimatic envelope of southern conifers using epidermal physiognomy?*

These aims have been addressed in the following chapters:

Chapter 2 – HYPEROVERLAP: detecting biological overlap in *n*-dimensional space

In this chapter I present HYPEROVERLAP, a novel application of support vector machines to detect overlap between point clouds in multi-dimensional space (e.g. climate space). I demonstrate the utility of this method compared to HYPERVOLUME, using global conifer occurrence records. This tool can therefore be used to detect and investigate no-analogue pairs in the fossil record. This chapter has been published (Brown *et al.*, 2020) and the package is available on CRAN (https://cran.r-project.org/web/packages/hyperoverlap/index.html).

Chapter 3 – No-analogue associations in the fossil record of southern conifers reveal conservatism in precipitation, but not temperature axes

In this chapter, I use HYPEROVERLAP to analyse the Cenozoic fossil record of southern conifers, to identify and examine no-analogue fossil associations. Further to this, I categorise each no analogue pair in terms of temperature and precipitation to determine which aspects of the climatic niche have been conserved, and which may be more labile. This chapter is published (Brown *et al.* 2021).

Chapter 4 – No cell is an island: improving characterisation of epidermal cells by considering neighbours

In Chapter 4, I present EPIDERMALMORPH, an R package that automates trait measurements from images of epidermal cells. This tool includes several new cell shape descriptors and is the first software to automate measurement of cell arrangement. EPIDERMALMORPH can be used to undertake broad-scale studies of epidermal traits in order to identify palaeoclimatic proxies. This package is available on GitHub (https://github.com/matildabrown/epidermalmorph).

Chapter 5 – The palaeoecological value of epidermal characters in the Podocarpaceae

In this chapter, I use EPIDERMALMORPH to examine the epidermal morphology of Podocarpaceae. I compare the epidermal traits from greenhouse plants to look for climatic adaptation that could be used to identify adapted ecotypes or for palaeoclimatic estimation.

Chapter 6 – General Discussion

In the final chapter, I synthesise the key findings of my thesis and discuss the potential for and limitations of using machine learning in palaeobiological studies.

Preface

This PhD thesis is composed of two published papers in peer-reviewed international journals (Chapters 2 and 3), and two chapters that are formatted as papers (Chapters 4 and 5). To enhance the structure of the thesis, I have removed the author addresses, keywords and acknowledgements from each, but have retained the reference lists.

References

Aasamaa, K., Sober, A. & Rahi, M. (2001) Leaf anatomical characteristics associated with shoot hydraulic conductance, stomatal conductance and stomatal sensitivity to changes of leaf water status in temperate deciduous trees. *Australian Journal of Plant Physiology*, **28**, 765-774.

Andruchow-Colombo, A., Escapa, I.H., Carpenter, R.J., Hill, R.S., Iglesias, A., Abarzua, A.M. & Wilf, P. (2019) Oldest record of the scale-leaved clade of Podocarpaceae, early Paleocene of Patagonia, Argentina. *Alcheringa*, **43**, 127-145.

Beerling, D.J., McElwain, J.C. & Osborne, C.P. (1998) Stomatal responses of the 'living fossil' *Ginkgo biloba* L. to changes in atmospheric CO_2 concentrations. *Journal of Experimental Botany*, **49**, 1603-1607.

Bidhendi, A.J., Altartouri, B., Gosselin, F.P. & Geitmann, A. (2019) Mechanical stress initiates and sustains the morphogenesis of wavy leaf epidermal cells. *Cell reports*, **28**, 1237-1250.

Blomenkemper, P., Bäumer, R., Backer, M., Abu Hamad, A., Wang, J., Kerp, H. & Bomfleur, B. (2021) Bennettitalean Leaves From the Permian of Equatorial Pangea—The Early Radiation of an Iconic Mesozoic Gymnosperm Group. *Frontiers in Earth Science*, **9**, 162.

Brodribb, T. & Hill, R.S. (2004) The rise and fall of the Podocarpaceae in Australia—A physiological explanation. *Evolution of Plant Physiology from Whole Plants to Ecosystems* (ed. by A.H.I. Poole), pp. 379-381. Academic Press, London.

Broennimann, O., Fitzpatrick, M.C., Pearman, P.B., Petitpierre, B., Pellissier, L., Yoccoz, N.G., Thuiller, W., Fortin, M.J., Randin, C., Zimmermann, N.E., Graham, C.H. & Guisan, A. (2012) Measuring ecological niche overlap from occurrence and spatial environmental data. *Global Ecology and Biogeography*, **21**, 481-497.

Brown, M.J., Holland, B.R. & Jordan, G.J. (2020) HYPEROVERLAP: Detecting biological overlap in n-dimensional space. *Methods in Ecology and Evolution*, **11**, 513-523.

Brown, M.J., Brodribb, T.J. & Jordan, G.J. (2021) No-analogue associations in the fossil record of southern conifers reveal conservatism in precipitation, but not temperature axes. *Global Ecology and Biogeography*, **30**(12), 2455-2466

Buschiazzo, E., Ritland, C., Bohlmann, J. & Ritland, K. (2012) Slow but not low: genomic comparisons reveal slower evolutionary rate and higher dN/dS in conifers compared to angiosperms. *BMC Evolutionary Biology*, **12**, 1-15.

Carpenter, R., Hill, R. & Jordan, G. (1994) Cenozoic vegetation in Tasmania: macrofossil evidence. *History of the Australian vegetation: Cretaceous to Recent* (ed. by R.S. Hill), pp. 276-298. University of Adelaide Press, Adelaide.

Carpenter, R.J., Jordan, G.J., Mildenhall, D.C. & Lee, D.E. (2011) Leaf fossils of the ancient Tasmanian relict *Microcachrys* (Podocarpaceae) from New Zealand. *American Journal of Botany*, **98**, 1164-72.

Chevalier, M., Cheddadi, R. & Chase, B.M. (2014) CREST (Climate REconstruction SofTware): a probability density function (PDF)-based quantitative climate reconstruction method. *Climate of the Past*, **10**, 2081-2098.
Deccetti, S.F.C., Soares, A.M., Paiva, R. & de Castro, E.M. (2008) Effect of the culture environment on stomatal features, epidermal cells and water loss of micropropagated *Annona glabra* L. plants. *Scientia Horticulturae*, **117**, 341-344.
Dunn, R.E., Le, T.Y.T. & Stromberg, C.A.E. (2015a) Light Environment and Epidermal Cell Morphology in Grasses. *International Journal of Plant Sciences*, **176**, 832-847.
Dunn, R.E., Stromberg, C.A., Madden, R.H., Kohn, M.J. & Carlini, A.A. (2015b) Linked canopy, climate, and faunal change in the Cenozoic of Patagonia. *Science*, **347**, 258-61.
Farjon, A. (2010) *A Handbook of the World's Conifers*. Brill, Leiden/Boston.
Farjon, A. & Filer, D. (2013) *An atlas of the world's conifers: an analysis of their distribution, biogeography, diversity and conservation status*. Brill, Leiden/Boston.
Gallaher, T.J., Akbar, S.Z., Klahs, P.C., Marvet, C.R., Senske, A.M., Clark, L.G. & Stromberg, C.A.E. (2020) 3D shape analysis of grass silica short cell phytoliths: a new method for fossil classification and analysis of shape evolution. *New Phytologist*, **228**, 376-392.
Harbert, R.S. & Baryiames, A.A. (2020) cRacle: R tools for estimating climate from vegetation. *Applications in Plant Sciences*, **8**, e11322.
Harris, A.J., Papes, M., Gao, Y.D. & Watson, L. (2014) Estimating paleoenvironments using ecological niche models of nearest living relatives: A case study of Eocene *Aesculus* L. *Journal of Systematics and Evolution*, **52**, 16-34.
Haworth, M., Heath, J. & McElwain, J.C. (2010) Differences in the response sensitivity of stomatal index to atmospheric CO2 among four genera of Cupressaceae conifers. *Annals of Botany*, **105**, 411-8.
Hill, R.S. (1995) Conifer origin, evolution and diversification in the Southern Hemisphere. *Ecology of the southern conifers* (ed. by N.J. Enright and R.S. Hill), pp. 10-29. Melbourne University Press, Carlton.
Hill, R.S. & Brodribb, T.J. (1999) Turner Review No. 2 - Southern conifers in time and space. *Australian Journal of Botany*, **47**, 639-696.
Holt, K., Allen, G., Hodgson, R., Marsland, S. & Flenley, J. (2011) Progress towards an automated trainable pollen location and classifier system for use in the palynology laboratory. *Review of Palaeobotany and Palynology*, **167**, 175-183.
Huff, P.M., Wilf, P. & Azumah, E.J. (2003) Digital future for paleoclimate estimation from fossil leaves? Preliminary results. *Palaios*, **18**, 266-274.
Jin, W.T., Gernandt, D.S., Wehenkel, C., Xia, X.M., Wei, X.X. & Wang, X.Q. (2021) Phylogenomic and ecological analyses reveal the spatiotemporal evolution of global pines. *Proceedings of the National Academy of Sciences*, **118**, e2022302118.

Johnsrud, S., Yang, H.G., Nayak, A. & Punyasena, S.W. (2013) Semi-automated segmentation of pollen grains in microscopic images: a tool for three imaging modes. *Grana*, **52**, 181-191.
Jordan, G.J. (1997a) Uncertainty in palaeoclimatic reconstructions based on leaf physiognomy. *Australian Journal of Botany*, **45**, 527-547.
Jordan, G.J. (1997b) Contrasts between the climatic ranges of fossil and extant taxa: Causes and consequences for palaeoclimatic estimates. *Australian Journal of Botany*, **45**, 465-474.
Jordan, G.J. (1997c) Evidence of Pleistocene plant extinction and diversity from Regatta Point, western Tasmania, Australia. *Botanical Journal of the Linnean Society*, **123**, 45-71.
Jordan, G.J. (2011) A critical framework for the assessment of biological palaeoproxies: predicting past climate and levels of atmospheric CO(2) from fossil leaves. *New Phytologist*, **192**, 29-44.
Jordan, M.I. & Mitchell, T.M. (2015) Machine learning: Trends, perspectives, and prospects. *Science*, **349**, 255-60.
Kennedy, E.M., Arens, N.C., Reichgelt, T., Spicer, R.A., Spicer, T.E.V., Stranks, L. & Yang, J. (2014) Deriving temperature estimates from Southern Hemisphere leaves. *Palaeogeography Palaeoclimatology Palaeoecology*, **412**, 80-90.
Khanzhina, N., Putin, E., Filchenkov, A. & Zamyatina, E. (2018) Pollen grain recognition using convolutional neural network. *European Symposium on Artificial Neural Networks, Computational Intelligence and Machine Learning* (ed by. Bruges.
Kooyman, R.M., Rossetto, M., Sauquet, H. & Laffan, S.W. (2013) Landscape patterns in rainforest phylogenetic signal: isolated islands of refugia or structured continental distributions? *PLoS One*, **8**, e80685.
Li, H., Yu, J.X., McElwain, J.C., Yiotis, C. & Chen, Z.Q. (2019) Reconstruction of atmospheric CO2 concentration during the late Changhsingian based on fossil conifers from the Dalong Formation in South China. *Palaeogeography Palaeoclimatology Palaeoecology*, **519**, 37-48.
Li, S.F., Jacques, F.M.B., Spicer, R.A., Su, T., Spicer, T.E.V., Yang, J. & Zhou, Z.K. (2016) Artificial neural networks reveal a high-resolution climatic signal in leaf physiognomy. *Palaeogeography Palaeoclimatology Palaeoecology*, **442**, 1-11.
Little, S.A., Kembel, S.W. & Wilf, P. (2010) Paleotemperature proxies from leaf fossils reinterpreted in light of evolutionary history. *PLoS One*, **5**, e15161.
Macphail, M. (2007) *Australian palaeoclimates: Cretaceous to Tertiary. A review of palaeobotanical and related evidence to the year 2000*. CRC LEME, Bentley.
Macphail, M., Carpenter, R.J., Iglesias, A. & Wilf, P. (2013) First evidence for Wollemi Pine-type pollen (*Dilwynites*: Araucariaceae) in South America. *PLoS One*, **8**, e69281.
McElwain, J.C. (2018) Paleobotany and global change: Important lessons for species to biomes from vegetation responses to past global change. *Annual Review of Plant Biology*, **69**, 761-787.

McElwain, J.C., Montañez, I., White, J.D., Wilson, J.P. & Yiotis, C. (2016) Was atmospheric CO_2 capped at 1000 ppm over the past 300 million years? *Palaeogeography, Palaeoclimatology, Palaeoecology*, **441**, 653-658.
Mosbrugger, V. & Utescher, T. (1997) The coexistence approach—a method for quantitative reconstructions of Tertiary terrestrial palaeoclimate data using plant fossils. *Palaeogeography, Palaeoclimatology, Palaeoecology*, **134**, 61-86.
Okanume, O.E., Joseph, O.M., Agaba, O.A., Habila, S., Oluwatobi, A.O. & Adebayo, O.B. (2017) Effect of Industrial Effluent on the Growth, Yield and Foliar Epidermal Features of Tomato (*Solanum lycopersicum* L.) in Jos, Plateau State, Nigeria. *Notulae Scientia Biologicae*, **9**, 549-556.
Peppe, D.J., Baumgartner, A., Flynn, A. & Blonder, B. (2018) Reconstructing paleoclimate and paleoecology using fossil leaves. *Methods in Paleoecology* (ed. by D.A. Croft, D. Su and S.W. Simpson), pp. 289-317. Springer, Cham.
Peppe, D.J., Royer, D.L., Cariglino, B., Oliver, S.Y., Newman, S., Leight, E., Enikolopov, G., Fernandez-Burgos, M., Herrera, F., Adams, J.M., Correa, E., Currano, E.D., Erickson, J.M., Hinojosa, L.F., Hoganson, J.W., Iglesias, A., Jaramillo, C.A., Johnson, K.R., Jordan, G.J., Kraft, N.J., Lovelock, E.C., Lusk, C.H., Niinemets, U., Penuelas, J., Rapson, G., Wing, S.L. & Wright, I.J. (2011) Sensitivity of leaf size and shape to climate: global patterns and paleoclimatic applications. *New Phytologist*, **190**, 724-39.
Pole, M. (2007) Plant-macrofossil assemblages during pliocene uplift, South Island, New Zealand. *Australian Journal of Botany*, **55**, 118-142.
Porter, A.S., Evans-Fitz.Gerald, C., Yiotis, C., Montañez, I.P. & McElwain, J.C. (2019) Testing the accuracy of new paleoatmospheric CO_2 proxies based on plant stable carbon isotopic composition and stomatal traits in a range of simulated paleoatmospheric O_2:CO_2 ratios. *Geochimica et Cosmochimica Acta*, **259**, 69-90.
Purcell, C., Batke, S.P., Yiotis, C., Caballero, R., Soh, W.K., Murray, M. & McElwain, J.C. (2018) Increasing stomatal conductance in response to rising atmospheric CO_2. *Ann Bot*, **121**, 1137-1149.
Rahim, M.A. & Fordham, R. (1991) Effect of Shade on Leaf and Cell-Size and Number of Epidermal-Cells in Garlic (*Allium sativum*). *Annals of Botany*, **67**, 167-171.
Royer, D.L., Wilf, P., Janesko, D.A., Kowalski, E.A. & Dilcher, D.L. (2005) Correlations of climate and plant ecology to leaf size and shape: potential proxies for the fossil record. *American Journal of Botany*, **92**, 1141-51.
Sniderman, J.M., Woodhead, J.D., Hellstrom, J., Jordan, G.J., Drysdale, R.N., Tyler, J.J. & Porch, N. (2016) Pliocene reversal of late Neogene aridification. *Proceedings of the National Academy of Sciences*, **113**, 1999-2004.
Spicer, R.A. (1988) Quantitative sampling of plant megafossil assemblages. *The Paleontological Society Special Publications*, **3**, 29-51.

Spicer, R.A., Yang, J., Spicer, T.E. & Farnsworth, A. (2020) Woody dicot leaf traits as a palaeoclimate proxy: 100 years of development and application. *Palaeogeography, Palaeoclimatology, Palaeoecology*,
Stark Schilling, D.M. & Mill, R.R. (2011) Cuticle micromorphology of Caribbean and Central American species of *Podocarpus* (Podocarpaceae). *International Journal of Plant Sciences*, **172**, 601-631.
Steinthorsdottir, M., Porter, A.S., Holohan, A., Kunzmann, L., Collinson, M. & McElwain, J.C. (2016) Fossil plant stomata indicate decreasing atmospheric CO_2 prior to the Eocene-Oligocene boundary. *Climate of the Past*, **12**, 439-454.
Stockey, R.A. (1982) The Araucariaceae - an Evolutionary Perspective. *Review of Palaeobotany and Palynology*, **37**, 133-154.
Sundaram, M. & Leslie, A.B. (2021) The influence of climate and palaeoclimate on distributions of global conifer clades depends on geographical range size. *Journal of Biogeography*, **48**, 2286-2297.
Thomas, P.W., Woodward, F.I. & Quick, W.P. (2004) Systemic irradiance signalling in tobacco. *New Phytologist*, **161**, 193-198.
Torre, S., Fjeld, T., Gislerod, H.R. & Moe, R. (2003) Leaf anatomy and stomatal morphology of greenhouse roses grown at moderate or high air humidity. *Journal of the American Society for Horticultural Science*, **128**, 598-602.
Truswell, E.M. & MacPhail, M.K. (2009) Polar forests on the edge of extinction: What does the fossil spore and pollen evidence from East Antarctica say? *Australian Systematic Botany*, **22**, 57-106.
Vőfély, R.V., Gallagher, J., Pisano, G.D., Bartlett, M. & Braybrook, S.A. (2019) Of puzzles and pavements: a quantitative exploration of leaf epidermal cell shape. *New Phytol*, **221**, 540-552.
Wei, G., Peng, C., Zhu, Q., Zhou, X. & Yang, B. (2021) Application of machine learning methods for paleoclimatic reconstructions from leaf traits. *International Journal of Climatology*, **41**, E3249-E3262.
Westerhold, T., Marwan, N., Drury, A.J., Liebrand, D., Agnini, C., Anagnostou, E., Barnet, J.S., Bohaty, S.M., De Vleeschouwer, D. & Florindo, F. (2020) An astronomically dated record of Earth's climate and its predictability over the last 66 million years. *Science*, **369**, 1383-1387.
Wilf, P. (2012) Rainforest conifers of Eocene Patagonia: attached cones and foliage of the extant Southeast Asian and Australasian genus *Dacrycarpus* (Podocarpaceae). *Am J Bot*, **99**, 562-84.
Wilf, P., Zhang, S., Chikkerur, S., Little, S.A., Wing, S.L. & Serre, T. (2016) Computer vision cracks the leaf code. *Proceedings of the National Academy of Sciences*, **113**, 3305-10.
Wilf, P., Little, S.A., Iglesias, A., Del Carmen Zamaloa, M., Gandolfo, M.A., Cuneo, N.R. & Johnson, K.R. (2009) *Papuacedrus* (Cupressaceae) in Eocene Patagonia: A new fossil link to Australasian rainforests. *Am J Bot*, **96**, 2031-47.
Wolf, J.A. (1990) Palaeobotanical evidence for a marked temperature increase following the Cretaceous/Tertiary boundary. *Nature*, **343**, 153-156.

Wolfe, J.A. (1993) *A method of obtaining climatic parameters from leaf assemblages*. US Government Printing Office, Washington DC.
Yang, J., Spicer, R.A., Spicer, T.E. & Li, C.-S. (2011) 'CLAMP Online': a new web-based palaeoclimate tool and its application to the terrestrial Paleogene and Neogene of North America. *Palaeobiodiversity and Palaeoenvironments*, **91**, 163-183.

Chapter 2 : HYPEROVERLAP: detecting biological overlap in *n*-dimensional space

This chapter has been published in Methods in Ecology and Evolution.

Brown, M.J.M., Holland, B.R., Jordan, G.J. (2020). HYPEROVERLAP: Detecting biological overlap in n-dimensional space. Methods in Ecology and Evolution.; 11: 513– 523. https://doi.org/10.1111/2041-210X.13363

Introduction

Many ecological and evolutionary questions revolve around the study of overlap: Do two species (or any other entity, **Table 2.1**) overlap in terms of climatic requirements? How have particular entities diverged (or converged) over evolutionary time? Under what conditions could two entities coexist? These questions of biological overlap are central to a broad range of studies including taxonomy (Rissler & Apodaca, 2007), investigating broad-scale evolution of climatic envelopes (Donoghue & Edwards, 2014), niche partitioning (Peterson *et al.*, 2013), predicting the spread of invasive species (Guisan *et al.*, 2014) and palaeoclimatic estimation (Mosbrugger & Utescher, 1997). Many of these studies have been made possible because of the relatively recent development of large online databases such as the Global Biodiversity Information Facility (GBIF), the Plant Trait Database (TRY; Kattge *et al*. 2020) and WorldClim (Fick & Hijmans, 2017), which make large amounts of biological data publicly available.

Table 2.1. Key terms in the hyperoverlap framework

decision boundary	The hypersurface that best separates the data of a pair of entities in *n*-dimensional space. May be linear or non-linear.
entity	Any group of individuals to be compared, as per Broennimann *et al.* (2012). Not limited to species; other examples may be genera, families, native or invasive populations or any other statistical population.
explicit hypervolume method/model	Any method or model which explicitly describes the geometry of the hypervolume. Examples include convex hulls (Habel *et al.* 2015), dynamic range boxes (Schreyer *et al.* 2015) and the HYPERVOLUME package (Blonder *et al.*, 2014; Blonder *et al.*, 2018).
hyperplane	An *n*-1-dimensional subspace of an *n*-dimensional space.
hypervolume	A contiguous *n*-dimensional region in *n*-dimensional space.
kernel	A function that transforms the original, *n*-dimensional data into higher dimensional space in such a way that a hyperplane can be fitted to the data (see Scholkopf & Smola, 2002).
nested hypervolumes	A qualitative relationship between two hypervolumes where one entity occurs entirely within the region of space occupied by the other entity.
overlap	The observed intersection in *n*-dimensional space of the hypervolumes occupied by two entities, where the dimensions represent biological variables.
single-entity method	An approach to overlap detection which constructs individual models for each entity, then measures overlap of these models.
support vector machine (SVM)	A machine learning classifier that finds the maximal-margin separating hyperplane within classes (see Scholkopf & Smola, 2002)

We can use hypervolume concepts to analyse patterns of overlap between sets of point data in multidimensional space (e.g. Blonder et al, 2018). Current hypervolume approaches first map each observation in an *n*-dimensional space, where the dimensions are the chosen variables. These approaches then create a multidimensional object (a “hypervolume”) that encloses the observations, often allowing for error. The hypervolume is then assumed to represent the set of phenotypes or environments occupied by the entity. Hypervolume concepts were first used to describe the ecological niche (see Holt, 2009) but they are broadly applicable to any multidimensional space and have been utilised in several other fields (e.g. morphometry, Sidlauskas, 2008; functional traits, Díaz *et al.*, 2016). However, such hypervolume-type studies typically seek to *predict* the distributions of entities, and require *a priori* assumptions about the distribution or shape of the hypervolume, so methods developed for this purpose may not be suited to answer questions which require qualitative inference of overlap.

Many hypervolume-based algorithms in ecology model the occupied region of a single entity – overlap detection is a by-product of this application. In this paper, we use the term ‘single-entity method’ to refer to any which constructs individual models for each entity and then compares them to analyse overlap. Joint species models (e.g. Pollock *et al.*, 2014; Ovaskainen *et al.*, 2016) are an emerging tool to incorporate biotic interactions into niche models but require absence data as well as presence data so they are not considered further here.

In this paper, we discuss the limitations of detecting biological overlap using single-entity methods and argue that all single-entity solutions to this problem share similar theoretical problems. We present the ‘hyperoverlap’ framework – a novel application of a machine learning classifier to detect overlap between point data sets sampled from hypervolumes in *n*-dimensional space. We also present an R package that implements this analytical framework – HYPEROVERLAP (see https://github.com/matildabrown/hyperoverlap). To highlight the conceptual novelty of our approach, we compare the performance of HYPEROVERLAP with the most comparable single-entity

approach: Blonder's 'HYPERVOLUME' algorithms (hereafter referred to as HYPERVOLUME to distinguish the R package from more general uses of the term hypervolume). We analyse a real-world example (the ecological ranges of genera of conifers) to demonstrate the advantages of our method and discuss the caveats that should be considered when using the hyperoverlap framework.

Current approaches

The geometry of the hypervolume may be measured in several ways, depending on *a priori* expectations about the shape of the hypervolume. A plethora of increasingly sophisticated algorithms have been developed to model this hypervolume, either directly or indirectly, and measure overlap between the estimated hypervolumes occupied by two entities. Although earlier approaches were computationally and/or conceptually limited to low-dimensional analyses (e.g. Broennimann *et al.*, 2012), several recent methods allow direct analysis in *n*-dimensional space.

Machine learning methods are used extensively to analyse landscape-scale, multidimensional data. In explicit hypervolume models, machine learning classifiers are used to predict the habitat suitability of each pixel in a landscape (e.g. MaxEnt; Phillips *et al.*, 2006); to classify points in ecological space as 'in' or 'out' of the modelled niche (e.g. 'hypervolume_exclusion_test'; Blonder *et al.*, 2018); or to define the boundary of the niche in n-dimensional space (e.g. 'hypervolume_svm'; Blonder *et al.*, 2018). Once described by an appropriate model, two hypervolumes may be compared and the volumes of the overlapping and unique regions can be measured (see 'hypervolume_set', 'hypervolume_overlap_statistics' functions; Blonder *et al.*, 2018).

Current methods of describing hypervolumes vary in the geometric model used. The simplest of these methods is the *n*-dimensional convex hull, implemented in the GEOMETRY R package (R Core Team, 2014; Habel *et al.* 2015). However, many biological hypervolumes are not convex. Similarly, the hypervolumes simulated by NICHEA software (Qiao *et al.*, 2016) are

constrained to ellipsoids, and so are not broadly applicable to the non-convex or irregular data common encountered in ecological problems. Dynamic range boxes (DYNRB PACKAGE; Schreyer *et al.* 2015) have the advantage that they do not assume normally or elliptically distributed data, but the authors acknowledge that correlated variables must be removed during pre-processing (Junker *et al.* 2016). Because many biological variables are strongly correlated, this method is limited in the variables that can be analysed. Blonder's HYPERVOLUME package (Blonder *et al.*, 2014; Blonder *et al.*, 2018) includes a range of functions for hypervolume modelling and comparison. In both HYPERVOLUME AND HYPEROVERLAP the shape of the hypervolume is not defined by *a priori* expectations, so we have used HYPERVOLUME as a standard to evaluate the performance of HYPEROVERLAP. Additionally, these methods use the same machine learning classifier (SVM), so conflicting results will be driven by conceptual rather than algorithmic differences.

Weaknesses of using single-entity methods for detecting overlap in multidimensional space

Reliable results from single-entity methods depend on meeting several assumptions, many of which are unlikely to hold for landscape-scale datasets (Jarnevich *et al.*, 2015). The most commonly violated of these assumptions is that the records are an unbiased sample of the biological range. Satisfying this assumption requires even sampling from the entire geographic and ecological and/or phenotypic range of an entity. For almost all entities in GBIF, occurrence sampling is substantially biased in geographic space (Boakes *et al.*, 2010; Beck *et al.*, 2014), with strong biases towards roads and urbanised areas, and especially strong biases towards rare species (Stolar and Nielsen, 2015).

Thus, real-world entities are often represented by sampled data that are irregular, holey, discontinuous, or include outliers (Blonder, 2016). Outliers are often treated as noise by modelling algorithms – which are designed to filter out noisy data – but sampling effort, habitat fragmentation, and the

geographical distribution of suitable habitat can each cause real occurrence records to appear as outliers. Highly restricted, often endangered entities with geographic outliers are often high priorities for conservation management but are also most likely to be misrepresented by these models. Adjusting the model-fitting parameters to ensure that every occurrence record is included in the model predictions (i.e. a 0% omission threshold) can result in severe extrapolation. In species distribution modelling, this means that conditions well outside the observed hypervolume are predicted to be suitable (Escobar *et al.*, 2018). This means that the choice of omission threshold may falsely inflate or decrease observations of overlap between entities.

These issues are unavoidable when attempting to resolve the complex problem of accurately modelling the hypervolume from sampled point data, and there is no universal best approach (Qiao *et al.*, 2015). However, we suggest that the detection and description of the observed overlap between two hypervolumes can be achieved by comparing the point data for entities directly and is thus a simpler task than explicitly modelling the hypervolume.

Hyperoverlap conceptual framework

We propose a qualitative method for detecting multidimensional overlap. There are three possible qualitative relationships between points sampled from two hypervolumes: nested, overlapping, or non-overlapping (Figure 2.1). If the observations from each hypervolume can be perfectly separated by a decision boundary (**Table 2.1**), we cannot identify a shared region and the entities do not overlap. If this decision boundary does not exist, the entities overlap (with misclassified points occupying the shared region). If we assume that all observations of an entity are within the hypervolume, this principle can be applied to samples of point data (but see *Caveats and Limitations*).

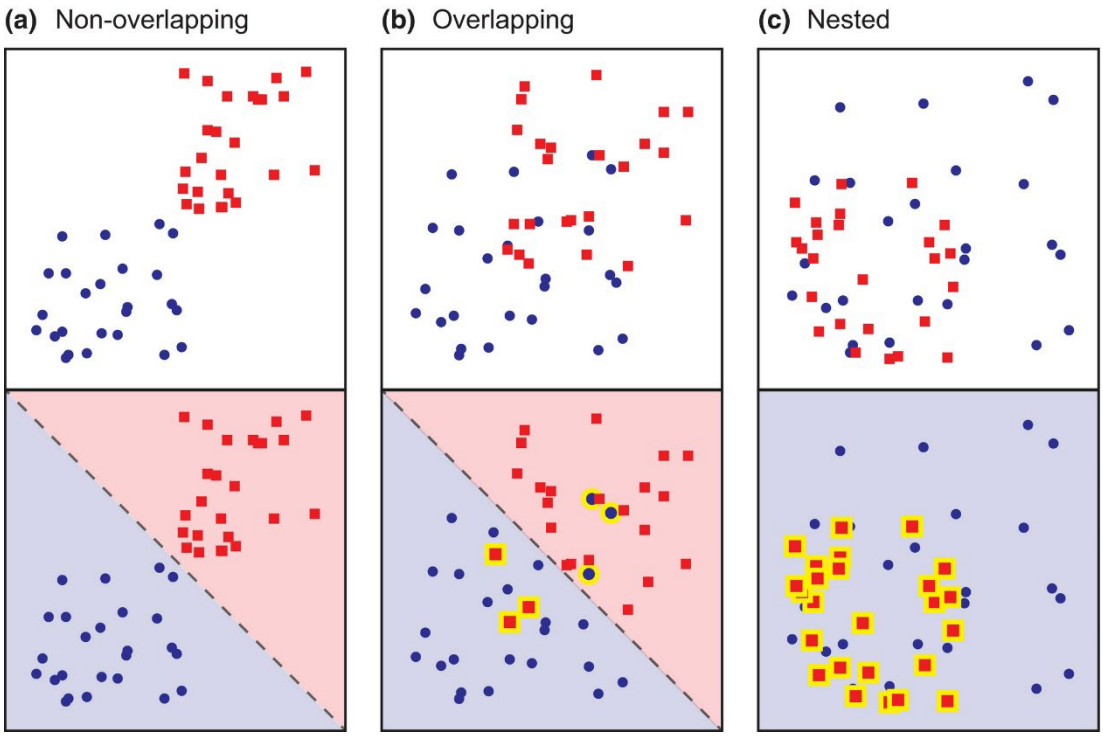

Figure 2.1 There are three possible relationships between two hypervolumes. Points sampled from two hypervolumes (top panels) can be used to train a classifier, find the optimal decision boundary (dashed line) and identify misclassified points (highlighted in yellow). The possible relationships are: the hypervolumes do not intersect (a); the hypervolumes intersect (b) or one hypervolume is contained within the other (c). This concept can be easily visualized in two or three dimensions but can be generalized to any *n*-dimensional space

The HYPEROVERLAP algorithm finds the optimal separating hyperplane between two entities using SVMs based on point data and calculates the number of points belonging to each entity on either side of this boundary. If there are no misclassified points, we infer that the hypervolumes for the entities do not overlap (Figure 2.1a, but see *Caveats and Limitations*). If at least one point is misclassified (Figure 2.1b), the two entities overlap. If no boundary can be found (Figure 2.1c), one hypervolume is 'nested' within the other (see *Terminology*).

If there is a single hyperplane (of *n*-1 dimensions) which perfectly separates the observations from each hypervolume, the entities are linearly separable (Figure 2.2a). For entities which cannot be separated using a linear plane but occupy distinct regions of space (Figure 2.2b), a kernel function (Scholkopf & Smola, 2002) can be used to find a curvilinear decision boundary. Polynomial kernel functions are preferred because other functions (e.g. sigmoidal or Gaussian) can create complex decision boundary shapes that are likely to overfit the classifier (Figure 2.2c). The order of the polynomial kernel function constrains the complexity of the decision boundary. Potential concerns about the biological meaningfulness of this boundary may be addressed by visualisation (functions provided in the HYPEROVERLAP package).

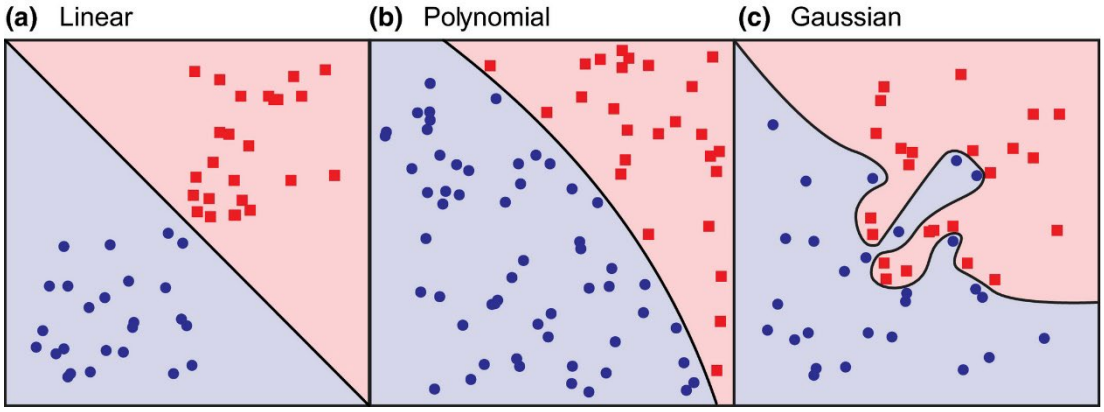

Figure 2.2. Decision boundaries generated using different kernel functions. A linear kernel (a) always produces a linear decision boundary, a polynomial kernel (b) may produce a curvilinear decision boundary and a Gaussian kernel (c) can produce a complex decision boundary which does not reflect the underlying biology

Sketch of the HYPEROVERLAP algorithm

Before implementing The HYPEROVERLAP workflow, it is important to pre-process data to exclude duplicate, incomplete or erroneous records, and to ensure that the dimensions are comparable (see Blonder, 2018). A support vector machine (SVM) is then trained on the data using the E1071 package (Meyer *et al.*, 2018). This creates a fitted linear model that is used to predict

the labels of the input data. If the model correctly classifies every point (i.e. the entities can be separated by the linear hyperplane) the function returns the result (non-overlap) and the coordinates of the decision boundary. If there are misclassified points, SVMs are trained using polynomial kernels of increasing complexity, each time evaluating the number of misclassified points until a separating hyperplane is found. If such a hyperplane is not found, the result ('overlap') is returned.

Finding the decision boundary for non-overlapping entities is fast (typically milliseconds) but can be much slower if the entities overlap. To prevent excessive searching, the algorithm does not attempt a non-linear kernel if the linear result is that the two entities are nested, or if a certain number of points representing significant overlap are misclassified. This parameter is user-defined (see `stoppage.threshold`; package documentation).

Machine learning classifiers are typically trained with the aim to correctly predict the labels of unknown data. Various caveats about relative and absolute sample sizes apply to SVMs when they are used to automate identification in this way. However, these caveats are not relevant to HYPEROVERLAP, which does not use SVMs in a predictive fashion. Instead, HYPEROVERLAP uses the SVM classifier as a descriptive tool and so overfitting is prevented by setting constraints on the shape of the decision boundary. This can be verified using visualisation of the decision boundary (in three or fewer dimensions) or visualisation of the data using ordination (in four or more dimensions) using functions in the HYPEROVERLAP R package (see Figure S2.1 in Supporting Information for example).

Theoretical advantages of HYPEROVERLAP

Dimensionality and sample size

The hyperoverlap algorithm considers the data for two entities simultaneously, unlike other hypervolume methods (e.g. HYPERVOLUME, BLONDER ET AL., 2018; NICHEA, Qiao *et al.*, 2016). It is often difficult or impossible to use single-entity methods to fit models to very small samples, and thus to investigate many relevant problems (e.g. those involving threats

to endangered species). This problem affects all methods which fit individual models to entities. However, the most relevant sample size for HYPEROVERLAP is *total* sample size for the pair of entities. As a result, this approach can be effective with sample sizes as small as 1 for one of the entities –provided that the number of observations of the other entity is at least moderately large (see *Evaluation: Results; Case Study 2*). However, care should be taken when analysing two very small entities, as discussed in *Caveats and Limitations*.

Computational effort

Conventional measurement of overlap from single-entity models require two phases; initial modelling, then pairwise comparison of models. Unless the number of entities is very small, conventional memory constraints demand that these models are written to disk and re-read for comparison, separating these two phases. Hyperoverlap builds models using the paired data, so does not require this storage step. Computational effort is further reduced by constraints on the shape of decision boundary; the decision boundary produced by HYPEROVERLAP is constrained to linear and low-degree polynomial kernels (unlike the edges of the hypervolumes modelled using HYPERVOLUME).

Evaluation

Methods

To evaluate the performance of HYPEROVERLAP, we compared parallel results between HYPEROVERLAP and HYPERVOLUME for 71 conifer genera (2485 pairs). Conifers are an ideal group for this because the group is diverse with regard to ecological and distributional range (e.g. *Pinus* occurs across the Northern Hemisphere; *Wollemia* is only found in one gorge near Sydney, Australia; Farjon & Filer, 2013) and because species of conifers have well-defined bioclimatic ranges (Brodribb & Hill, 1999). The data are geographic point records for each genus of conifer used by Larcombe *et al.* (2018). We extracted climatic data for each point record from WorldClimV2 at 30”

(approximately 1km^2) resolution and used DISMO (Hijmans *et al.*, 2015) to build the values for three variables which are known to correlate to physiological stresses in conifers. These variables were mean minimum temperature of the coldest month (mint.cm) reflecting frost tolerance (Sakai & Larcher, 2012); mean temperature of the warmest quarter (at.warmq) reflecting growing season temperature (Prentice et al., 1992); and mean precipitation of the driest quarter (p.dryq) reflecting drought tolerance (Mackey, 1994). Although HYPEROVERLAP has been developed for *n*-dimensional analyses, using only three dimensions for evaluation allowed the results to be inspected directly, without requiring ordination. We also conducted analyses using two additional variables (mean precipitation of the warmest and wettest quarters, respectively) to assess computational performance in higher dimensional space.

Precipitation records (p.dryq) were transformed to an approximately normal distribution by taking the fourth root and all variables were *z*-transformed to the global (-90° to 90° latitude) mean and standard deviation of each variable. We compared the overlap/non-overlap results, computational time and stability of the two methods (HYPEROVERLAP and HYPERVOLUME). To evaluate stability, each overlap detection function was run ten times (a larger number of runs was not computationally feasible). We then compiled and compared the results from each method. For each entity pair that gave conflicting results, we visually inspected the data to assess the accuracy of each method.

Runtimes are given for scripts run on an Intel i7-8700k CPU.

Results

Overlap detection

HYPEROVERLAP detected 1134 non-overlapping pairs of entities (of 2485 pairs; Figure 2.3). Of these non-overlapping pairs, 1082 (95%) could be separated with a linear decision boundary, and only 52 (2.1%) required a curvilinear hyperplane (polynomial kernel function) to identify ecological non-overlap. The number of non-overlapping pairs identified by HYPERVOLUME

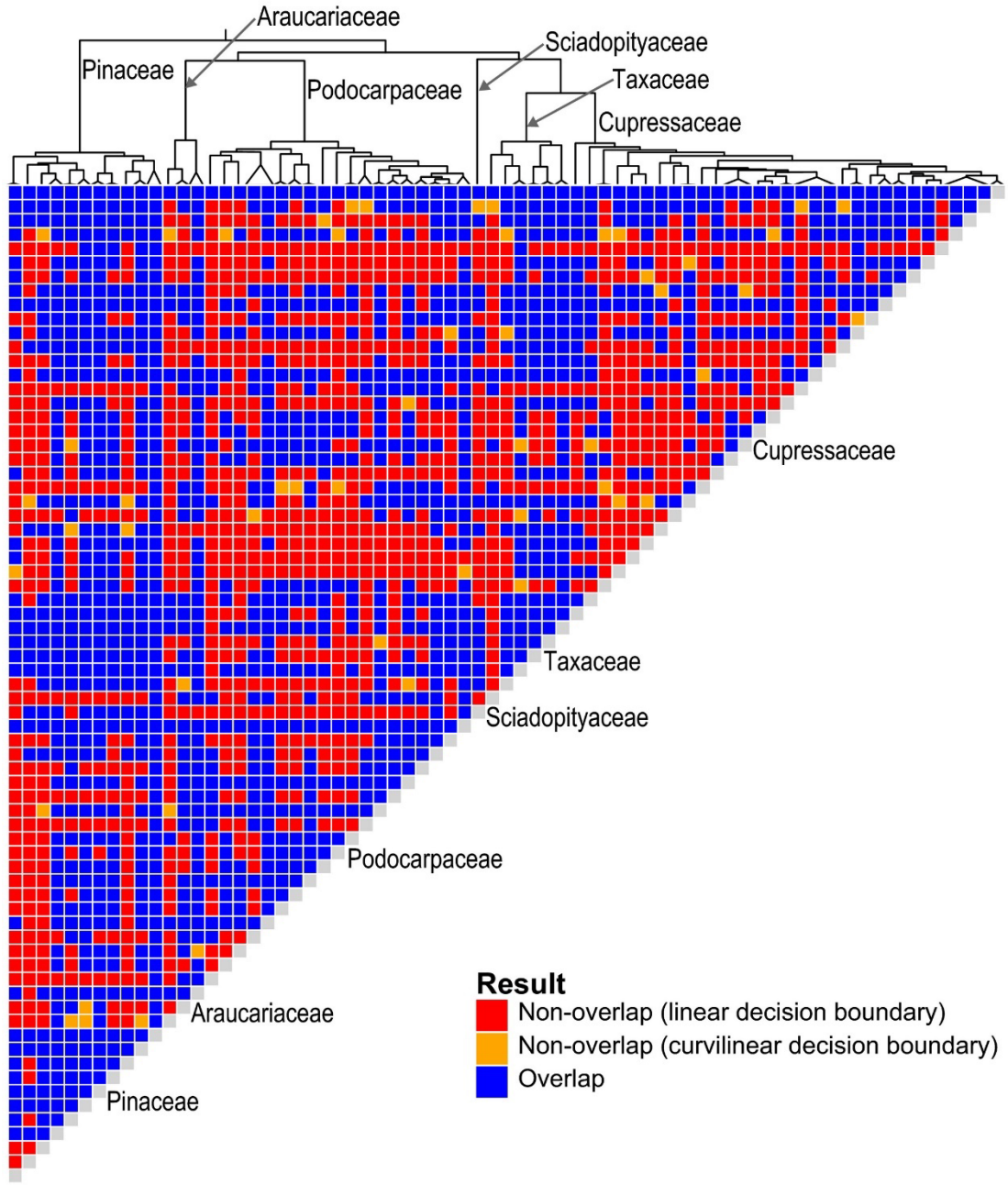

Figure 2.3 Pairwise comparison of climatic distributions of conifer genera (grouped phylogenetically) using hyperoverlap. A fully labelled version of this figure is available in Figure S2.2). Phylogeny from Leslie et al. (2012).

varied with run, ranging from 1076 to 1092 (see *Computational Time and Stability*).

There were differences in the results given by different methods. HYPEROVERLAP reported 133 non-overlaps (5.5% of the 2415 pairs excluding *Wollemia*) that were classified as overlaps by HYPERVOLUME (see *Case Study 1*), and 33 overlaps (1.4% of total) where HYPERVOLUME reported non-overlap (see *Case Study 2*). Visualisation confirmed the status of all the non-overlaps identified by HYPEROVERLAP that were reported as overlaps by HYPERVOLUME. There was no discernible pattern in these conflicts; they do not cluster by taxonomic group or sample size (

Figure 2.4). In addition, while HYPEROVERLAP satisfactorily created models to compare *Wollemia* with each other genus, HYPERVOLUME could not produce a hypervolume for this taxon because, with only two unique points in ecospace, it was not possible to build a model in three dimensions. Although *Wollemia* cannot be included in comparisons of stability or computation times between HYPERVOLUME and HYPEROVERLAP, it should be noted that the small number of points for this entity is not an artefact of sampling effort. These data represent the entire range of this genus at this spatial resolution.

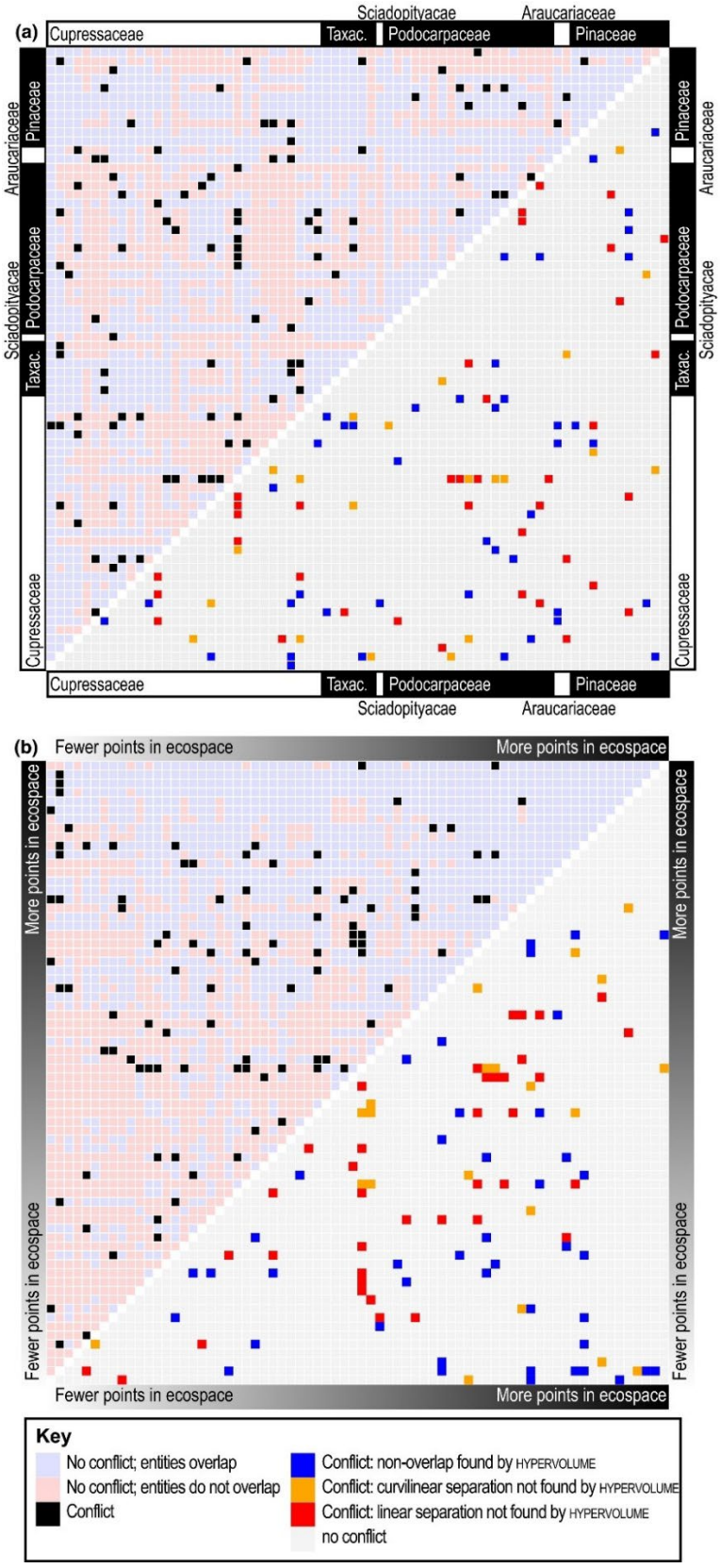

Figure 2.4 Conflicting results between hyperoverlap and hypervolume, with entities ordered phylogenetically (a) and by number of unique points in hyperspace (b)

Computational time & stability

At the default parameters (cost = 1000, kernel = ”polynomial”, kernel.degree = 5, stoppage.threshold = 0.4), the mean total runtime (all pairwise comparisons) for HYPEROVERLAP was 228 minutes (range 212-239 minutes). The results from HYPEROVERLAP were exceptionally stable; the results for identifying overlap versus non-overlap, shape, polynomial order and number of misclassified points were identical in all 10 runs. When the algorithm was constrained to linear decision boundaries, the average runtime was 85 minutes.

At default parameters, computation of HYPERVOLUME results took 16 minutes. However, these results were less stable than those produced by HYPEROVERLAP. Qualitative results (overlap/non-overlap) were inconsistent for 109 pairs of entities (4.5%). Increasing the `samples.per.point` parameter by a factor of 100 reduced this instability to 38 pairs (1.6%) but increased the average runtime to 327 minutes.

Preliminary tests in five-dimensional ecospace (adding mean precipitation of the warmest and wettest quarters) emphasised the computational advantage of HYPEROVERLAP in higher dimensions; the average runtime at default parameters was 147 minutes for HYPEROVERLAP and 855 minutes for HYPERVOLUME.

Case Study 1: *Dacrycarpus* and *Cupressus*

The comparison of *Dacrycarpus* (555 unique points in ecospace) and *Cupressus* (133 points) illustrates the main reason for the observed conflicting results between HYPEROVERLAP and HYPERVOLUME (points in orange and red, Figure 2.3). HYPERVOLUME finds that these entities overlap (Figure 2.5b; overlap shown in green), but HYPEROVERLAP finds that the points of each entity occupy distinct regions of ecospace. This can be verified by visualisation of the decision boundary (Figure 2.5a). The region of overlap found by HYPERVOLUME is the result of small but non-trivial extrapolation by

the model-building algorithm; none of the original observations are within this region of apparent overlap. This extrapolation effect was observed for all entity pairs for which HYPEROVERLAP detected non-overlap, but HYPERVOLUME reported overlap (80% of total conflicts). If our goal is to predict potential overlap, then this extrapolation may be sensible. However, if we are aiming to identify regions of multidimensional space *occupied by both entities*, we suggest that the result given by HYPEROVERLAP is more accurate.

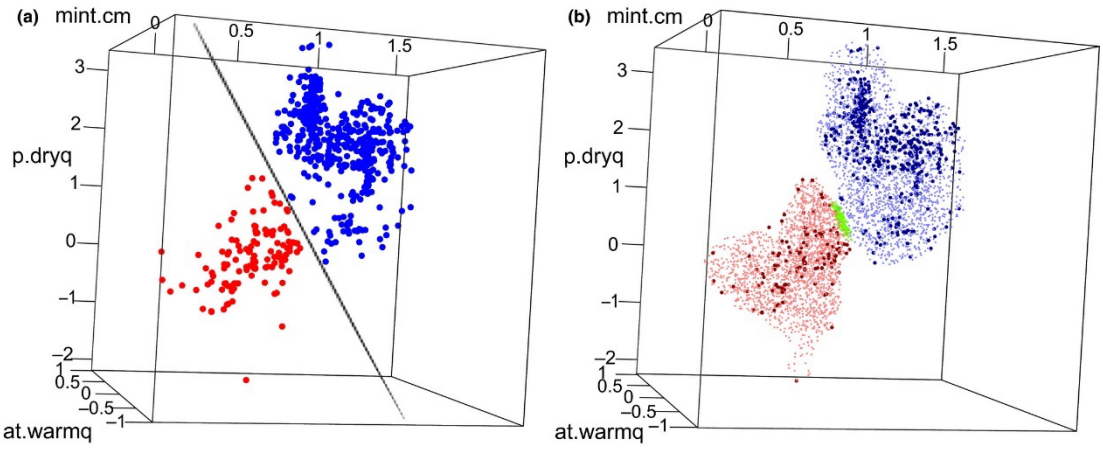

Figure 2.5 The ecological occupation of *Dacrycarpus* (blue) and *Cupressus* (red). These entities can be separated by a single linear hyperplane using hyperoverlap (a), but hypervolume predicts a region of overlap, shown in green (b)

Case study 2: *Metasequoia*

Metasequoia (representing the single species, *M. glyptostroboides*) is a narrowly endemic genus of conifers with only three unique points in ecospace at our sampling resolution. Its native range is limited to a small region of Hubei Province, China, although fossils indicate that it was previously widespread (LePage *et al.*, 2005). This entity proved the most problematic for HYPERVOLUME; for over 20% of pairs involving *Metasequoia* (15 pairs) the results for HYPEROVERLAP and HYPERVOLUME were in conflict. Although the conflicting result for *Metasequoia* and *Cathaya* is a case of false

separation like those discussed in *Case Study 1,* all the other conflicts represent cases in which HYPERVOLUME finds a false separation between *Metasequoia* and the other entity. In these latter cases, HYPEROVERLAP identified overlap, and visualisation shows that the region occupied by *Metasequoia* is deeply nested within the hypervolume occupied by the other entity (Figure 2.6). It is not clear what is driving this anomalous result from HYPERVOLUME, but large differences in sample size may contribute.

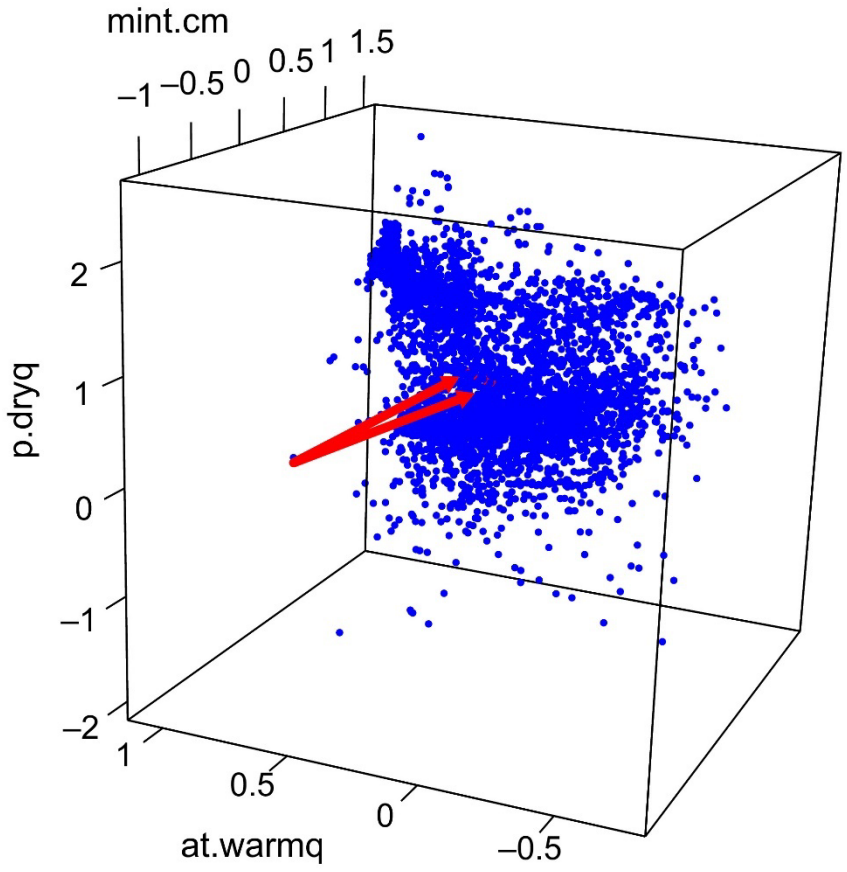

Figure 2.6 The ecological occupation of *Metasequoia* and *Taxus*. The occurrences of *Metasequoia* (position indicated by arrows) are nested within the region occupied by *Taxus*, but the models produced by hypervolume do not intersect, despite obvious visual overlap.

Caveats and limitations

The first obvious limitation of the hyperoverlap framework is that while it effectively *detects* overlap or non-overlap, it does not *measure the amount* of overlap. The overlapping region may be studied by visualisation or inspection of misclassified points, but to measure its volume or calculate a similarity index between the two entities would require the edges of each entity to be defined. This would then invoke the assumptions and challenges associated with single-entity models that this framework was designed to circumvent. However, the shared hypervolume may be modelled based on misclassified points using existing methods.

There are certain theoretical situations where entities do not overlap but cannot be separated using the HYPEROVERLAP algorithm (see Fig. 7 for examples). Although some of these situations may be biologically plausible, we did not find evidence of any in this study. However, such cases may be identified by using the visualisation functions in the HYPEROVERLAP package.

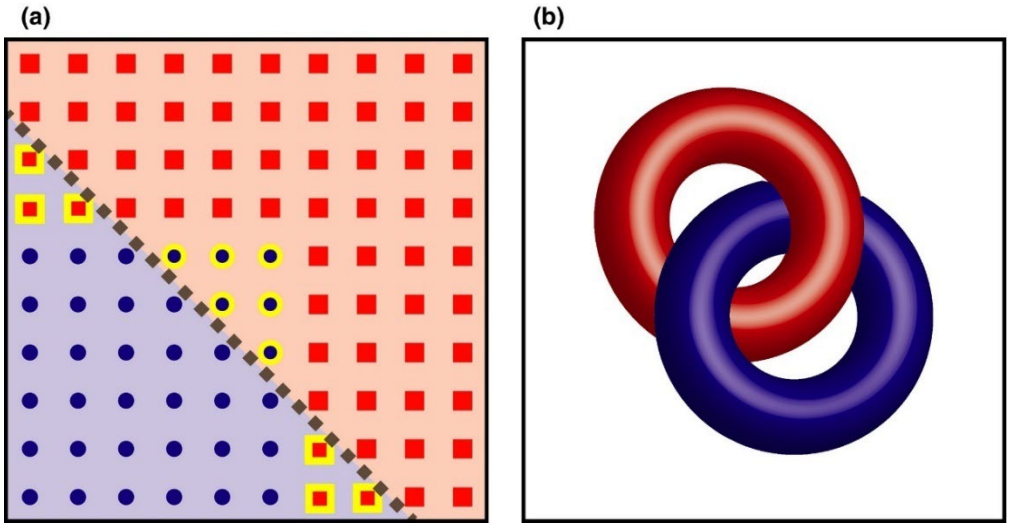

Figure 2.7 Two possible relationships between two entities for which HYPEROVERLAP would be expected to falsely detect overlap. The pattern shown in (a) could be caused by a combination of biological thresholds (e.g. enzyme thermal tolerances) and competitive exclusion. In (b), biological, geographic or other factors could cause the hypervolume geometry to be holey or otherwise very complex. In both cases, the HYPEROVERLAP decision boundary (shown by dotted line in (a)) cannot separate the two entities when constrained to a polynomial kernel. However, these scenarios can be resolved using visualization.

HYPEROVERLAP is also subject to many caveats that apply to the use of hypervolume concepts. Incomplete records cannot be placed in hyperspace so must be excluded or otherwise augmented (see Blonder 2014). Although SVMs handle high dimensionality well, care should be taken when comparing entities that are both highly restricted in multidimensional space. The extreme case is that if the total number of unique points for a pair of entities is lower than $n+1$, where n is the number of dimensions, the two entities can always be separated perfectly with a linear hyperplane. Curvilinear separation is not recommended for small total sample sizes.

It should also be noted that observations represent points in time as well as space; the occupation of morphological or ecological space by an entity is dynamic and is likely to change through time – the fossil record of conifers shows evidence of major changes in ecological occupation during the Cenozoic (Macphail, 2007). A significant caveat is that hyperoverlap does not directly identify overlap between pairs of hypervolumes, instead it identifies overlap between observations sampled from those hypervolumes. Thus, there will be a false identification of non-overlap if there are no observations from the true region of intersection. Other methods deal with this issue mainly by padding each point, in effect extrapolating the range of each entity. However, this solution is problematic, as discussed above (*Case Study 1*). In any case, no approach can fully overcome poor sampling. In particular, care should be taken when using databased occurrence records, which are likely to include some erroneous observations. Visualisation of results and expert knowledge of the entities concerned are both vital to using HYPEROVERLAP and to identify errors such as those illustrated in Fig. 2.7.

Extensions to HYPEROVERLAP

Here, we have focused on overlap versus non-overlap, rather than exploring the question of nested hypervolumes, but this type of relationship can also be explored using the hyperoverlap framework. This has several possible applications in studying recent changes in hypervolumes, including phenological shifts and detection of ecological range expansion in invasive

species. Although this conceptual extension has not been tested, it is a promising avenue for further research and potential inclusion in future versions of the HYPEROVERLAP R package.

Conclusions

The hyperoverlap framework presented here has potential applications in many disciplines – although the concepts underpinning this method have been used widely within ecology, they are not specific to this field. HYPEROVERLAP can be used to investigate ecological and evolutionary partitioning, palaeoclimatic conditions, taxonomy and historical changes in ecology or morphology.

For many biological questions, it is not necessary to model the underlying hypervolume to evaluate overlap. By comparing the space occupied by entities without explicitly describing the geometry of the underlying hypervolumes, fewer assumptions are required to be met and results can be more accurate and reliable than existing methods, as demonstrated clearly for our real-world example (conifers). The approach is particularly effective when the set of entities to be compared is very large and includes entities with a small number of occurrences relative to the dimensionality of the analysis (e.g. species with highly restricted distributions), or when there are potential complex interactions between variables. The HYPEROVERLAP R package provides a user-friendly, intuitive machine-learning method to detect overlap in *n*-dimensional space, and is an additional tool to use in analyses of many biological datasets.

References

Beck, J., Böller, M., Erhardt, A. & Schwanghart, W. (2014) Spatial bias in the GBIF database and its effect on modeling species' geographic distributions. *Ecological Informatics*, **19**, 10-15. doi: 10.1016/j.ecoinf.2013.11.002

Blonder, B. (2016) Do hypervolumes have holes? *The American Naturalist*, **187**, E93-E105. doi: 10.1086/685444

Blonder, B. (2018) Hypervolume concepts in niche-and trait-based ecology. *Ecography*, **41**, 1441-1455. doi: 10.1111/ecog.03187

Blonder, B., Lamanna, C., Violle, C. & Enquist, B.J. (2014) The *n*-dimensional hypervolume. *Global Ecology and Biogeography*, **23**, 595-609. doi: 10.1111/geb.12146

Blonder, B., Morrow, C.B., Maitner, B., Harris, D.J., Lamanna, C., Violle, C., Enquist, B.J. & Kerkhoff, A.J. (2018) New approaches for delineating n-dimensional hypervolumes. *Methods in Ecology and Evolution*, **9**, 305– 319. doi: 10.1111/2041-210x.12865

Boakes, E.H., McGowan, P.J., Fuller, R.A., Chang-qing, D., Clark, N.E., O'Connor, K. & Mace, G.M. (2010) Distorted views of biodiversity: spatial and temporal bias in species occurrence data. *PLoS Biology*, **8**, e1000385. doi: 10.1371/journal.pbio.1000385

Brodribb, T. & Hill, R. (1999) The importance of xylem constraints in the distribution of conifer species. *New Phytologist*, **143**, 365-372. doi: 10.1046/j.1469-8137.1999.00446.x

Broennimann, O., Fitzpatrick, M.C., Pearman, P.B., Petitpierre, B., Pellissier, L., Yoccoz, N.G., Thuiller, W., Fortin, M.J., Randin, C., Zimmermann, N.E., Graham, C.H. & Guisan, A. (2012) Measuring ecological niche overlap from occurrence and spatial environmental data. *Global Ecology and Biogeography*, **21**, 481-497. doi: 10.1111/j.1466-8238.2011.00698.x

Díaz, S., Kattge, J., Cornelissen, J.H., Wright, I.J., Lavorel, S., Dray, S., Reu, B., Kleyer, M., Wirth, C. & Prentice, I.C. (2016) The global spectrum of plant form and function. *Nature*, **529**, 167. doi: 10.1038/nature16489

Donoghue, M.J. & Edwards, E.J. (2014) Biome shifts and niche evolution in plants. In: *Annual Review of Ecology, Evolution, and Systematics*, pp. 547-572. doi: 10.1146/annurev-ecolsys-120213-091905

Escobar, L.E., Qiao, H., Cabello, J. & Peterson, A.T. (2018) Ecological niche modeling re-examined: A case study with the Darwin's fox. *Ecology and Evolution*, **8**, 4757-4770. doi: 10.1002/ece3.4014

Farjon, A. & Filer, D. (2013) *An atlas of the world's conifers: an analysis of their distribution, biogeography, diversity and conservation status*. Brill, Leiden. doi: 10.1163/9789004211810

Fick, S.E. & Hijmans, R.J. (2017) WorldClim 2: new 1-km spatial resolution climate surfaces for global land areas. *International Journal of Climatology*, **37**, 4302-4315. doi: 10.1002/joc.5086

Guisan, A., Petitpierre, B., Broennimann, O., Daehler, C. & Kueffer, C. (2014) Unifying niche shift studies: insights from biological invasions. *Trends Ecol Evol*, **29**, 260-9. doi: 10.1016/j.tree.2014.02.009

Habel, K., Grasman, R., Gramacy, R.B., Stahel, A. & Sterratt, D.C. (2015). Package 'geometry'. Available online at: http://cran.r-project.org/web/packages/geometry/index.html

Kattge, J, Bönisch, G, Díaz, S, et al. (2020) TRY plant trait database – enhanced coverage and open access. *Glob Change Biol*, **26**, 119-188. doi: 10.1111/gcb.14904

Hijmans, R.J, Phillips, S., Leathwick, J. and Elith, J. (2011), Package 'dismo'. Available online at: http://cran.r-project.org/web/packages/dismo/index.html.

Holt, R.D. (2009) Bringing the Hutchinsonian niche into the 21st century: Ecological and evolutionary perspectives. *Proceedings of the National Academy of Sciences of the United States of America*, **106**, 19659-65. doi: 10.1073/pnas.0905137106

Jarnevich, C.S., Stohlgren, T.J., Kumar, S., Morisette, J.T. & Holcombe, T.R. (2015) Caveats for correlative species distribution modeling. *Ecological Informatics*, **29**, 6-15. doi: 10.1016/j.ecoinf.2015.06.007

Junker, R. R., Kuppler, J., Bathke, A. C., Schreyer, M. L., & Trutschnig, W. (2016). Dynamic range boxes–a robust nonparametric approach to

quantify size and overlap of n-dimensional hypervolumes. *Methods in Ecology and Evolution*, **7**(12), 1503-1513. doi: 10.1111/2041-210x.12611

Larcombe, M.J., Jordan, G.J., Bryant, D. & Higgins, S.I. (2018) The dimensionality of niche space allows bounded and unbounded processes to jointly influence diversification. *Nature Communications*, **9**, 4258. doi: 10.1038/s41467-018-06732-x

LePage, B.A., Yang, H. & Matsumoto, M. (2005) The evolution and biogeographic history of Metasequoia. *The geobiology and ecology of Metasequoia*, pp. 3-114. Springer, Dordrecht. doi: 10.1007/1-4020-2764-8_1

Leslie, A. B., Beaulieu, J. M., Rai, H. S., Crane, P. R., Donoghue, M. J., & Mathews, S. (2012). Hemisphere-scale differences in conifer evolutionary dynamics. *Proceedings of the National Academy of Sciences*, **109**(40), 16217-16221. doi: 10.1073/pnas.1213621109

Mackey, B.G. (1994) Predicting the potential distribution of rain-forest structural characteristics. *Journal of Vegetation Science*, **5**, 43-54. doi: 10.2307/3235636

Macphail, M. (2007) *Australian palaeoclimates: Cretaceous to Tertiary a review of palaeobotanical and related evidence to the year 2000*. CRC LEME, Bentley.

Meyer, D., Dimitriadou, E., Hornik, K., Weingessel, A., Leisch, F., Chang, C.-C., Lin, C.-C. & Meyer, M.D. (2018) Package 'e1071'. Available online at: https://cran.r-project.org/web/packages/e1071/index.html

Mosbrugger, V. & Utescher, T. (1997) The coexistence approach—a method for quantitative reconstructions of Tertiary terrestrial palaeoclimate data using plant fossils. *Palaeogeography, Palaeoclimatology, Palaeoecology*, **134**, 61-86. doi: 10.1016/s0031-0182(96)00154-x

Ovaskainen, O., Roy, D.B., Fox, R. & Anderson, B.J. (2016) Uncovering hidden spatial structure in species communities with spatially explicit joint species distribution models. *Methods in Ecology and Evolution*, **7**, 428-436. doi: 10.1111/2041-210x.12502

Peterson, M.L., Rice, K.J. & Sexton, J.P. (2013) Niche partitioning between close relatives suggests trade-offs between adaptation to local environments and competition. *Ecol Evol*, **3**, 512-22. doi: 10.1002/ece3.462

Phillips, S.J., Anderson, R.P. & Schapire, R.E. (2006) Maximum entropy modeling of species geographic distributions. *Ecological Modelling*, **190**, 231-259. doi: 10.1016/j.ecolmodel.2005.03.026

Pollock, L.J., Tingley, R., Morris, W.K., Golding, N., O'Hara, R.B., Parris, K.M., Vesk, P.A. & McCarthy, M.A. (2014) Understanding co-occurrence by modelling species simultaneously with a Joint Species Distribution Model (JSDM). *Methods in Ecology and Evolution*, **5**, 397-406. doi: 10.1111/2041-210x.12180

Prentice, I.C., Cramer, W., Harrison, S.P., Leemans, R., Monserud, R.A. & Solomon, A.M. (1992) A Global Biome Model Based on Plant Physiology and Dominance, Soil Properties and Climate. *Journal of Biogeography*, **19**, 117-134. doi: 10.2307/2845499

Qiao, H., Soberón, J. & Peterson, A.T. (2015) No silver bullets in correlative ecological niche modelling: insights from testing among many potential algorithms for niche estimation. *Methods in Ecology and Evolution*, **6**, 1126-1136. doi: 10.1111/2041-210x.12397

Qiao, H., Peterson, A.T., Campbell, L.P., Soberón, J., Ji, L. & Escobar, L.E. (2016) NicheA: creating virtual species and ecological niches in multivariate environmental scenarios. *Ecography*, **39**, 805-813. doi: 10.1111/ecog.01961

R Core Team. (2018). R: A language and environment for statistical computing. Vienna, Austria: R Foundation for Statistical Computing.

Rissler, L.J. & Apodaca, J.J. (2007) Adding more ecology into species delimitation: ecological niche models and phylogeography help define cryptic species in the black salamander (Aneides flavipunctatus). *Systematic Biology*, **56**, 924-942. doi: 10.1080/10635150701703063

Sakai, A. and Larcher, W. (1987) *Frost Survival of Plants. Responses and Adaptation to Freezing Stress*, Springer-Verlag, New York.

Scholkopf, B. & Smola, A.J. (2002) Kernels. *Learning with kernels: support vector machines, regularization, optimization, and beyond*. MIT press. doi: 10.7551/mitpress/4175.003.0005

Schreyer, M., Trutschnig, W., Junker, R.R, Kuppler, J., Bathke, A., Parkinson, J.H. & Kutil, R. (2018). Package 'dynRB'. Available online at: https://cran.r-project.org/web/packages/dynRB/index.html

Sidlauskas, B. (2008) Continuous and arrested morphological diversification in sister clades of characiform fishes: a phylomorphospace approach. *Evolution: International Journal of Organic Evolution*, **62**, 3135-3156. doi: 10.1111/j.1558-5646.2008.00519.x

Soberon, J. & Peterson, A.T. (2005) Interpretation of models of fundamental ecological niches and species' distributional areas. *Biodiversity Informatics,* **2**, 1–10. doi: 10.17161/bi.v2i0.4

Stolar, J. & Nielsen, S.E. (2015) Accounting for spatially biased sampling effort in presence-only species distribution modelling. *Diversity and Distributions*, **21**, 595-608. doi: 10.1111/ddi.12279

Chapter 3 : No-analogue pairs in the fossil record of southern conifers reveal conservatism in precipitation, but not temperature axes

This chapter has been published in Global Ecology and Biogeography.

Brown, M.J.M., Holland, B.R., Jordan, G.J. (2021). No-analogue pairs in the fossil record of southern conifers reveal conservatism in precipitation, but not temperature axes. *Global Ecology and Biogeography* (in press).

Introduction

No-analogue assemblages – fossil assemblages in which the nearest living relatives of some taxa occupy dissimilar climates to the nearest living relatives of other taxa from the same palaeocommunity – challenge the assumption that fossil species inhabited similar climatic conditions to their modern relatives. Such assemblages (also termed nonanalogue communities, disharmonious assemblages, mixed floras, intermingled, mosaic, anomalous assemblages and extraprovincial biotas) have been identified in the fossil records of vascular plants (Jordan, 1997; Macphail, 2007; Williams & Jackson, 2007), marine and terrestrial invertebrates (Coope, 2000; Preece & Bridgland, 2012), birds (Brasso & Emslie, 2006), mammals (Graham *et al.*, 1996). Although palaeoclimatic estimations often allow for such assemblages by excluding certain fossil taxa from analyses (Mosbrugger & Utescher, 1997), no-analogue assemblages can provide valuable insights into past changes in the climatic ranges of taxa. Previous studies of no-analogue assemblages have examined relatively recent fossil biota, with a focus on rapid community changes (e.g. in response to Pleistocene glaciation; Jackson & Williams 2004). To the best of the authors'

knowledge, no ‘true’ no-analogue (i.e., not due to transport or other taphonomic mixing) assemblages from earlier than the Pleistocene have been quantitatively analysed. However, if the fossils can be attributed to living groups or species, it is possible to study no-analogue associations from much further back in time.

One approach to understanding no-analogue assemblages is to partition them into pairs of co-occurring fossils. We can then identify no-analogue pairs as those pairs of fossil taxa for which their extant counterparts have non-overlapping bioclimatic envelopes. We can assemble these pairwise data to compare fossil assemblages in detail and consider trends in time and space. The results can then be interpreted based on an understanding of how no-analogue pairs form.

Some no-analogue pairs may arise through misidentification of fossils, transport of the fossils from areas with different climates or inaccurate modelling of the bioclimatic envelopes of the fossils’ extant relatives (see Jordan, 1997; Stewart, 2009 for discussion). However, the most likely explanation for many no-analogue pairs is that the bioclimatic envelope occupied by the fossilised taxon was not the same as that occupied by its nearest living relatives.

For two co-occurring fossil taxa to become a no-analogue pair, there must be a loss of part of the bioclimatic envelope of one or both members of the pair. This restriction can occur via several mechanisms (Figure 3.1). There could be environmental change leading to loss of available bioclimatic space (Figure 3.1b-c); this represents a change in the existing niche *sensu* Peterson et al. (2011). The bioclimatic envelope can also be restricted by non-climatic variables (e.g. biotic or anthropogenic factors; Figure 3.1e), these would typically involve changes in the realised niche (*sensu* Peterson et al. 2011), or extinction of ecotypes (including ecologically distinct taxa, Figure 3.1f); this can represent a change in the fundamental or scenopoetic niche (*sensu* Peterson et al., 2011). Adaptive evolution can create no-analogue pairs (Figure 3.1g), but only if it involves a simultaneous loss of part

of the bioclimatic envelope (e.g. if the evolution involves an adaptive trade-off). One important consideration is that the current bioclimatic envelope may be affected by earlier range restrictions (Figure 3.1d) –habitat suitable for both taxa may be currently available, but either or both taxa may be in climatic disequilibrium (Svenning & Skov, 2007), potentially obscuring the cause of no-analogue pairs. Importantly, these scenarios are not mutually exclusive, which can make it even more difficult to identify the mechanism causing a no-analogue pair to arise.

The 'southern conifers' – Podocarpaceae, Araucariaceae, Callitroideae (Cupressaceae), *Athrotaxis* (Cupressaceae), and *Austrotaxus* (Taxaceae) – provide a good group for the study of no-analogue associations. This mostly southern hemisphere group has, with the exception of *Austrotaxus,* an exceptional Cenozoic fossil record (Hill & Brodribb, 1999). In a spectacular display of morphological stasis for 30 million years, the Eocene species *Pherosphaera microfolia* is almost indistinguishable from the extant *P. hookeriana* (Wells & Hill, 1989). There is significant evidence that conifer distributions are physiologically constrained by climatic factors (Enright & Hill, 1995; Brodribb & Hill, 1999; Brodribb *et al.,* 2014) and it is widely assumed that conifers show high levels of evolutionary niche conservatism, as has been demonstrated for southern hemisphere plants (Crisp et al., 2009). This assumption underpins the widespread use of taxonomic information in palaeoclimatic estimations (Jordan 2011). However, variation among closely related species in both climatic range and in physiology (*see* Larter *et al.,* 2017) shows that many taxa have changed their bioclimatic ranges. Furthermore, the presence of no-analogue assemblages in the fossil record as recently as the Pleistocene is clear evidence that some of these changes are both large, and relatively recent (Jordan 1997).

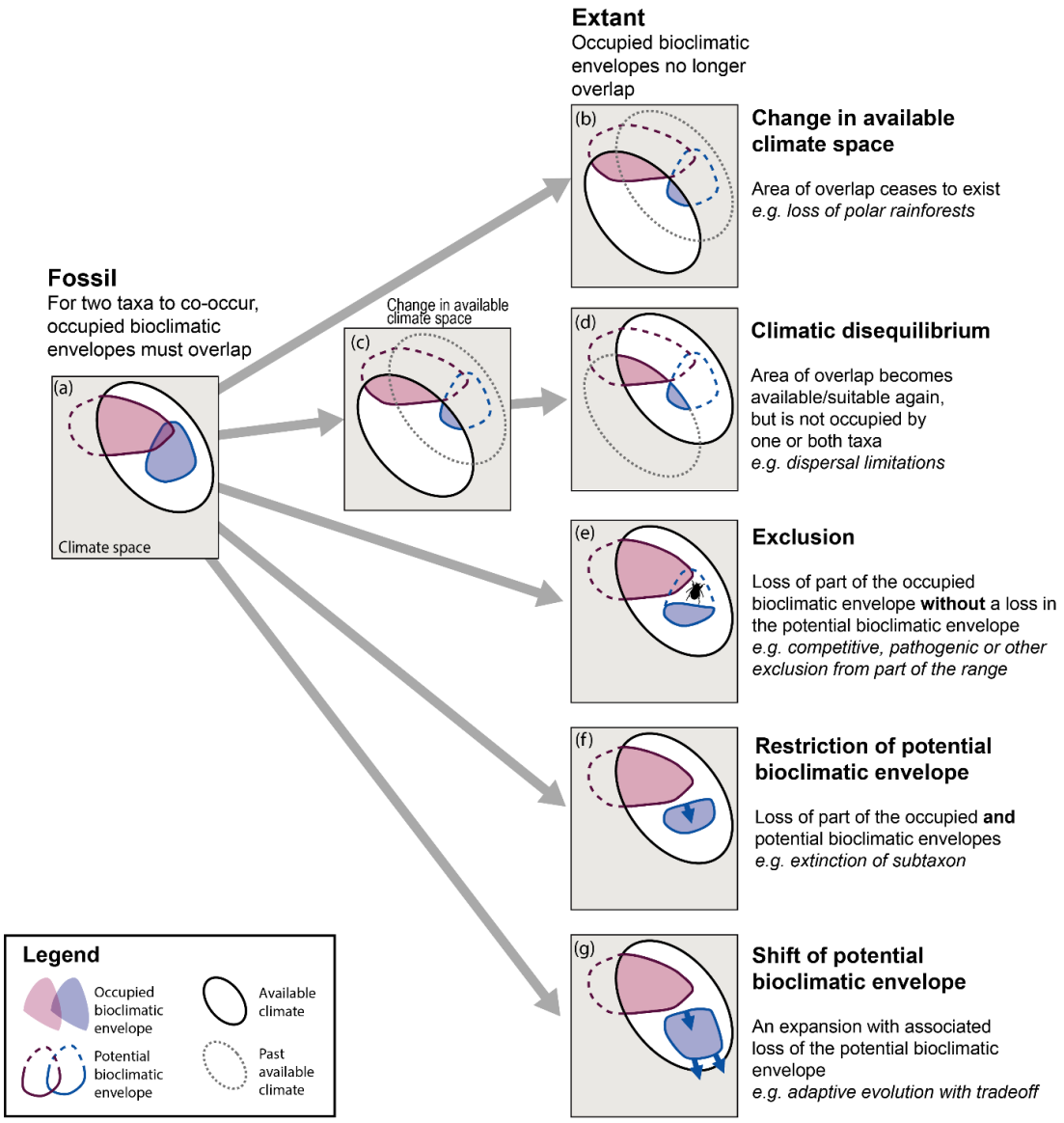

Figure 3.1 No-analogue pair formation via changes in bioclimatic envelope. The bioclimatic envelopes of two taxa (red, blue) are depicted here in two-dimensional climate space. The occupied bioclimatic envelope of a taxon (shaded red and blue) is limited by the set of climatic conditions that are favourable for that taxon (the potential bioclimatic envelope; red and blue outlines), as well as the availability of climate space (black outline). If two taxa co-occurred in the past, there must have been overlap between their occupied bioclimatic envelopes (a). If they no longer overlap, there must have been a change in either one or both of these bioclimatic envelopes. This could take place via changes in the available environment (b) that may also have a legacy effect leading to climatic disequilibrium (c, d), loss of the bioclimatic envelope via other biotic or abiotic factors (e, f), or even adaptive evolution (g), as long as there is a concomitant loss of part of the bioclimatic range. These processes are not mutually exclusive, and although we have only illustrated climatic disequilibrium with regard to climatic availability, other processes shown here can also have similar legacy effects.

Here, we use a recently developed method, HYPEROVERLAP (Brown et al., 2020) to identify no-analogue pairs in the southern conifer fossil record, then consider the roles of temperature and precipitation in the incidence of these associations. We examined: (1) whether no-analogue associations are associated with a particular time period; (2) the relative importance of temperature and precipitation in these shifts by identifying no-analogue pairs that can be explained by changes in either temperature or precipitation requirements allowing us to estimate the specific climatic drivers of Cenozoic conifer extinctions. Given the well-documented importance of drought tolerance for southern conifer distributions (Brodribb *et al*., 2014; Larter *et al*., 2017), we hypothesized that the fossil record will reflect greater conservatism in precipitation dimensions than in thermal dimensions – i.e., we expect that most of the implied changes in bioclimatic envelopes between fossil and extant conifers will be in thermal dimensions, rather than those related to rainfall.

Methods

Fossil assemblages and taxa

We used species lists from 43 Cenozoic fossil sites from the southern hemisphere in which at least three coniferous taxa reliably attributed to extant genera have been identified (Figure 3.2). For each site, we assembled complete lists of seed plant fossils from these sites from the literature (see Supporting Information Table S3.1). The nearest living relative of each identified fossil was defined as the smallest extant clade to which the fossil can be attributed (for stem lineages, the nearest living relative was assigned as the nearest crown group). For some fossils, this was a single species (e.g. *Microcachrys tetragona*), for others it was necessary to use a genus or family as the nearest living relative (e.g. the extinct genus *Willungia* could only be attributed to Podocarpaceae; Hill & Pole, 1992). Where there was uncertainty in the extant affinity, we took a conservative approach (with the fossil taxon either being excluded or attributed to a higher taxonomic level, see Table S3.1). We included only fossils that were likely to have been derived from

plants close to the fossil site: macrofossils, highly abundant wind-dispersed pollen, and moderately abundant animal-dispersed pollen. Fossils were excluded if the authors indicated that were likely to have been reworked (deposited, unearthed and redeposited in younger sediments).

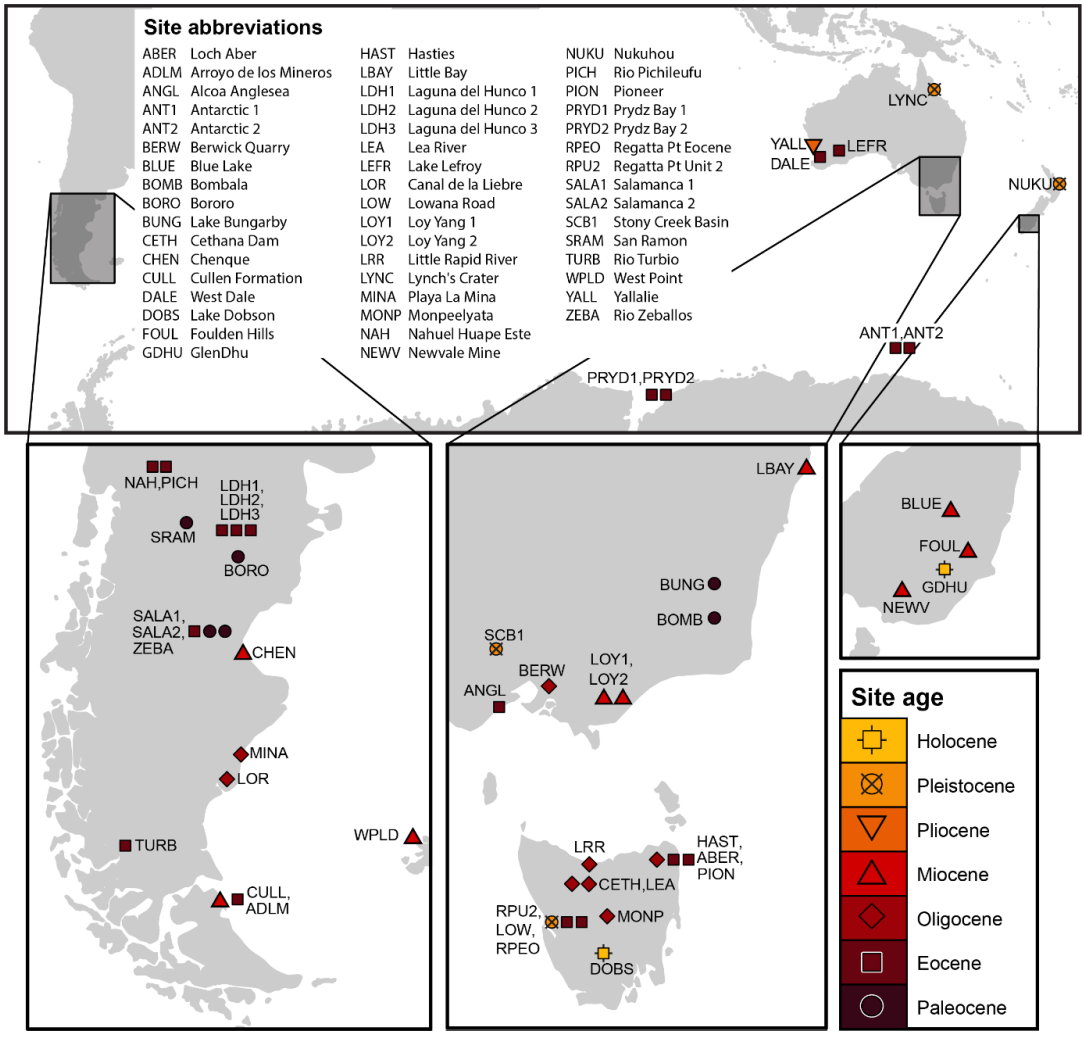

Figure 3.2 Sites analysed in this study. Site details, including specific layers/core depths and sources, are available in Supplementary Information (Table S3.1).

Climatic occurrence records

For each nearest living relative, we collated occurrence records for that taxon from the dataset used in in Larcombe et al. (2018) and Brown et al. (2020). These data represent individual species records and have been manually cleaned thoroughly to exclude cultivated, naturalised and duplicate records, as well as including latitudes and longitudes for sites supported by precise location descriptions as determined from Google Earth (see Larcombe et al., 2018 for details). Cleaning involved careful assessment of all observations near the periphery of the apparent climatic range of each taxon. Potential outlier locations were also visually assessed using Google Earth to ensure that the habitat at that site was consistent with the known habitat for the species. Unverified climatic outliers (e.g. where the coordinates listed on a vouchered specimen were not supported by a location description) were excluded. Occurrences that were deleted during this process were carefully compared to documented distributions of species (from Farjon & Filer, 2013) to avoid eliminating true records.

For each occurrence of each nearest living relative, we extracted five contemporary environmental variables that are linked to physiological stresses in plants (Table 3.1) from WorldClim V2 (Fick & Hijmans, 2017) at a resolution of 30 seconds (approximately 1km^2). Precipitation variables were fourth-root transformed to an approximately normal distribution to account for the non-linear physiological responses to precipitation (as per Blackman et al., 2012). The environmental variables (both temperature and transformed-precipitation) were then normalised to the global means and standard deviations to ensure that axes were comparable (as per Blonder, 2018).

Sampling effort for different taxa was reasonably even relative to area of extent of each taxon. Occurrence records for each taxon were downsampled to exclude duplicate points in climate space (approximately equivalent to a 30” grid in geographic space). The number of unique climatic records varied markedly from 23 (*Fitzroya*) to 10778 (Cupressaceae) points per taxon. These differences are largely explained by differences in geographic extent

of the taxa, although some differences appear to be explained by high original sampling densities in some regions (e.g. Australia and New Zealand, compared to New Guinea, south-east Asia and South America).

Table 3.1 Climatic variables used in analyses of the nearest living relatives of fossils

Abbreviation	Variable	Biological importance
mint.cm	Mean minimum temperature of the coldest month	Freezing tolerance (Sakai & Larcher, 2012)
at.warmq	Mean temperature of the warmest quarter	Growing season heat availability (Prentice *et al.*, 1992)
p.drym	Mean precipitation of the driest month	Drought tolerance (Mackey, 1994)
p.warmq	Mean precipitation of the warmest quarter	Growing season water availability; thermal-seasonal sites (Prober *et al.*, 2012)
p.wetq	Mean precipitation of the wettest quarter	Growing season water availability; rainfall-seasonal sites (Prober *et al.*, 2012)

No-analogue pair detection

No-analogue pairs were identified using the *HYPEROVERLAP* package (Brown *et al.*, 2020) in *R* (R Core Team, 2014), using default parameters. This method uses a machine learning classifier to attempt to find a dividing line (or plane/hyperplane in three or more dimensions) which separates two groups of points. Here, we have constrained the shape of the boundary to a third-order polynomial kernel as recommended by Brown et al. (2020); see this work for a discussion of kernel choice and boundary shape. Because this method does not create a model of the environmental distribution of each taxon, it is relatively insensitive to sampling effort and sample size. It is sensitive to sampling near the periphery of the bioclimatic envelope of the taxa, but the distribution data used here were sampled to minimise errors from such sampling effects. Overall, this approach has been shown to be more accurate than niche-modelling methods for detecting bioclimatic

overlap (and therefore identifying no-analogue pairs), particularly for conifers, which are climatically and geographically well-sampled and have unequally sized geographic distributions (see Brown et al., 2020).

Climatic factors relating to no-analogue pairs

We performed detection of no-analogue pairs in the five-dimensional climate space defined by the variables in Table 3.1. No-analogue pairs were then re-analysed under two additional scenarios.

Scenario 1: Removal of thermal dimensions (including rainfall seasonality, which is inherently linked to temperature). If the pair is still a no-analogue pair in the remaining precipitation dimensions (p.drym and p.wetq), at least one of the fossil entities in the pair occupied a different precipitation niche to its extant counterpart.

Scenario 2: Removal of precipitation dimensions. If the pair is still a no-analogue pair in the remaining thermal dimensions (mint.cm, at.warmq), at least one of the fossil entities in the pair occupied a different thermal niche to its extant counterpart.

Each no-analogue pair was then categorised as one of four types, depending on its persistence under these two scenarios (Figure 3.3). We can view each of these scenarios through the lens of ecological conservatism; if the thermal niche is highly conserved we would expect to see changes in the occupied precipitation niche (type ‘P’), and vice versa.

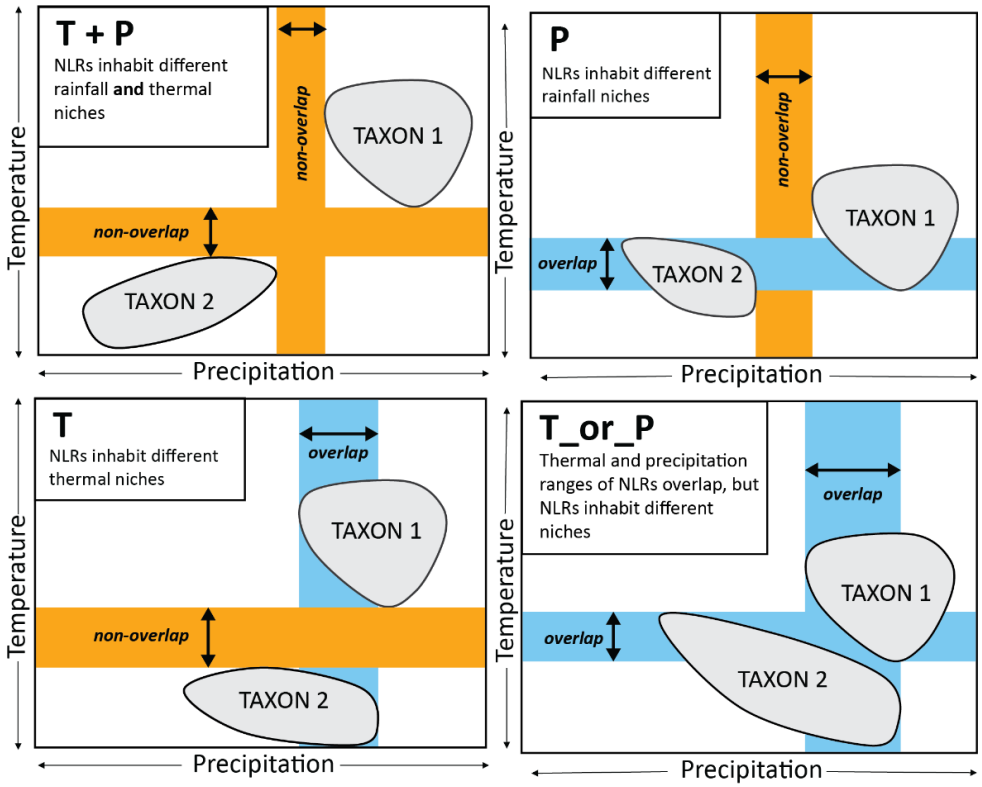

Figure 3.3 The four types of no-analogue pairs depending on whether or not the no-analogue nature of the pair persisted when certain subsets of environmental dimensions were analysed. The text in each box describes the inferences we can draw from each type of no-analogue association in terms of the difference in bioclimatic envelope between the fossil taxon and its nearest living relative (NLR). In this conceptual figure, temperature and precipitation are each represented in one dimension, but in our analyses we used two temperature dimensions (mint.cm, at.warmq) and two precipitation dimensions (p.drym, p.wetq).

Temporal analyses

To account for differences in assemblage diversity and non-independence of pairs we calculated no-analogue scores for each site as the square root of the proportion of no-analogue pairs relative to the total number of pairs (including the pairs of entities with themselves). The square root converts the score to be independent of sample size (i.e. number of species per sample) because the number of pairs increases as the square of the number of species. Generalised additive models (GAMs) were fitted to the median age for each assemblage and the no-analogue score using the *gam* function in the *mgcv* package (Wood, 2011). Because extant communities are assemblages without no-analogue pairs, we added a number of modern

pseudo-assemblages (points of age 0 and no-analogue score of 0) to the GAM-fitting dataset for each region for which we fitted GAMs (Australia, New Zealand, South America). We performed this analysis several times, using different numbers of points to anchor the GAM. We also fitted GAMS that were either unweighted or weighted by the total number of pairs in each assemblage (to reduce the leverage of depauperate assemblages). To account for uncertainty in fossil ages, we fitted 9999 GAMs with a uniformly randomly sampled age from the age range of the assemblages. To test for major changes in slope in the GAM we also fitted a segmented regression using the 'segmented' package (Muggeo, 2008) to obtain approximate p-values for the approximately linear parts of the GAMs.

Results

We identified 240 no-analogue pairs (pairs of fossils that have nearest living relatives with non-overlapping climatic ranges) from 2407 co-occurring pairs of fossils (Supporting Information Table S3.2). These no-analogue associations were represented by 73 unique no-analogue pairs involving 27 modern conifer taxa (from 41; Supporting Information Figure S3.1).

Fourteen assemblages did not contain any no-analogue pairs (Table S3.2). All these sites are either recent (<1Ma), depauperate (<6 fossil conifer taxa), pollen-only assemblages, or some combination of the above. Four assemblages contained 15 or more no-analogue pairs: Monpeelyata, Pioneer, Little Rapid River and Cethana. These are all Oligocene or Early Miocene Tasmanian assemblages with notably high conifer diversity (12-16 fossil taxa; Fig.S3.2).

The no-analogue score for each assemblage (reflecting the proportion of no-analogue pairs, corrected for assemblage size) increases with assemblage age (Figure 3.4). There was no trend in no-analogue scores from the beginning of the Paleocene (65 million years ago) to the middle Oligocene (~28Ma), but no-analogue scores decreased from that time onwards (Fig 4). This was the case for all GAMs, at all numbers of anchoring points, both weighted and unweighted (Fig S3.3). This was also confirmed by the results

of the segmented regression (Fig S3.4); all regions showed a significant relationship between no-analogue score and age in assemblages from the Late Oligocene onwards (respective p-values of 1.7×10^{-3}, 1.54×10^{-6}, and 2×10^{-16} for each region). Uncertainty in the ages of the fossils had no effect; GAMs fitted to randomly sampled ages were not significantly different to those fitted to the median ages. Australian assemblages tended to contain more no-analogue pairs than South American assemblages (Figure 3.4, S3.2-3.4).

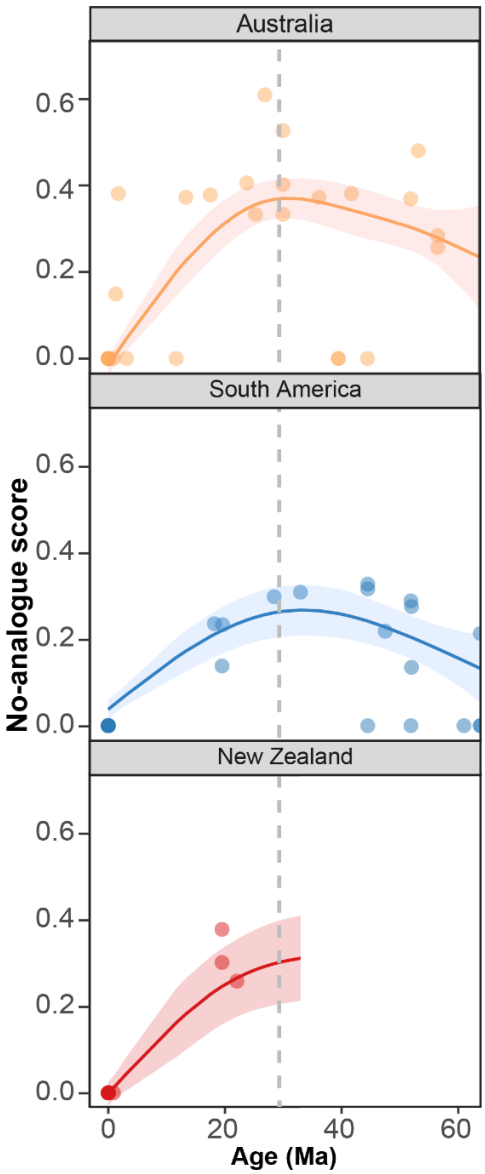

Figure 3.4 Generalised additive models fitted to the no-analogue score and median age of each fossil site, plus or minus standard error (shaded). The grey dotted line is at 28Ma. This is the model fitted using 20 anchor points at 0Ma, with a gamma value of 3 and points weighted by the number of pairs in each assemblage.

Climatic types of no-analogue pairs

Most (75.4%) no-analogue pairs can be explained by a change in temperature *without* a change in precipitation (types 'T', 'T_or_P';**Table 3.2**). Only 40.4% of no-analogue pairs can be explained by a change in precipitation *without* a change in temperature (types 'P', 'T_or_P'; **Table 3.2**). A minority (20.4%) of no-analogue pairs require changes in both temperature and precipitation dimensions (type 'T+P'; Table 3.2). Thus, most no-analogue pairs are associated with a past change in the thermal distribution of one or both taxa in the pair. In 50% of no-analogue assemblages (17 sites; Figure 3.5), changes in thermal distribution could explain all observed no-analogue pairs (i.e. the no-analogue pairs were all of types "T" or "T_or_P") and the proportion of temperature no-analogue pairs was higher than precipitation no-analogue pairs in all sites. No assemblages contained only pairs of type "P" – a change in precipitation was always associated with an accompanying change in temperature. There was no clear temporal or geographic pattern in no-analogue pairs that could be explained by temperature, when expressed as proportion of all no-analogue pairs (**Figure 3.5**).

Table 3.2 No-analogue pair type frequency (see Figure 3.5).

No-analogue pair type	count	percentage
Temperature + precipitation (T+P)	49	20.4%
Temperature (T)	94	39.2%
Precipitation (P)	10	4.2%
Temperature or precipitation (T_or_P)	87	36.2%
Total	240	

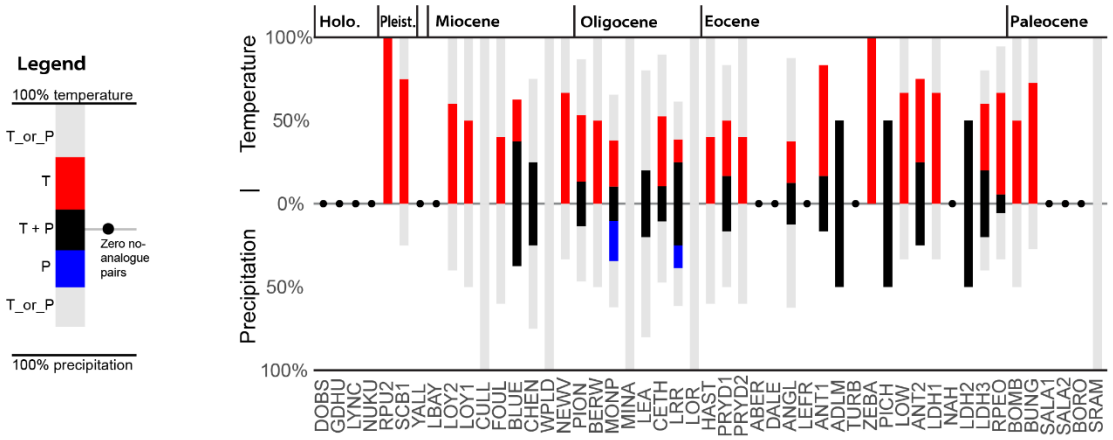

Figure 3.5 Climatic aspects of no-analogue pairs. Each fossil site is represented by a vertical bar or point. Points denote assemblages with no no-analogue pairs. The coloured components of each bar show the proportion of no-analogue pairs of each type (from Fig. 3). Red shows the proportion of thermal no-analogue pairs (T); blue shows the proportion of precipitation no-analogue pairs (P), black shows the proportion of thermal **and** precipitation no-analogue pairs (T+P), and grey shows no-analogue pairs that are ambiguous (T_or_P). If the bar (red or grey) reaches 1, all no-analogue pairs can be explained by a change in temperature (i.e. without invoking a change in precipitation). If the bar (blue or grey) reaches -1, all no-analogue pairs in that assemblage can be explained by change in precipitation (i.e. without invoking a change in temperature).

Discussion

Our results suggest that changes in the bioclimatic envelope of southern conifers have been largely thermal, rather than hydrological, and that this pattern does not vary significantly with assemblage age. This inference assumes that the patterns in no-analogue pairs observed here are due to past changes in bioclimatic envelopes (Figure 3.1). The main alternative causes – errors in reconstructing extant bioclimatic range and taphonomic biases – should apply more-or-less equally to all fossils, and therefore should not have created the systematic change through time observed here (Figure 3.4).

The overwhelming predominance of no-analogue pairs in which the non-overlap is in thermal dimensions (“T” pairs; Figure 3.5) implies that the changes in bioclimatic ranges have mostly been in temperature. We argue that this is the result of much greater long-term stability in the hydro-climatic envelope than the thermal envelope in southern conifers. It is worth noting

that the physiological impacts of temperature and precipitation are interlinked (Jones, 2014) – this may be contributing to the reasonable proportion (20.4%) of no-analogue pairs that are both thermal and hydrological (T+P). We further argue that the temporal correspondence between no-analogue pairs (climatically incongruous pairs of fossils) and broad-scale climatic changes in both temperature and rainfall (Westerhold *et al.* 2021) suggests that the no-analogue associations in southern conifers are linked (either directly or indirectly) to climate change in the last 30 million years. These links may be direct, through the reduction in fundamental niche through loss of warm- or cold-adapted ecotypes or species, consistent severe range contraction and extinction of the relevant taxa through this time. They may also be indirect, through reduction in realised niche via competition with angiosperms (Condamine et al., 2020), including competition mediated by fire (Belcher et al., 2021).

Regional and temporal patterns

Australian assemblages tend to contain more no-analogue pairs than New Zealand and South America, and a high proportion of all the no-analogue pairs are due to cool-climate palaeoendemic genera now restricted to southern Australia (*Microcachrys, Lagarostrobos, Athrotaxis, Diselma, Pherosphaera*; Jordan *et al.,* 2016) co-occurring with now tropical taxa. However, this does not mean that the processes considered here are due to idiosyncrasies of Australia's history. No-analogue associations are common in assemblages outside Australia (Figure 3.4, S2) and include multiple taxa that are centred outside Australia (Fig S1). In particular, taxa now restricted to temperate regions outside Australia (e.g. *Lepidothamnus* from New Zealand and South America, *Austrocedrus* from South America) also co-occur with tropical taxa. Overall, no-analogue associations are not restricted to any one region, habitat or taxon; this argues that the no-analogue pairs in southern conifers are better explained by hemisphere-scale processes than by local idiosyncrasies of history (e.g. local anthropogenic extinctions). It is worth noting that similar co-occurrences in the fossil record of now temperate

and tropical angiosperm taxa are well known from all the southern continents (Hill, 2004).

It is possible that lower taxonomic resolution in identifying the living relatives of older fossils has artefactually suppressed the true numbers of no-analogue pairs in older assemblages. Older fossils are less likely to be attributable to an extant genus or species and thus, no-analogue pairs are less likely to be detected. However, it is clear that no-analogue pairs have decreased in at least the last 20-30Ma (Figure 3.4); there are assemblages with no-analogue pairs in all regions at 20Ma, but none in assemblages younger than 1Ma (Fig. S2). This is consistent with the theory that conifers suffered extinctions during the cooling and drying of the Oligocene and Miocene (Hill 2004; Brodribb & Hill, 2004). The success of the drought-adapted Cupressaceae (e.g. *Callitris*) compared to their mesic relatives (e.g. *Athrotaxis*) also suggests that precipitation has been a dominant selection pressure acting on southern conifers (Pitterman et al., 2012; Larter et al., 2017). This contrasts with the northern conifers, which inhabit environments that extend into much more extreme thermal environments than their southern counterparts. Thus, a comparable study of northern conifer no-analogue fossils may reveal strikingly different climatic patterns to those found in this study, as predicted by Leslie et al., (2012).

Limits on southern conifer distributions

Four climate-related factors provide major limits on the distributions of most southern hemisphere conifer species– aridity and the need for tolerance of water deficit; freezing conditions and the need for freezing tolerance; climatic equability and the capacity to compete in tropical forests associated with warm, wet climates; and finally the frequency and intensity of fire (Brodribb & Hill, 2004; Bannister & Lord, 2006; Pittermann *et al.*, 2012; Brodribb *et al.*, 2014; Kooyman et al., 2014; Eiserhardt *et al.*, 2015). Of these factors, physiological evidence and current distributions suggest that intolerance of dry climates is critical, and our results imply that this has been the case throughout the Cenozoic. Brodribb and Hill (1999; 2002) found that xylem

vulnerability to damage under water deficit and water-use efficiency are closely correlated to dry season rainfall in conifers from across the southern hemisphere (although noting that fire sensitivity and frost tolerance may be important covariates in this relationship; Laughlin *et al.,* 2020). Furthermore, the physiological limitations underpinning this relationship are well-studied and have strong evolutionary bases (Brodribb *et al*., 2014; Larter *et al*., 2017). Although thermal distributional limits appear to be present in some Australian conifers, Bush *et al.,* (2018) found that thermal disequilibrium (i.e., species not inhabiting their full range of thermal tolerances) is common in the Australian flora, suggesting that temperature does not directly limit the distributions of many tree species.

The current distributions of conifers have also been influenced by factors other than current climates, including distributions in ecological disequilibrium due to past events, and these past events may have caused some of the no-analogue pairs. At least some southern conifers are thought to be extremely dispersal-limited (Holz et al. 2015) and may be in a state of climatic disequilibrium, so that they do not fully occupy their potential bioclimatic envelope (or realised niche *sensu* Peterson et al. (2011). Recent work by Sundaram and Leslie (in press) showing that climatic stability affects conifer distributions is in accordance with our findings of conservatism, as taxa that are unable to adapt to climatic changes are most likely to persist in stable, climatically suitable environments.Overall, the effects of past climates on southern conifers may be smaller than observed in northern hemisphere conifers because the southern conifers have not been substantially affected by either severe freezing climates or extensive Pleistocene glaciation – two factors that are considered to have been critical in determining the distribution and composition of northern floras (Leslie et al., 2012). However, other historical processes or events may have contributed to the distribution of southern conifers.

Past and present fires are likely to have affected the bioclimatic envelopes of many southern conifers (Enright & Hill 1995; Farjon & Filer, 2013) and evidence from charcoal in sediments indicates a major increase in fire from

the late Neogene onwards (Herring 1985). However, fire is intimately linked to both temperature and precipitation, as well as the abundance and type of angiosperms (Belcher et al., 2021). Some no-analogue pairs may have been caused by disturbances that are decoupled from climate, but the strong preciptiation signal we observed implies that this is not the case for the majority of no-analogue pairs.

Formation of no-analogue pairs

Most of the no-analogue associations studied here represent changes in the thermal envelope of one or both members of the pair. These changes inevitably involve loss of part of the climatic ranges of one or both of the taxa involved in these associations. Although geographic and climate space are not perfectly correlated (see Peterson et al. 2011), loss of geographic range is strongly linked to loss of climatic range, and the fossil record of southern conifers demonstrates a massive loss of geographic range. For example, two genera in many of the no-analogue associations detected in this study (*Microcachrys* and *Lagarostrobos*; Table S2) were present on all southern hemisphere landmasses during the Cretaceous and Palaeogene, but are now restricted to Tasmania (Hill & Brodribb 1999). Many other southern conifer taxa, including taxa involved in almost all of the no-analogue pairs, have contracted from multiple continents to much more restricted ranges (Hill & Brodribb 1999; Wilf, 2012).

Furthermore, the geographic and climatic range loss in southern conifers involved substantial extinction. Hill and Brodribb (1999) demonstrated very high diversity of southern conifers in the Cenozoic, including many extinct species and some extinct genera. Such estimates of fossil diversity may even be underestimates because species are often represented in the palaeobotanical record by pollen or vegetative fragments, so many fossils can only be referred to extant families or genera, rather than species. Even so, many currently species-poor genera are represented by multiple species in the fossil record – *Microcachrys* has one extant species, endemic to the alpine regions of Tasmania, but there is at least one additional species

described from New Zealand fossils, and there are at least five distinct pollen types which have been linked to the genus (Carpenter et al., 2011). Many authors have concluded that southern conifers suffered high levels of extinction during the Cenozoic (Jordan, 1995; Brodribb & Hill, 2004; Carpenter et al., 2011; Crisp & Cook, 2011), so we find it reasonable to assume that most no-analogue associations in the fossil record are the result of extinctions. However, it is unclear whether these extinctions were driven by aridification, temperature fluctuations, or other factors (e.g. fire, biotic interactions).

However, these changes in bioclimatic envelopes implicit in the no-analogue pairs may well also include adaptation to novel climates. The fact that many of the southern conifers involved in no-analogue pairs now occupy climatic conditions that were absent or much more restricted in the Paleogene in the southern hemisphere (e.g. freezing temperatures; Pross et al., 2012; Westerhold et al., 2021) suggests that the thermal envelope of conifers has expanded in response to changes in the available climatic space. However, only one southern conifer clade (*Callitris*, Larter et al., 2017) has been able to expand its range into the drier climates that expanded during the Cenozoic, suggesting that the precipitation requirements of most of these plants are highly stable and unlikely to respond to future aridification. In this study, the other members of the no-analogue pairs involving *Callitris* are likely to be the driving members of those pairs: *Microcachrys*, *Fitzroya* and *Diselma*, and only the latter of these involves a change in the precipitation niche (Table S2). We suggest that the radiation of *Callitris* has not produced any no-analogue associations because, although the genus is generally considered a specialist of arid environments, it has retained occupation of wet regions (e.g. *C. macleayana),* so no regions of climatic space have been lost.

It is also possible that some fossil taxa co-occurred in no-analogue climates (combinations of climatic conditions that no longer exist; Williams & Jackson, 2004). This could lead to no-analogue pairs via a reduction in available climate space (i.e. a reduction in the existing niche; Figure 3.1b), and can have long-term legacy effects even if suitable climatic conditions become

available once more (Figure 3.1c, d). It seems plausible that this may be the case for at least some no-analogue pairs, and could well be a major contributing factor to the extinctions described above. It may never be possible to disentangle the exact processes leading to no-analogue pairs, but all plausible explanations discussed here are consistent with high levels of niche conservatism, specifically of the precipitation niche.

Implications

In a remarkable display of ecological conservatism, our study suggests that the hydraulic limitations (sensitivity of the water transport system to water deficit) on current conifer distributions (see Brodribb & Hill 1999; Brodribb et al., 2014) have existed for at least the last 50 million years. This conservatism may be linked to morphological constraints – Hill (2004) suggested that morphological changes in the leaves of *Dacrycarpus* were adaptations to a drying climate, shortly before the genus became extinct in Australia. Recently, Condamine *et al.,* (2020) found that an angiosperm-driven extinction model was a better fit to extant conifer diversity patterns than climate-driven models, and suggested that competition with angiosperms was the main cause of Cenozoic extinctions. However, our results highlight the importance of including water availability in studies of palaeoecological changes – precipitation was not included in the model set evaluated in Condamine et al. (2020) – so while our findings support the conclusions of these authors with regard to the limited influence of temperature, we find evidence for the role of changing precipitation regimes in directly or indirectly driving Cenozoic contraction of southern conifers. This is consistent with observations that the most hydraulically vulnerable conifers (e.g. *Acmopyle*) also have the earliest last appearances in the fossil record of Australia (Brodribb & Hill, 2004).

Studies on the effect of climate on deep-time biodiversity patterns have been largely centred on temperature both in marine (Yasuhara et al., 2012; Yasuhara et al., 2020) and terrestrial systems (e.g., Shiono et. al, 2018), but our results emphasise the need to consider changes in precipitation regime

as long-term drivers of change in terrestrial systems. Furthermore, our results highlight the potential for using fossils as proxies for precipitation. We show that the nearest living relatives of fossils of southern conifers provide reliable indicators of palaeoprecipitation, but – for pre-Quaternary sites – are less reliable indicators of palaeotemperatures. In this context it is worth noting that palaeoprecipitation is more difficult to estimate than palaeotemperature using other methodologies, including foliar physiognomy (leaf size and shape; Wolfe, 1993; Wei et al., 2021), marine fossils and biochemistry. Although there is some risk in making inferences from negative results (the absence of precipitation no-analogue pairs), conservatism remains the most parsimonious explanation for our observations. It may thus be possible to assess other palaeoproxies using no-analogue pairs to identify which aspects of the niche have remained stable through geological time.

Here, we show that analysis of no-analogue pairs in the fossil record can be used to infer changes in the evolutionary and ecological history of taxa. The pair-oriented approach employed here also has the advantage of detecting changes in climatic envelopes without the need to reconstruct past climates. While the focus of this study is restricted to southern conifers, our novel analyses using no-analogue pairs in multidimensional environmental space are applicable to any sets of fossil assemblages. Of particular interest for future study are northern hemisphere conifers – Leslie et al., (2012) reported hemisphere-scale evolutionary differences in conifers that may be driven by the differences between the largely continental northern environment and the more oceanic southern hemisphere. Additionally, we highlight the utility of southern conifers for palaeoprecipitation estimation.

Although our evidence is consistent with very high levels of evolutionary conservatism in climatic niches of conifers, this conservatism is largely in dimensions related to water, not to temperature. This emphasises current and future threats to many southern conifers posed by drying climates (Brodribb et al 2020).

References

Bannister, P., & Lord, J. M. (2006). Comparative winter frost resistance of plant species from southern Africa, Australia, New Zealand, and South America grown in a common environment (Dunedin, New Zealand). *New Zealand Journal of Botany*, **44**, 109-119.

Belcher, C. M., Mills, B. J. W., Vitali, R., Baker, S. J., Lenton, T. M., & Watson, A. J. (2021). The rise of angiosperms strengthened fire feedbacks and improved the regulation of atmospheric oxygen. *Nature Communications*, **12**, 503.

Blackman, C. J., Brodribb, T. J., & Jordan, G. J. (2012). Leaf hydraulic vulnerability influences species' bioclimatic limits in a diverse group of woody angiosperms. *Oecologia* **168**, 1-10.

Blonder, B. (2018), Hypervolume concepts in niche- and trait-based ecology. *Ecography*, **41**, 1441-1455.

Brasso, R. L., & Emslie, S. D. (2006). Two new late Pleistocene avifaunas from New Mexico. *The Condor*, **108**, 721-730.

Brodribb, T., & Hill, R. (1999). The importance of xylem constraints in the distribution of conifer species. *The New Phytologist*, **143**, 365-372.

Brodribb, T., & Hill, R. S. (2002). The photosynthetic drought physiology of a diverse group of southern hemisphere conifer species is correlated with minimum seasonal rainfall. *Functional Ecology*, **12**, 465-471.

Brodribb, T., & Hill, R. S. (2004). The rise and fall of the Podocarpaceae in Australia - A physiological explanation. In A.R. Helmsley & I. Poole (Eds.) *The evolution of plant physiology* (pp. 381-399). London: Elsevier Academic Press.

Brodribb, T. J., McAdam, S. A., Jordan, G. J., & Martins, S. C. (2014). Conifer species adapt to low-rainfall climates by following one of two divergent pathways. *Proceedings of the National Academy of Sciences*, **111**, 14489-14493.

Brodribb, T. J., Powers, J., Cochard, H., & Choat, B. (2020). Hanging by a thread? Forests and drought. *Science*, **368**, 261-266.

Brown, M. J., Holland, B. R., & Jordan, G. J. (2020). hyperoverlap: Detecting biological overlap in n-dimensional space. *Methods in Ecology and Evolution*, **11**, 513-523.

Bush, A., Catullo, R. A., Mokany, K., Thornhill, A. H., Miller, J. T., & Ferrier, S. (2018). Truncation of thermal tolerance niches among Australian plants. *Global Ecology and Biogeography*, **27**, 22-31.

Carpenter, R. J., Jordan, G. J., Mildenhall, D. C., & Lee, D. E. (2011). Leaf fossils of the ancient Tasmanian relict *Microcachrys* (Podocarpaceae) from New Zealand. *American Journal of Botany*, **98**, 1164-72.

Condamine, F. L., Silvestro, D., Koppelhus, E. B., & Antonelli, A. (2020). The rise of angiosperms pushed conifers to decline during global cooling. *Proceedings of the National Academy of Sciences*, **117**, 28867-28875.

Coope, G. R. (2000). Middle Devensian (Weichselian) coleopteran assemblages from Earith, Cambridgeshire (UK) and their bearing on the interpretation of ‘Full glacial’ floras and faunas. *Journal of Quaternary Science*, **15**, 779-788.

Crisp, M. D., Arroyo, M. T., Cook, L. G., Gandolfo, M. A., Jordan, G. J., McGlone, M. S., ... & Linder, H. P. (2009). Phylogenetic biome conservatism on a global scale. *Nature*, **458**, 754-756.

Crisp, M. D., & Cook, L. G. (2011). Cenozoic extinctions account for the low diversity of extant gymnosperms compared with angiosperms. *New Phytologist*, **192**, 997-1009.

Eiserhardt, W. L., Borchsenius, F., Sandel, B., Kissling, W. D., & Svenning, J. C. (2015). Late Cenozoic climate and the phylogenetic structure of regional conifer floras world-wide. *Global Ecology and Biogeography*, **24**, 1136-1148.

Enright, N. J., & Hill, R. S. (1995). *Ecology of the southern conifers*. Carlton, Vic : Melbourne University Press.

Farjon, A., & Filer, D. (2013). An atlas of the world's conifers: an analysis of their distribution, biogeography, diversity and conservation status. Leiden: Brill.

Fick, S. E., & Hijmans, R. J. (2017). WorldClim 2: new 1-km spatial resolution climate surfaces for global land areas. *International Journal of Climatology*, **37**, 4302-4315.

Graham, R. W., Lundelius, E.L., Graham, M. A., Schroeder, E. K., Toomey, R. S., Anderson, E., Barnosky, A. D., Burns, J. A., Churcher, C. S., & Grayson, D. K. (1996). Spatial response of mammals to late Quaternary environmental fluctuations. *Science*, **272**, 1601-1606.

Herring, J. R. (1985). Charcoal fluxes into sediments of the North Pacific Ocean: the Cenozoic record of burning. In: *The carbon cycle and atmospheric CO_2: Natural variations Archean to Present*, *Geophysical Monographs*, **32**, 419–442.

Hill, R. S. (2004). Origins of the southeastern Australian vegetation. *Philosophical Transactions of the Royal Society of London. Series B: Biological Sciences*, **359**, 1537-1549.

Hill, R. S., & Brodribb, T. J. (1999). Turner Review No. 2 - Southern conifers in time and space. *Australian Journal of Botany*, **47**, 639-696.

Hill, R. S., & Pole, M. S. (1992). Leaf and shoot morphology of extant *Afrocarpus*, *Nageia* and *Retrophyllum* (Podocarpaceae) species, and species with similar leaf arrangement, from Tertiary sediments in Australasia. *Australian Systematic Botany*, **5**, 337-358.

Holz, A., Wood, S. W., Veblen, T. T., & Bowman, D. M. (2015). Effects of high-severity fire drove the population collapse of the subalpine Tasmanian endemic conifer *Athrotaxis cupressoides*. *Global Change Biology*, **21**, 445-458.

Jackson, S. T., & Williams, J. W. (2004). Modern analogs in Quaternary paleoecology: here today, gone yesterday, gone tomorrow? *Annual Review of Earth and Planetary Sciences*, **21**, 495-537

Jones, H. G. (2014). *Plants and microclimate. 3rd Edn.* Cambridge: Cambridge University Press.

Jordan, G. J. (1995). Extinct conifers and conifer diversity in the Early Pleistocene of western Tasmania. *Review of Palaeobotany and Palynology*, **84**, 375-387.

Jordan, G. J. (1997). Contrasts between the climatic ranges of fossil and extant taxa: Causes and consequences for palaeoclimatic estimates. *Australian Journal of Botany*, **45**, 465-474.
Jordan, G. J. (2011). A critical framework for the assessment of biological palaeoproxies: Predicting past climate and levels of atmospheric CO2 from fossil leaves. *New Phytologist* **192**: 29-44.
Jordan, G. J., Harrison , P. A., Worth, J. R. P., Williamson, G. J., & Kirkpatrick, J. B. (2016). Palaeoendemic plants provide evidence for persistence of open, well-watered vegetation since the Cretaceous. *Global Ecology and Biogeograph*y, **25**, 127-140.
Kooyman, R. M., Wilf, P., Barreda, V. D., Carpenter, R. J., Jordan, G. J., Sniderman, J. M. K., … Weston, P. H. (2014). "Paleo-Antarctic rainforest into the modern old world tropics: The rich past and threatened future of the "southern wet forest survivors"." *American Journal of Botany*, **101**, 2121-2135.
Larcombe, M. J., Jordan, G. J., Bryant, D., & Higgins, S. I. (2018). The dimensionality of niche space allows bounded and unbounded processes to jointly influence diversification. *Nature Communications*, **9**, 4258.
Larter, M., Pfautsch, S., Domec, J. C., Trueba, S., Nagalingum, N., & Delzon, S. (2017). Aridity drove the evolution of extreme embolism resistance and the radiation of conifer genus *Callitris*. *New Phytologist*, **215**, 97-112.
Laughlin, D.C., Delzon, S., Clearwater, M. J., Bellingham, P. J., McGlone, M. S., & Richardson, S. J. (2020). Climatic limits of temperate rainforest tree species are explained by xylem embolism resistance among angiosperms but not among conifers. *New Phytologist*, **226**, 727-740.
Leslie, A. B., Beaulieu, J. M., Rai, H. S., Crane, P. R., Donoghue, M. J., & Mathews, S. (2012). "Hemisphere-scale differences in conifer evolutionary dynamics." *Proceedings of the National Academy of Sciences* **109**, 16217-16221.
Mackey, B. G. (1994). Predicting the potential distribution of rain-forest structural characteristics. *Journal of Vegetation Science*, **5**, 43-54.
Macphail, M. (2007). Australian palaeoclimates: Cretaceous to Tertiary a review of palaeobotanical and related evidence to the year 2000. Bentley: CRC LEME.
Mosbrugger, V., & Utescher, T. (1997). The coexistence approach—a method for quantitative reconstructions of Tertiary terrestrial palaeoclimate data using plant fossils. *Palaeogeography, Palaeoclimatology, Palaeoecology*, **134**, 61-86.
Muggeo, V. M. (2008). Segmented: An R package to fit regression models with broken-line relationships. *R News* **8**, 20-25
Peterson, A. T., Soberón, J., Pearson, R. G., Anderson, R. P., Martínez-Meyer, E., Nakamura, M., & Araújo, M. B. (2011). *Ecological niches and geographic distributions.* Princeton: Princeton University Press.
Pittermann, J., Stuart, S. A., Dawson, T. E., & Moreau, A. (2012). Cenozoic climate change shaped the evolutionary ecophysiology of the Cupressaceae conifers. *Proceedings of the National Academy of Sciences*, **109**, 9647-52.

Preece, R., & Bridgland, D. R. (2012). Late Quaternary environmental change in North-west Europe: Excavations at Holywell Coombe, South-east England: Excavations at Holywell Coombe, South-east England. Springer Science & Business Media.

Prentice, I. C., Cramer, W., Harrison, S. P., Leemans, R., Monserud, R. A., & Solomon, A. M. (1992). A global biome model based on plant physiology and dominance, soil properties and climate. *Journal of Biogeography*, **19**, 117-134.

Prober, S. M., Thiele, K. R., Rundel, P. W., Yates, C. J., Berry, S. L., Byrne, M., Christidis, L., Gosper, C. R., Grierson, P. F., & Lemson, K. (2012) Facilitating adaptation of biodiversity to climate change: a conceptual framework applied to the world's largest Mediterranean-climate woodland. *Climatic Change*, **110**, 227-248.

Pross, J., Contreras, L., Bijl, P. K., Greenwood, D. R., Bohaty, S. M., Schouten, S., ... Brinkhuis, H. (2012). Persistent near-tropical warmth on the Antarctic continent during the early Eocene epoch. *Nature*, **488**, 73-77.

R Core Team (2014). R: *A language and environment for statistical computing*. Vienna, Austria: R Foundation for Statistical Computing.

Sakai, A., & Larcher, W. (2012). *Frost survival of plants: responses and adaptation to freezing stress*. Springer Science & Business Media.

Shiono, T., Kusumoto, B., Yasuhara, M., & Kubota, Y. (2018). Roles of climate niche conservatism and range dynamics in woody plant diversity patterns through the Cenozoic. *Global Ecology and Biogeography*, **27**, 865-874.

Stewart, J. R. (2009). The evolutionary consequence of the individualistic response to climate change. *Journal of Evolutionary Biology*, **22**, 2363-75.

Sundaram, M., & Leslie, A. B. (in press). The influence of climate and palaeoclimate on distributions of global conifer clades depends on geographical range size. *Journal of Biogeography*.

Svenning, J. C., & Skov, F. (2007). Could the tree diversity pattern in Europe be generated by postglacial dispersal limitation? *Ecology Letters*, **10**, 453–460.

Wei, G., Peng, C., Zhu, Q., Zhou, X., & Yang, B. (2021). Application of machine learning methods for paleoclimatic reconstructions from leaf traits. *International Journal of Climatology*, **41**(Suppl. 1): E3249– E3262.

Wells, P., & Hill, R. S. (1989). Fossil imbricate-leaved Podocarpaceae from Tertiary sediments in Tasmania. *Australian Systematic Botany*, **2**, 387-423.

Westerhold, T., Marwan, N., Drury, A. J., Liebrand, D., Agnini, C., Anagnostou, E., … Zachos, J. C. (2020). An astronomically dated record of Earth's climate and its predictability over the last 66 million years. *Science*, **369**, 1383-1387.

Wilf, P. (2012). Rainforest conifers of Eocene Patagonia: attached cones and foliage of the extant Southeast Asian and Australasian genus *Dacrycarpus* (Podocarpaceae). *American Journal of Botany*, **99**, 562-84.

Wolfe, J. A. (1993). A method of obtaining climatic parameters from leaf assemblages. *US Geological Survey Bulletin* **2040**.
Williams, J. W., & Jackson, S. T. (2007). Novel climates, no-analog communities, and ecological surprises. *Frontiers in Ecology and the Environment*, **5**, 475-482.
Wood, S. (2018). *Package 'mgcv'. R package version 1.8.* Vienna, Austria: R Foundation for Statistical Computing.
Yasuhara, M., Hunt, G., Dowsett, H. J., Robinson, M. M., & Stoll, D. K. (2012). Latitudinal species diversity gradient of marine zooplankton for the last three million years. *Ecology Letters,* **15**, 1174-1179.
Yasuhara, M., Huang, H., Hull, P., Rillo, M., Condamine, F., Tittensor, D., . . . Saupe, E. (2020). Time machine biology: cross-timescale integration of ecology, evolution, and oceanography. *Oceanography*, **33**, 16-28.

Chapter 4 : No cell is an island: characterising the epidermis using EPIDERMALMORPH, a new R package

Abstract

The leaf epidermis is the interface between the plant and its environment, and is highly variable in morphology. This diversity shows links to both phylogeny and environment, and is relevant to several fields; the epidermis is important in physiology, functional traits, palaeobotany, taxonomy, and developmental biology.

However, describing and measuring leaf epidermal traits remains challenging. Current approaches are either extremely labour-intensive and not feasible for large studies, or are limited to measurements of individual cells.

Here, we present a method to characterise individual cell shape, cell arrangement and the effect of neighbouring cells on shape from light microscope images of the cuticle. We have implemented this method in an R package, EPIDERMALMORPH and provide an example workflow using this package, which includes functions to evaluate trait reliability and optimal sampling effort for any given group of plants. We demonstrate that our new metrics of cell shape are independent of gross cell shape, unlike existing metrics.

EPIDERMALMORPH provides a broadly applicable method for quantifying epidermal traits that we hope can be used to disentangle the fundamental relationships between form and function in the leaf epidermis.

Introduction

The plant epidermis controls transpiration and gas exchange via stomata, protects the plant from both environmental stressors and biological invasions, and can even act as a mechano-sensory organ (Hamant et al. 2008). There is extreme diversity in epidermal traits that can be observed from light microscopy – the size, shape, arrangement and number of pavement cells, stomatal and other specialised cells (e.g. trichomes) – but the physiological function of each of these traits under different environmental conditions remains unclear, despite extensive study (Sharma, 1972; Royer, 2001; Dunn *et al.*, 2015a). The functions of epidermal traits may also vary among groups of plants, highlighting the need for broad-scale studies of epidermal traits (as noted by Vőfély *et al.*, 2019), and thus the need for a universally applicable approach to quantifying and comparing the epidermis.

Leaf epidermal traits are easy to observe in fresh or dried material, and cell imprints are readily preserved via the cuticle, which can retain epidermal information for hundreds of millions of years (Blomenkemper *et al.*, 2021). This means that we have a record of epidermal traits spanning deep time that can provide a wealth of evolutionary and palaeoecological information. These traits are used widely in the identification of fossil plants (Dilcher, 1974; Deng *et al.*, 2017) as well as estimating past climate, vegetation structure and atmospheric carbon dioxide, through either nearest-living-relative or

physiognomic approaches (Mosbrugger & Utescher, 1997; Dunn *et al.*, 2015b). The epidermis has also been studied in developmental (Bidhendi *et al.*, 2019) and functional trait contexts (e.g. Osunkoya *et al.*, 2014), as some epidermal traits have been linked to life-history strategies. However, the physiological significance of many epidermal traits is unclear – some traits appear to have contrasting relationships with climate in different groups of plants (Thomas *et al.*, 2004; Dunn *et al.*, 2015a). It is possible that these contradictory results could be explained by differences in methodology – there are many metrics that can be used to quantify the epidermis, ranging from very simple and intuitive (e.g. cell area) to extremely complicated (e.g. Fourier analysis, Sánchez-Corrales *et al.*, 2018).

Most current methods of quantifying the epidermis fall into one of two categories:

1) High-throughput measurements of individual cells (e.g. PAVEQANT, Möller *et al.*, 2017; GRAVIS, Nowak *et al.*, 2021). These methods employ sophisticated algorithms to describe cell shape, but do not consider either the effect of neighbouring cells or measure the arrangement of cells. Some of these methods have been shown to accurately distinguish subtle differences in the cell shape between genotypes (Nowak *et al.*, 2021), but the result can difficult to interpret in terms of functional traits.
2) Manual description of epidermal measurements (e.g. Stark Schilling & Mill, 2011). These methods take into account a wider range of traits (e.g. how cells are arranged, stomatal spacing) but are slow, labour

intensive and suffer from subjectivity in terms of choice of measurements. The low-throughput nature of these methods means that there is a significant compromise between sample size of both taxa and cells, which limits the scope of interpretations that can be made from such studies.

Furthermore, both types of approach tend to suffer from a common limitation – cell shape is measured on individual cells, without considering the effect of neighbours. The shape of an individual cell is strongly affected by that of its neighbours. Stomata and underlying venation also affect the shapes of cells (Vőfély *et al.*, 2019) so we propose that a) the epidermis should be measured as a mosaic of connected cells and b) that measurement of epidermal cells should include metrics of both cell shape and the relationships among cells. It is also unclear how many epidermal cells are needed to get a reliable estimate of trait values for an individual. Most authors take the mean value for 25-30 cells (Carins Murphy *et al.*, 2016; Vőfély *et al.*, 2019), though some values are based on as few as seven cells (Bush *et al.*, 2017), which is unlikely to be a reliable estimate for species, or even individual plants (Clugston *et al.*, 2017).

Here we present a new R package 'EPIDERMALMORPH', which contains a wide range of cell descriptors including cell area, aspect ratio and angle as well as several novel shape descriptors, a unique set of cell arrangement descriptors, and functions to optimise sampling effort. We also compare some of these descriptors to those from other algorithms, and provide an example workflow for using EPIDERMALMORPH.

Description of epidermalmorph

The input image format should be a tracing of the cells such that the cell walls, interiors of pavement cells, stomata and subsidiary cells are each represented by a single value (colour; Figure 4.1). Our package does not explicitly include tracing functions, but we recommend using the Ridge Detection function in ImageJ (Steger, 1998; Thorsten Wagner, 2017) as a form of semi-automation. Tracings produced by this method normally need to be manually edited before use. EPIDERMALMORPH also includes a pre-processing function to coerce images into the appropriate form ('image_preprocess'). The group of pixels for each cell are then converted into a single, spatial polygon object.

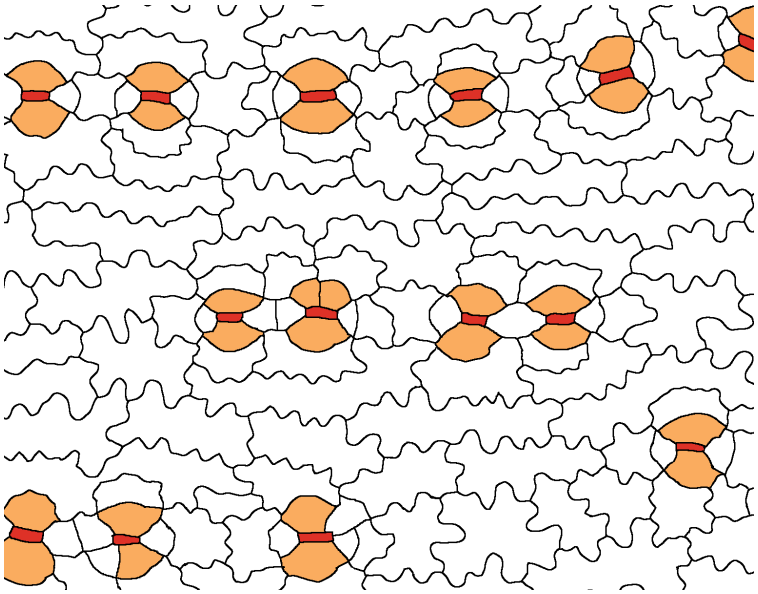

Figure 4.1 An example of the input required for EPIDERMALMORPH. The cell walls are shown in black, the pavement cells in white, stomata in red and the subsidiary cells in orange. This image has been cropped for clarity – the field of view should include at least 20-30 stomata.

At the core of the EPIDERMALMORPH package is the automated measurement of epidermal traits, using the 'extract_epidermal_traits' function. These traits include metrics of size, shape and alignment of epidermal cells (**Figure 4.2**) and stomata (**Figure 4.3**), as well as measurements of cell arrangement (**Figure 4.4**). Neighbouring cells are identified, so that the shortest paths between cell types can be calculated (e.g. mean number of cells between stomata, **Figure 4.4**). Cells on the edge of the image are excluded from shape measurements, but cells on the top and left edges are counted to calculate stomatal index (as per Kubínová, 1994).

Because the orientation of the image relative to the original leaf is uncertain in many cases, we used the mean angle of the stomata as a proxy for leaf axis (stomata are arranged parallel to the leaf axis in many plants). To identify stomatal north, we fit ellipses to each stomate and extract the mean angle of the long axis. The angles of pavement cells and individual stomata are calculated relative to this angle. This can be disabled if the leaf axis is known (see package documentation). Other measurements for which EPIDERMALMORPH provides novel automation are the arrangement and spacing of stomata and subsidiary cells (**Figure 4.4**).

For shape measurements, the pixelated outlines of each cell are smoothed using the SMOOTHR package (Strimas-Mackey, 2021) and the cell junctions are used to define the simplified shape of the cell (**Figure 4.2**). This use of the junction points is a novel way to describe the shape of the cell that has advantages over existing methods (*see Comparison to other approaches*). Where other methods try to exclude cell junctions, we use them to

disentangle gross cell shape from wall undulation. Given the junction points, we can define the simplified cell, and can then compute three main measures of undulation (Figure 4.2): the number of times that the cell wall crosses the simplified perimeter per millimetre (analogous to frequency), the maximum distance between the cell wall and the simplified perimeter (the size of the undulations, analogous to wavelength), and the ratio between the minimum perimeter and actual perimeter (complexity).

We implemented EPIDERMALMORPH in R, because it is a widely used program by biologists and we wanted to make this method accessible. The R package is available on GitHub (https://github.com/matildabrown/epidermalmorph).

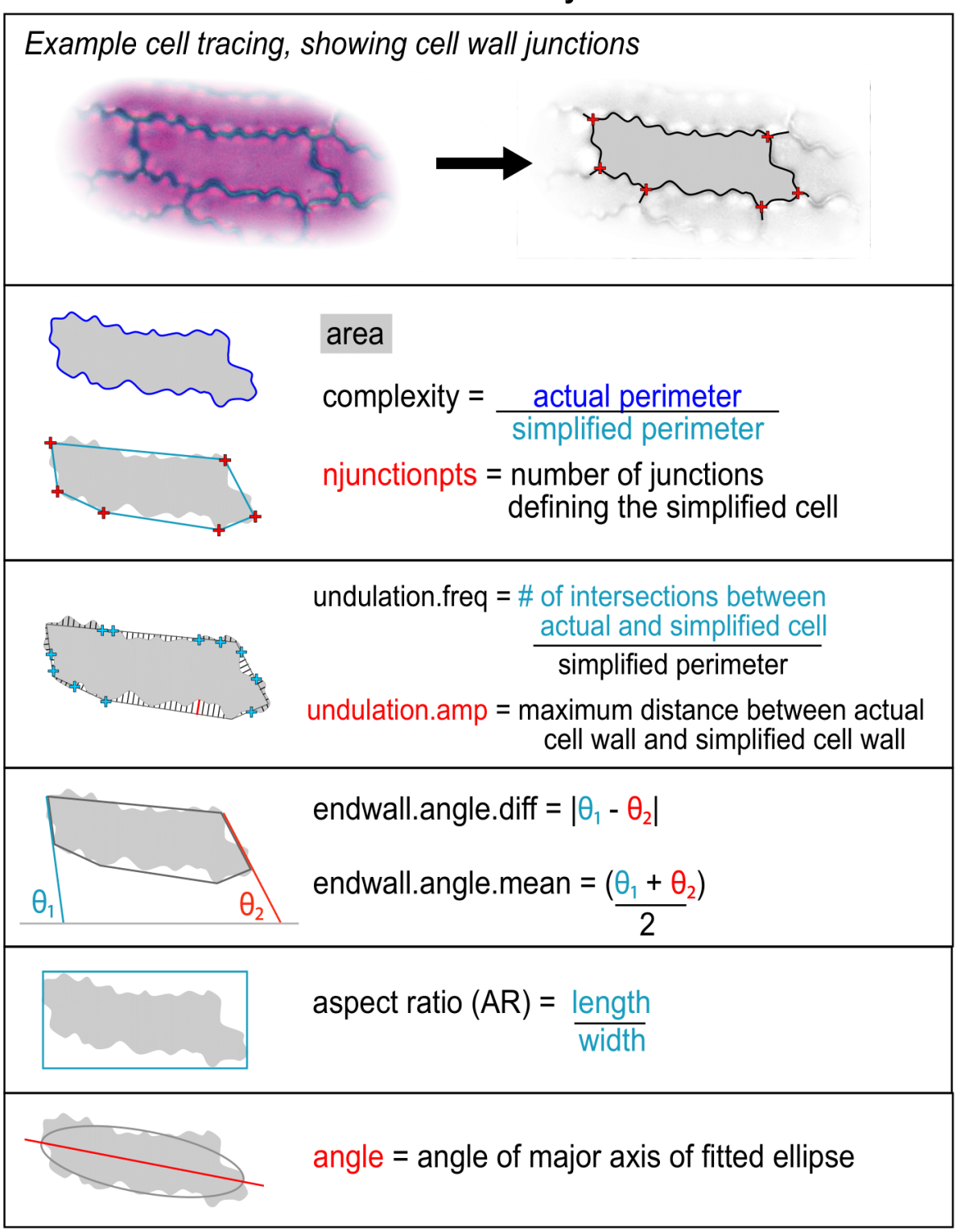

Figure 4.2 Graphical description of the individual pavement cell metrics that can be measured using epidermalmorph.

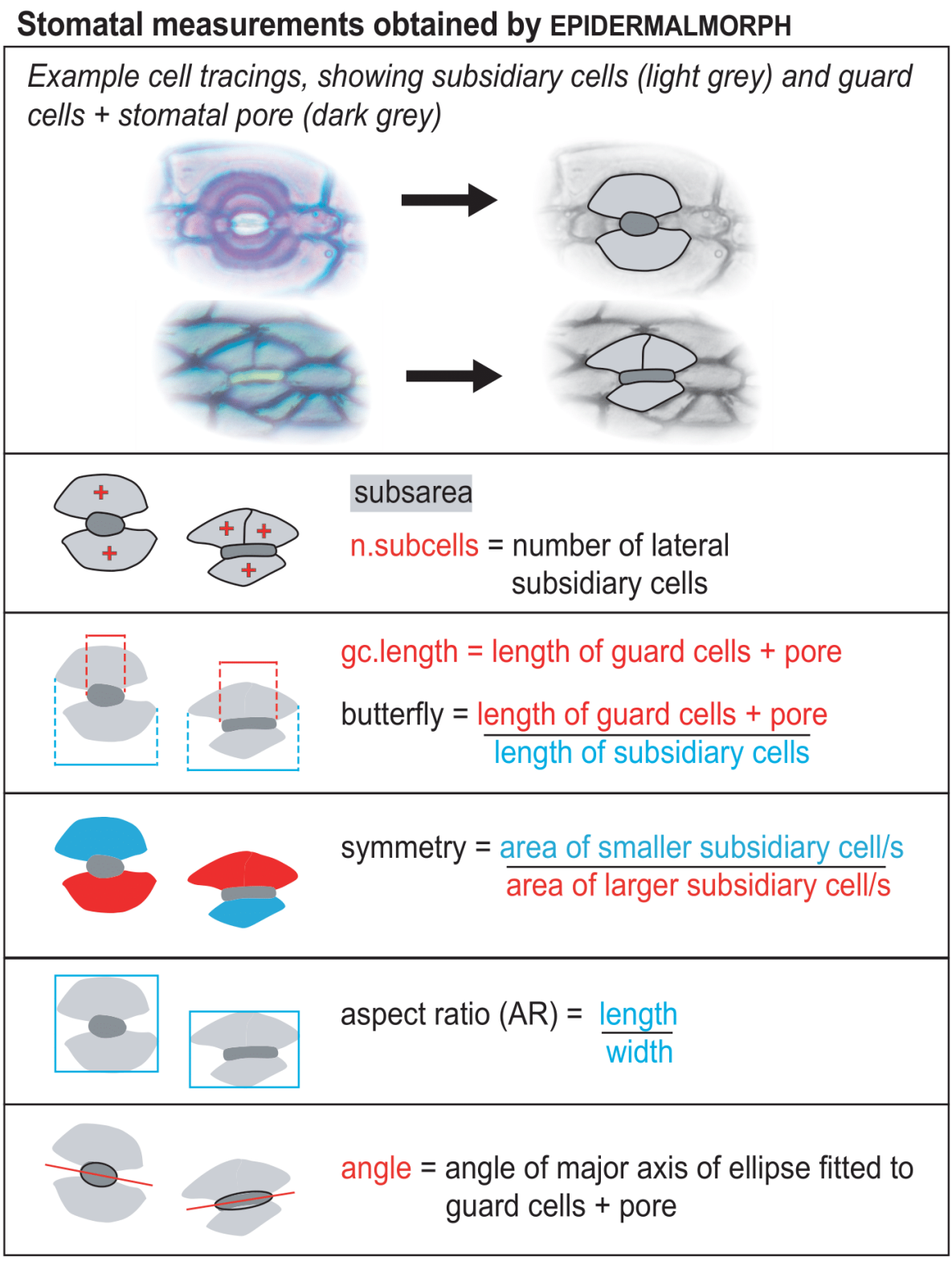

Figure 4.3 Graphical description of individual stomatal metrics that can be measured using EPIDERMALMORPH.

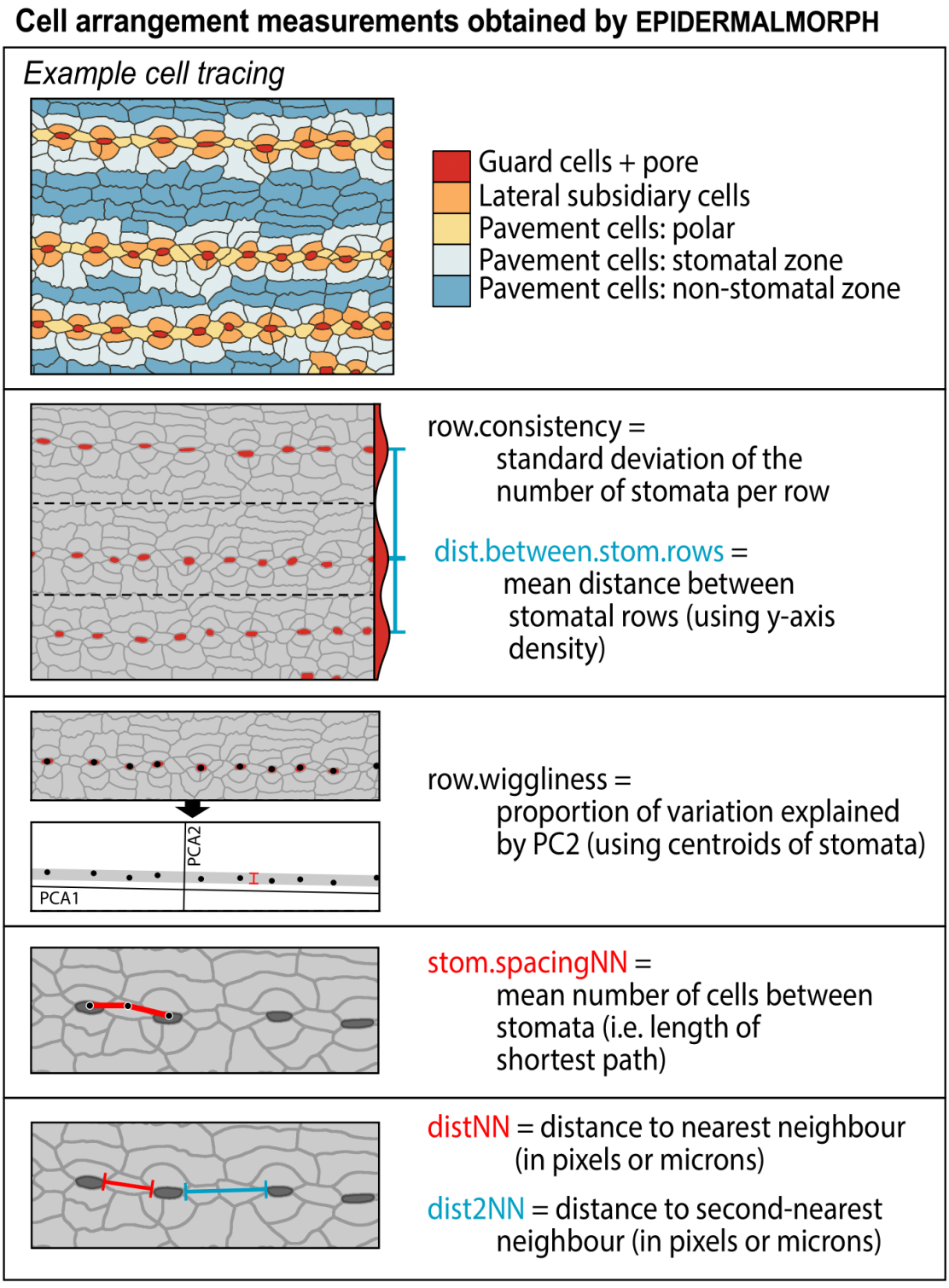

Figure 4.4 Graphical description of the cell arrangement metrics that can be measured by EPIDERMALMORPH. Pavement cells are categorised as being in the 'pavement zone', 'stomatal zone' or 'polar', depending on how far they are from the nearest stomate. Stomatal arrangement is measured in terms of both row characteristics, as well as spacing.

Sampling effort

Tracing epidermal cells can be laborious, despite attempts to automate this process (see *Segmentation* in *Discussion*), so finding a balance between effort and information is crucial. We have included a workflow to identify optimum sampling effort in the EPIDERMALMORPH package that employs subsampling of cells within images.

For each image, a set of random, contiguous patches of cells are sampled, then measured. This is implemented using the patch_sampler() function for patches of varying sizes (e.g. 50, 100, 200, 400 cells). This function finds a random, contiguous patch of cells as follows: a single cell is randomly selected, then the neighbours of that cell are added to the patch, then the neighbours of those cells, and so forth until the patch exceeds the required size. Where part of a stomatal complex is encountered, all cells from that complex are automatically added to the patch. This process is illustrated in Figure 4.5 below.

The variance in measured trait values from patches can then be used to identify a minimum number of cells, either by using an arbitrary threshold (e.g. the number of cells required to achieve less than 10% variance in samples) or some other measure of convergence (see package documentation for details). We also recommend carrying out a pilot study for any group of plants to evaluate trait reliability, as not all traits that can be measured using EPIDERMALMORPH are useful for all plants (see *Trait Reliability* in *Example Workflow*).

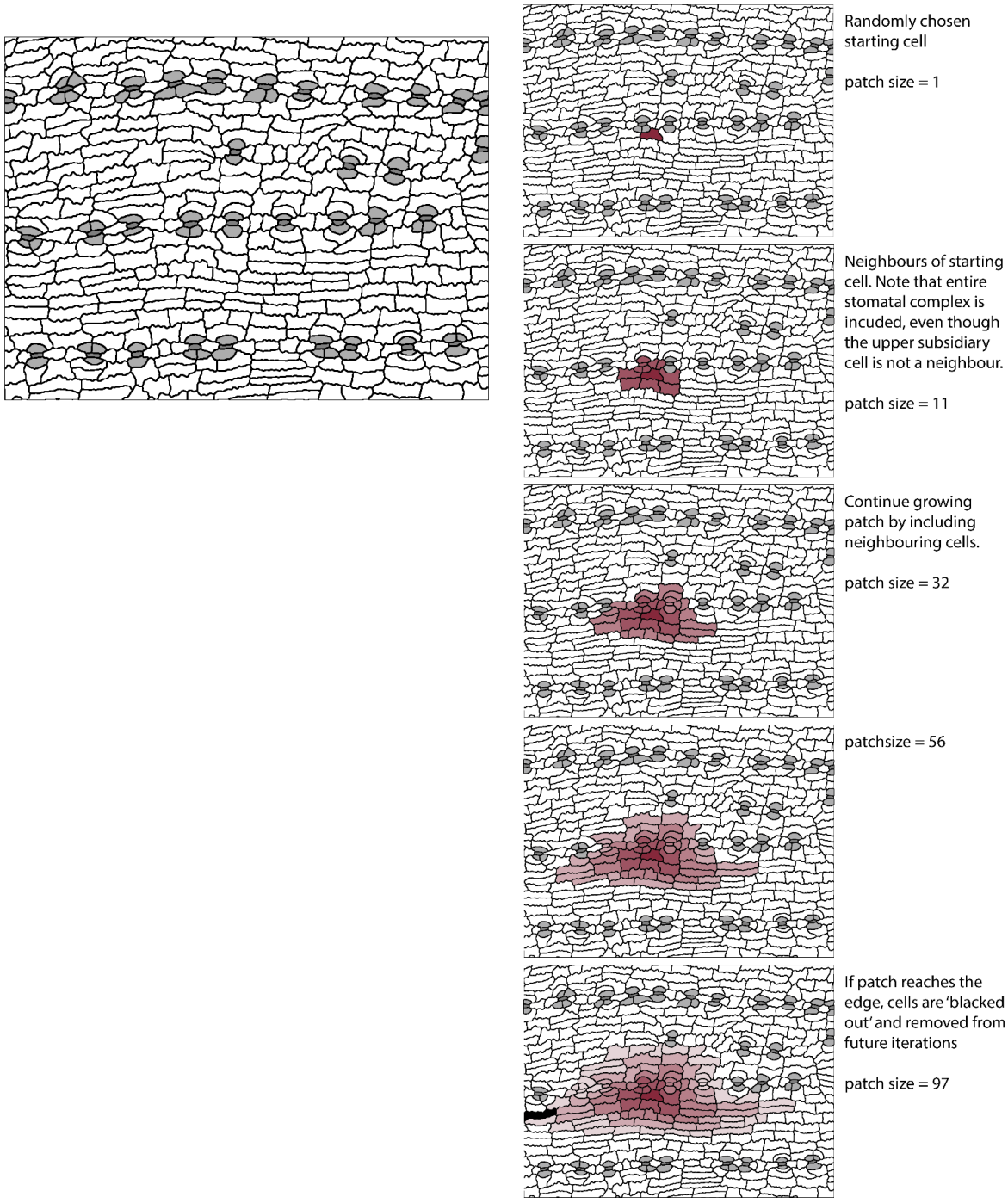

Figure 4.5 Example of cell patch sampling. From a starting cell, the region is grown iteratively by including neighbouring cells. If part of a stomatal complex is included, the algorithm automatically includes all other cells from that complex. If an edge is reached, the cell that is broken by the edge is removed and not included in future iterations.

Comparison with existing methods

To the best of our knowledge, this is the first piece of software that describes the spatial distribution of stomata on the leaf surface. EPIDERMALMORPH measures six traits describing the arrangement of stomata (Figure 4.4), including the spacing of both individual complexes and rows of stomata, as well as whether these rows are discontinuous (row.consistency) and straight/crooked (row.wiggliness). These traits can be distinctive in certain groups of plants and have been used to identify fossils (Hill, 1992; Andruchow-Colombo *et al.*, 2019) so we envisage that one application of EPIDERMALMORPH may be in the automated identification of plants from cuticle fragments. (Wilf *et al.*, 2016) demonstrated that automated identification of leaf fossils has significant potential, but epidermal cells have not yet been utilised in this way – possibly because the individual shapes of fern, angiosperm and conifer cells overlap considerably (despite significant differences in mean trait values; Vofely *et al*., 2019), making identification at even such a coarse taxonomic resolution impossible. By integrating individual cell measurements with stomatal arrangement traits, we expect to find that there is more clear separation between these groups.

While there is some overlap between EPIDERMALMORPH and other ways of quantifying the size and shape of cells (e.g. cell area, aspect ratio), our method describes the shape in the context of the cell's neighbours. The polygon formed by the tri-cell junctions defines the hypothetical shape of the cell if there were no undulations in the shared wall between cells (here termed the simplified cell). We can then measure certain traits from this

simplified cell (aspect ratio, endwall angles), but the key advantage this provides is in measuring the undulation of the cell. The degree and type of undulation of the cell wall is one of the most obvious differences between epidermal cells from different plant groups or environments, and unlike other traits (e.g. cell area) there is no obvious single measurement to describe these differences. As such, numerous approaches to measuring undulation have been proposed (Table 4.1). Good undulation metrics should have the following properties:

1. A cell with straight cell walls will have the lowest possible value of the metric, regardless of aspect ratio or gross cell shape.
2. The metric value/s should increase with both the size and number (or frequency) of undulations.
3. The metric/s should be applicable to cells with very slight undulations as well as those with very large undulations (e.g. the puzzle-shaped cells of *Arabidopsis*).
4. If undulation is to be described by multiple metrics, they should be readily interpretable (not requiring principal component analysis to compare cells).
5. Ideally, the metric should be able to be implemented easily across a wide range of platforms (should not require specialised software).

To identify the limitations of existing metrics and illustrate the advantages of EPIDERMALMORPH, we simulated 1200 cells of varying shapes and degrees of undulation (see Figure S4.1) then compared the measured values of undulation. The cells from Vofely *et al.*, (2019) and used by Nowak *et al.*

(2021) could not be used to evaluate EPIDERMALMORPH, which requires the cell junction coordinates, which were not captured in that dataset. Most existing methods of describing undulation (Table 4.1) compare the perimeter or area of the cell to some baseline, usually either the convex hull of the cell or a circle with the same area. Circle-based measurements are extremely sensitive to changes in the gross cell shape – elongated, straight-walled cells can have the same undulation index as isodiametric, undulated cells (Figure S4.2). Convex hull measurements are affected by non-convex cells (e.g. boomerang or crescent shape), and none of the single-value metrics can differentiate between many small undulations and few large undulations (Vofely *et al*., 2019, though see Figure S4.3)

Table 4.1 Current measurements of cell undulation and their limitations

Measurement name	Description	Implemented in/by	Limitations
Undulation index, Circularity, Form factor	Ratio of cell perimeter compared to the perimeter of a circle with the same area	Andriankaja *et al.* (2012), Bai *et al.* (2010) Thomas *et al.* (2004)	Affected by aspect ratio
Solidity	Ratio of cell area to area of convex hull	Vőfély *et al.* (2019); similar but not identical to that used by Dunn *et al.* (2015a)	Affected by non-convex (e.g. crescent shaped) cells
Convexity, Lobeyness,	Ratio of cell perimeter to perimeter of convex hull	PaCeQuant (Möller *et al.*, 2017); Sapala *et al.* (2019)	Affected by non-convex (e.g. crescent shaped) cells, though much less than Solidity
Margin roughness	The average angle between points on the cell wall compared to the average angle between the same number of points on a circle	McLellan and Endler (1998); PaCeQuant (Möller *et al.*, 2017)	Difficult to implement for large numbers of cells, Does not behave as expected with amplitude and or frequency
Completeness of visibility graph	Related to the direct 'lines of sight' between points on the perimeter of the cell; see Nowak *et al.* (2021) for details.	GraVis (Nowak *et al.*, 2021)	Likely to be affected by non-convex cells; downloaded software (GraVis, github link) does not work for all cell shapes
Skeleton measurements, lobe measurements	Numerous (15) measurements including: average basal lobe width, non-lobe area, average branch length. See supporting information of Möller *et al.* (2017) for details.	PaCeQuant (Möller *et al.*, 2017)	Large number of metrics not linked to traits, limited applicability outside of *Arabidopsis*
Elliptical Fourier Analysis	Based on the Fourier Series.	Sapala *et al.* (2019)	Good at picking up aspect ratio but performs poorly for undulation description (Vofely et al. 2018). Cannot deal with cells where the lobes 'double back' on themselves (non-holomorphic)
Lobe Contribution Elliptical Fourier Analysis (LOCO-EFA)	Modification of Elliptical Fourier analysis, see Sánchez-Corrales *et al.* (2018) for details	Sánchez-Corrales *et al.* (2018)	Different shapes use different numbers of L_n metrics, difficult to relate to traits

Other measures are indifferent to gross cell shape, but produce a large set of variables that can be difficult to interpret in a trait framework – e.g. GraVis, a recently developed method that uses visibility graphs to describe the cell (Nowak *et al.*, 2021). GraVis generates a graph for each cell by placing a number of nodes along the cell wall, then joining pairs of these nodes with edges if they can 'see' each other (without being occluded by the cell wall). These edges can then be weighted according to their distance and cell shape can be described as an $n \times n$ visibility matrix (where n is the number of nodes). This can be compared between cells using distance metrics, or condensed to a single value (the graph density). GraVis performs extremely well when classifying different genotypes or identifying cell lobes of *Arabidopsis,* and is able to reproduce cell shapes, but cannot be applied to all of our simulated cells so may be of limited utility for analysing broad-scale relationships between form and function.

Another relatively recent method is PaCeQuant (Pavement Cell Quantifier), developed by Möller *et al.* (2017). This can be run as a plugin through ImageJ and quantifies cell shape in 27 variables, including skeleton-based and contour-based measurements. Cell undulation is captured by several of these measurements, including circularity, solidity, convexity and margin roughness (Table 1). Margin roughness (described by McLellan *et al.,* 1998) represents an alternative approach to measuring undulation as it compares the *angles* between points to the expected angle if they were on a circle (rather than area or perimeter). PaCeQuant has largely been used to study the cells of *Arabidopsis*, possibly because many of the features measured

are specific to the extreme lobing displayed by the model species (but that is uncommon in other plants).

Our method separates gross cell shape (e.g. aspect ratio) from undulation by using the junction points with neighbouring cells to define the shape of the cell if all cell walls were straight (the simplified cell). From this, we introduce the ‘complexity’ metric - the ratio of the cell perimeter to the perimeter of the simplified cell. This is conceptually similar to undulation index, convexity and lobeyness but is not affected by the underlying shape of the cell (Fig. S4). To further characterise the pattern of undulation, we also introduce two additional new measurements: maximum undulation amplitude (undulation.amp; Figure 4.2, S4.5) and undulation frequency (undulation.freq, **Figure 4.2**, S6). A few, large undulations will be represented as high maximum undulation amplitude, but low undulation frequency, while the opposite will be true for cells with many small undulations. These measurements are approximately analogous to the ‘pitch’ and ‘amplitude’ of Sánchez-Corrales *et al.* (2018).

On our simulated cells, we found that existing methods performed poorly on elongated or non-convex cells (Figures S4.2-S4.3), but that the metrics from EPIDERMALMORPH were not affected (Figures S4.4-S4.6) As a single metric, complexity fulfills all of the requirements for a good undulation metric, but the addition of undulation amplitude and frequency improve the characterisation of undulation patterning.

Unlike other methods of stomatal quantification (e.g. Song *et al.*, 2020) we do not directly measure the guard cells – our ‘stomate’ cell class is similar to the

‘internal stomatal apparatus’ described by Stark Schilling and Mill (2011). This avoids many of the issues associated with measuring sunken stomata, where guard cells are obscured by subsidiary cells or lie in a different plane to the rest of the epidermis.

Example workflow

Example image dataset: Podocarpaceae

To demonstrate the implementation of EPIDERMALMORPH, here we present an example workflow using the Podocarpaceae, a conifer family with a largely southern hemisphere distribution comprising 20 genera and 196 species (Farjon, 2010; Page, 2019). Podocarps occupy a wide range of environments from alpine (e.g. *Podocarpus lawrencei*), tropical (e.g. *Acmopyle pancheri*) to understorey shrubs in fire-prone environments (e.g. *P. drouynianus*). They also have a strong fossil record (Hill & Brodribb, 1999), and several epidermal studies have been carried out (Stark Schilling & Mill, 2011; Clugston *et al.*, 2017), so it is possible to verify that our interpretation of light photomicrographs is consistent with images captured using a scanning electron microscope.

There is significant variation in the epidermal characters in the Podocarpaceae (Figure 4.6). Although stomata generally have two lateral subsidiary cells in a paracytic arrangement, extra divisions often result in additional subsidiary cells. Polar subsidiary cells may be present or absent, and the epidermal cell wall may be straight or strongly sinuous. Gross cell shape ranges from more or less isodiametric (e.g. *Acmopyle*), to rectangular (e.g. *P. dispermus*) to irregular (e.g. *P. drouynianus*). Epidermal traits are

known to vary between species in the Podocarpaceae (e.g.Stark Schilling & Mill, 2011), and there are well-resolved phylogenies of this family (Kelch, 2002; Biffin *et al.*, 2011; Leslie *et al.*, 2018; Page, 2019).

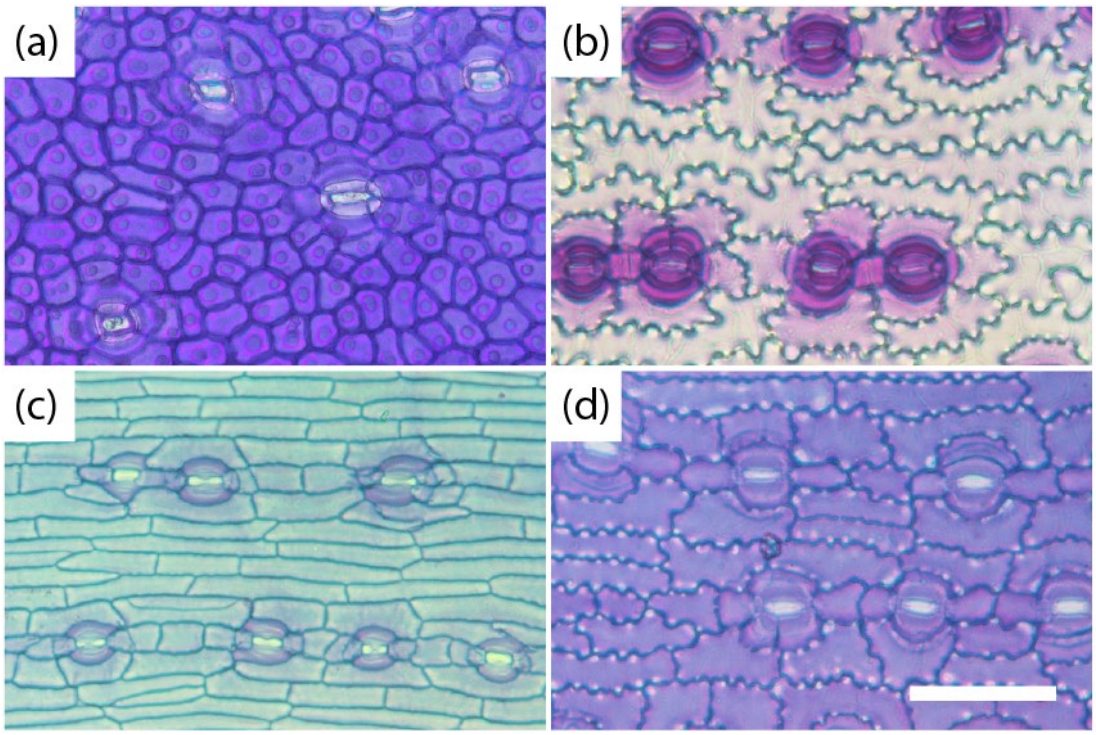

Figure 4.6 Cuticle diversity in the Podocarpaceae. *Phyllocladus aspleniifolius* (a), *Sundacarpus amarus* (b), *Afrocarpus gracilior* (c) and *Podocarpus costalis* (d). Scale bar is 0.1 mm; same scale for all images.

Image preparation

We collected, prepared and imaged cuticles from 26 individual greenhouse-grown plants (spanning 20 species and seven genera, see Table S4.1). For each plant, we captured between three and five images from 2-4 leaves, which were then traced using a combination of the Ridge Detection plugin from ImageJ (based on the method described by Steger, 1998) and manual tracing. Stomata and subsidiary cells were manually annotated using a flood fill (using different values for different cell types, see Figure 4.1 for example).

Trait reliability

We then used EPIDERMALMORPH to convert these images to polygons using the ‘image_to_poly’ function and extracted values for all measurements using the ‘extract_epidermal_traits’ function. We scaled and centred these measurements using a z-transformation, then calculated the mean within-plant standard deviation for each trait (Figure 4.7). We removed all variables that had a mean within-plant standard deviation greater than 0.2 (i.e., where the average within-plant standard deviation exceeded 20% of the total standard deviation for that trait).

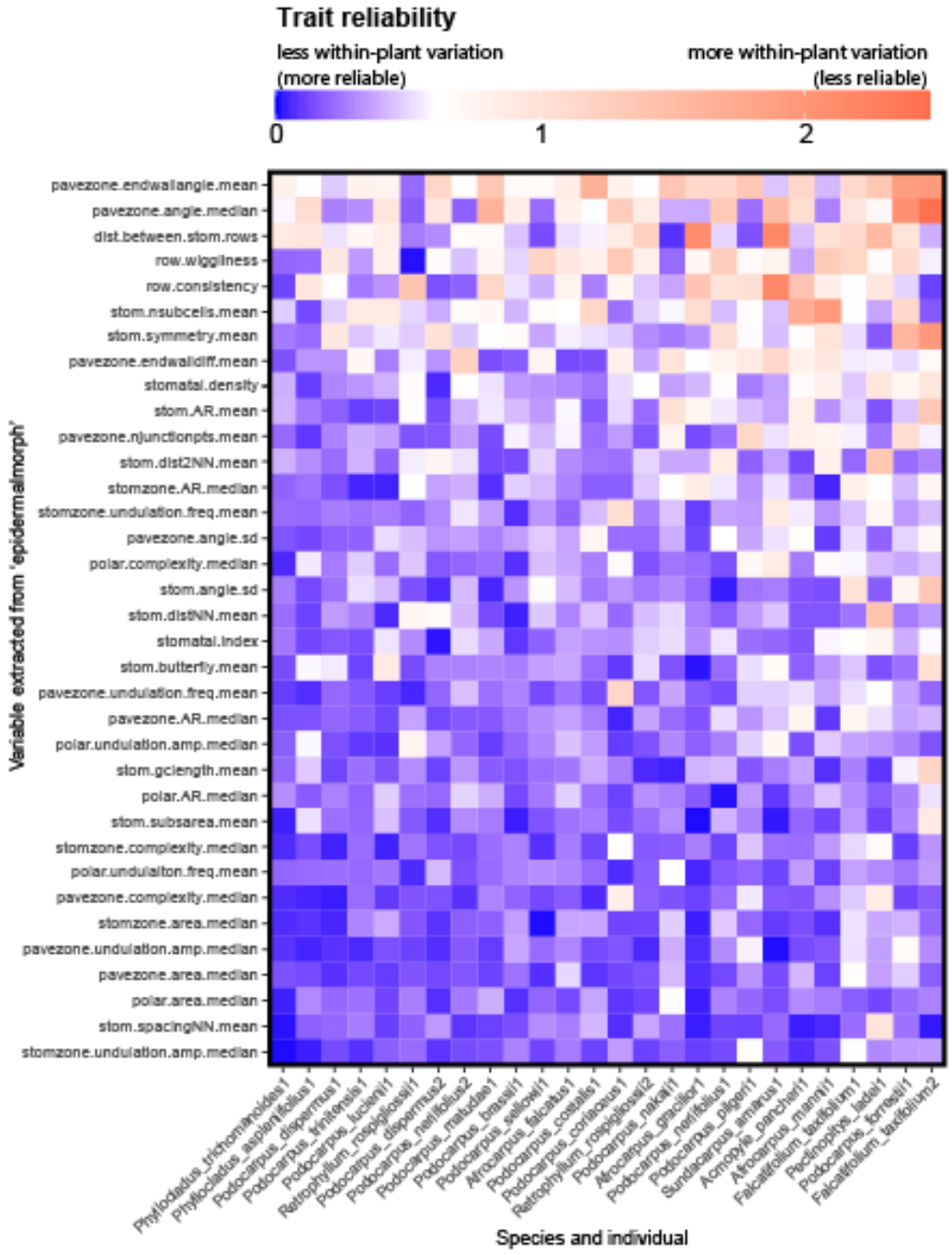

Figure 4.7 Within-plant trait reliability scores. The reliability score is calculated as the standard deviation of the standardised trait values measured from the same plant. A reliability score of 1 means that the variation in the plant is equal to the variation across plants, a score of 3 means that the within-plant variation is three times higher than that of the whole dataset (red; unreliable), while a reliability score of 0.2 means that the within-plant variation is 20% of the variation across plants (blue; reliable). In this dataset, the traits at the top of the figure (endwall.angle.mean, pavezone.angle.median) are the least reliable (i.e. most variable) when averaged across all plants. Similarly, the plants towards the right of the figure tend to be less reliable (*Falcatifolium taxoides* 2, *Podocarpus forrestii* 1). See Figs 2, 3, 4 for illustrations of each measured trait.

To calculate optimum sampling effort, we re-measured our metrics on sub-regions of each image. Measurements were then extracted from each patch as for the whole image, and scaled using the mean and standard deviations of the trait across the whole-image dataset. We repeated this 100 times for each image at each minimum patch size (50, 100, 200 and 400 cells) and recorded the number of cells of each cell type (pavement, stomata, subsidiary) for each iteration. We then calculated the difference between the patch and whole-image value (the delta-value) to allow us to compare measurement error between images. From this, we calculated the standard deviation of the delta-values (see Figure 4.8) at various patch sizes. Low standard deviations of delta-values indicate that all patch measurements were similar to each other (i.e. convergent), and high values indicate that the measurements varied depending on which cells were included in the patch (i.e. the patch size was too small to provide a consistent measurement). For Podocarpaceae, 100-200 pavement cells and 30-40 stomata are required to get a reliable estimate of trait value (Figure 4.8). We provide a function that runs these steps on a set of images (‘cell_resample’).

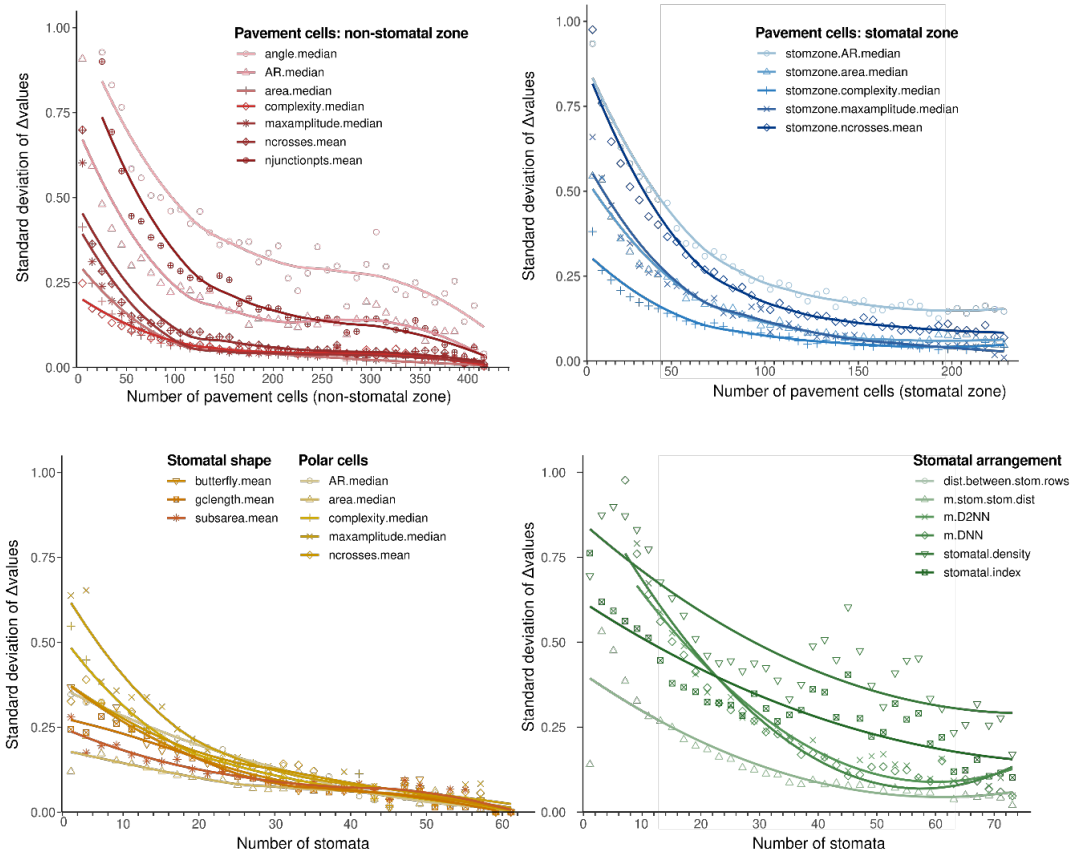

Figure 4.8 The convergence of measurements taken from subsamples of images. Cells from each image were sampled 100 times at a minimum patch size of 50, 100, 200 and 400 cells. Each of these samples were measured, and the difference between the sample and the whole image was calculated for each trait (the Δvalues). We then calculated the standard deviation of the Δvalues to evaluate convergence, to determine the optimal number of cells to sample. From these plots, we can infer that for Podocarpaceae, a minimum of 100 pavement cells and 30-50 stomatal complexes should be measured to allow estimation of all traits; smaller numbers may be adequate for some traits.

Discussion

EPIDERMALMORPH is the first software to synthesise the low-throughput measurements used by palaeobotanists and the quantitative, big-data approach that has been widely adopted to study individual cell traits. Our new metrics of cell wall undulation are unaffected by gross cell shape, and can be easily interpreted in a functional trait context. Our method is open-source,

modular and can be applied to a wide range of plants, which is vital to understanding the functional significance of leaf epidermal traits.

Part of the problem with untangling the functionality of epidermal traits seems to be that traits are under the control of different factors in different groups of plants. Some traits are controlled by evolutionary history (e.g. monocot stomatal shape), and there is evidence of phylogenetic signal in pavement cell shape (Vőfély *et al.*, 2019), but environment can also have significant direct effects on epidermal traits – one example of this is the difference between sun and shade leaves of the same individual (e.g. Bruschi *et al.*, 2000). Another widely-utilised trait-environment relationship is the correlation between stomatal index and atmospheric carbon dioxide concentration in *Ginkgo* (McElwain *et al.*, 2016), though this is not without controversy (Jordan, 1997, 2011).

It may be that trait-climate relationships are not simple and universal because they are clade-specific. Undulation in the periclinal walls of pavement cells is a prime example; it has been linked to light environment in many angiosperms (Metcalfe & Chalk, 1979; Kürschner, 1997; Thomas *et al.*, 2004), but not in grasses (Dunn *et al.*, 2015a). Furthermore, some species have deeply lobed cells regardless of environment (e.g. *Arabidopsis*), while others show significant plasticity in this trait (e.g. *Quercus*; Bruschi *et al*., 2000). Several functions of undulation have been hypothesised, including increased support for larger cells (Sapala *et al.*, 2019), leaf flexibility (Sotiriou *et al.*, 2018), biomechanical integrity (Jacques *et al.*, 2014) and increased surface area for cell-cell transport (Galletti & Ingram, 2015), but none of

these explanations explain undulation at a broad phylogenetic scale (Vőfély *et al.*, 2019). Cell elongation (aspect ratio) is another example – it can be used to predict the leaf aspect ratio (length to width) in monocots, ferns and gymnosperms, but not in angiosperms (Vőfély *et al.*, 2019). These findings demonstrate the limitations of generalising trait-function relationships in closely related species and the need to account for phylogenetic scope and structure in analyses of epidermal traits, something that we hope EPIDERMALMORPH will facilitate.

The limiting step in using EPIDERMALMORPH is tracing and annotating the cells. Automating this process is an exercise in semantic segmentation (see Marmanis *et al.*, 2016), and it may be possible to train a machine learning algorithm to perform this step. However, as noted by Vofely *et al.,* (2019), accurate segmentation of images is non-trivial, and poses a significant obstacle to high-throughput studies (though see recent work on stomatal detection by Fetter et al, 2019; Aono et al., 2021; Li et al., 2022). We found that the automated segmentation method implemented in PaCeQuant (Möller *et al.*, 2017) performed poorly on our image set (Figure S4.7). However, we found that complete segmentation of an image using our hybrid approach took between 10 minutes and 2 hours, and this can be substantially reduced by a) maximising the quality of the image (avoiding areas where the cuticle is folded/creased or where residual mesophyll is visible beneath the epidermis) and b) using only the optimal minimum number of cells as described above (*Sampling Effort*). Our dataset of fully annotated images is a valuable source of training data for future endeavours in this area. However, fully automated

segmentation may also introduce or amplify sampling biases; many species have epidermal cells that, regardless of preparation, are difficult to image with a high enough quality for automation (but are clear enough be traced manually). While automatic segmentation remains a promising avenue for epidermal image processing (e.g. Berg *et al.*, 2019; Aigouy *et al.*, 2020), we suggest that all images should be manually checked before trait extraction, as cell measurements could be significantly affected by poor segmentation.

Future development

We envisage that the EPIDERMALMORPH package will remain in active development and welcome suggestions for future trait inclusions.

This version of EPIDERMALMORPH is compatible with paracytic stomatal morphologies found in most Podocarpaceae. Because subsidiary cells are manually annotated, this version of EPIDERMALMORPH will still be able to process non-paracytic stomata. However, not all traits can be accurately measured for species that have stomata with a double layer of subsidiary cells (e.g. pericytic, polocytic stomata; Van Cotthem, 1970). We aim to include this functionality in future versions of the package.

We were unable to design an algorithmic approach to identifying and annotating hypoplastic (non-functional) stomata; this presents an opportunity for further development as the presence of hypoplastic stomata is a distinctive feature of some taxa (e.g. *Acmopyle*; Hill & Carpenter, 1991)) and quantification of non-functional stomata has not, to the best of our knowledge, been studied.

Conclusions

The leaf epidermis contains a wealth of information that is affected by both taxonomic identity and the growing environment. It can be studied in both living and fossil plants to provide insights into plant ecology, physiology and evolution, as well as being useful for palaeoclimatic estimation, but interpretations of epidermal traits remain clouded by convoluted relationships between form, function and ecology. It is our hope that taking a big-data approach to epidermal traits may help to reveal the evolutionary and physiological signals in the epidermis, and here we provide a suitable method to do so. Our novel approach to separating gross cell shape from undulation provides more robust measures of undulation that are not affected by cell elongation or non-convexity. This R package provides a fast and thorough method of quantifying epidermal traits that, with modification, can be applied both universally and to targeted groups of plants.

References

Aigouy, B., Cortes, C., Liu, S. & Prud'Homme, B. (2020) EPySeg: a coding-free solution for automated segmentation of epithelia using deep learning. *Development*, **147**, dev194589.

Andriankaja, M., Dhondt, S., De Bodt, S., Vanhaeren, H., Coppens, F., De Milde, L., Mühlenbock, P., Skirycz, A., Gonzalez, N. & Beemster, G.T. (2012) Exit from proliferation during leaf development in Arabidopsis thaliana: a not-so-gradual process. *Developmental cell*, **22**, 64-78.

Andruchow-Colombo, A., Escapa, I.H., Carpenter, R.J., Hill, R.S., Iglesias, A., Abarzua, A.M. & Wilf, P. (2019) Oldest record of the scale-leaved clade of Podocarpaceae, early Paleocene of Patagonia, Argentina. *Alcheringa*, **43**, 127-145.

Aono, A. H., Nagai, J. S., Dickel, G. D. S., Marinho, R. C., de Oliveira, P. E., Papa, J. P., & Faria, F. A. (2021). A stomata classification and detection system in microscope images of maize cultivars. *PloS one*, **16**(10), e0258679.

Bai, Y., Falk, S., Schnittger, A., Jakoby, M.J. & Hülskamp, M. (2010) Tissue layer specific regulation of leaf length and width in Arabidopsis as revealed by the cell autonomous action of ANGUSTIFOLIA. *The Plant Journal*, **61**, 191-199.

Berg, S., Kutra, D., Kroeger, T., Straehle, C.N., Kausler, B.X., Haubold, C., Schiegg, M., Ales, J., Beier, T. & Rudy, M. (2019) Ilastik: interactive machine learning for (bio) image analysis. *Nature Methods*, **16**, 1226-1232.

Bidhendi, A.J., Altartouri, B., Gosselin, F.P. & Geitmann, A. (2019) Mechanical stress initiates and sustains the morphogenesis of wavy leaf epidermal cells. *Cell reports*, **28**, 1237-1250.

Biffin, E., Conran, J. & Lowe, A.J. (2011) Podocarp evolution: a molecular phylogenetic perspective. *Ecology of the Podocarpaceae in tropical forests* (ed. by L.a.C. B. L. Turner), pp. 1-20. Smithsonian Contributions to Botany.

Blomenkemper, P., Bäumer, R., Backer, M., Abu Hamad, A., Wang, J., Kerp, H. & Bomfleur, B. (2021) Bennettitalean Leaves From the Permian of Equatorial Pangea—The Early Radiation of an Iconic Mesozoic Gymnosperm Group. *Frontiers in Earth Science*, **9**, 162.

Bruschi, P., Vendramin, G.G., Bussotti, F. & Grossoni, P. (2000) Morphological and molecular differentiation between *Quercus petraea* (Matt.) Liebl. and *Quercus pubescens* Willd.(Fagaceae) in northern and central Italy. *Annals of Botany*, **85**, 325-333.

Bush, R.T., Wallace, J., Currano, E.D., Jacobs, B.F., McInerney, F.A., Dunn, R.E. & Tabor, N.J. (2017) Cell anatomy and leaf δ13C as proxies for shading and canopy structure in a Miocene forest from Ethiopia. *Palaeogeography, Palaeoclimatology, Palaeoecology*, **485**, 593-604.

Carins Murphy, M.R., Jordan, G.J. & Brodribb, T.J. (2016) Cell expansion not cell differentiation predominantly co-ordinates veins and stomata within and among herbs and woody angiosperms grown under sun and shade. *Annals of Botany*, **118**, 1127-1138.

Clugston, J., Jeffree, C., Ahrends, A. & Mill, R. (2017) Do environmental factors affect the taxonomic reliability of leaf cuticular micromorphological characters? A case study in Podocarpaceae. *Edinburgh Journal of Botany*, **74**, 299-343.

Deng, M., Jiang, X.-L., Song, Y.-G., Coombes, A., Yang, X.-R., Xiong, Y.-S. & Li, Q.-S. (2017) Leaf epidermal features of Quercus Group Ilex (Fagaceae) and their application to species identification. *Review of Palaeobotany and Palynology*, **237**, 10-36.

Dilcher, D.L. (1974) Approaches to the identification of angiosperm leaf remains. *The Botanical Review*, **40**, 1-157.

Dunn, R.E., Le, T.Y.T. & Stromberg, C.A.E. (2015a) Light Environment and Epidermal Cell Morphology in Grasses. *International Journal of Plant Sciences*, **176**, 832-847.

Dunn, R.E., Stromberg, C.A., Madden, R.H., Kohn, M.J. & Carlini, A.A. (2015b) Linked canopy, climate, and faunal change in the Cenozoic of Patagonia. *Science*, **347**, 258-61.

Farjon, A. (2010) *A Handbook of the World's Conifers*. Brill, Leiden/Boston.

Fetter, K. C., Eberhardt, S., Barclay, R. S., Wing, S., & Keller, S. R. (2019). StomataCounter: a neural network for automatic stomata identification and counting. *New Phytologist*, **223**(3), 1671-1681.

Galletti, R. & Ingram, G.C. (2015) Communication is key: Reducing DEK1 activity reveals a link between cell-cell contacts and epidermal cell differentiation status. *Communicative & Integrative Biology*, **8**, e1059979.

Hill, R. & Carpenter, R. (1991) Evolution of Acmopyle and Dacrycarpus (Podocarpaceae) foliage as inferred from macrofossils in south-eastern Australia. *Australian Systematic Botany*, **4**, 449-479.

Hill, R.S. & Brodribb, T.J. (1999) Turner Review No. 2 - Southern conifers in time and space. *Australian Journal of Botany*, **47**, 639-696.

Hill, R.S., & Pole, M. S. (1992) Leaf and Shoot Morphology of Extant Afrocarpus, Nageia and Retrophyllum (Podocarpaceae) Species, and Species with Similar Leaf Arrangement, from Tertiary Sediments in Australasia. *Australian Systematic Botany*, **5**, 337-358.

Jacques, E., Verbelen, J.-P. & Vissenberg, K. (2014) Review on shape formation in epidermal pavement cells of the Arabidopsis leaf. *Functional Plant Biology*, **41**, 914-921.

Jordan, G.J. (1997) Uncertainty in palaeoclimatic reconstructions based on leaf physiognomy. *Australian Journal of Botany*, **45**, 527-547.

Jordan, G.J. (2011) A critical framework for the assessment of biological palaeoproxies: predicting past climate and levels of atmospheric CO(2) from fossil leaves. *New Phytol*, **192**, 29-44.

Kelch, D.G. (2002) Phylogenetic assessment of the monotypic genera *Sundacarpus* and *Manoao* (Coniferales: Podocarpaceae) utilising evidence from 18S rDNA sequences. *Australian Systematic Botany*, **15**, 29-35.

Kubínová, L. (1994) Recent stereological methods for measuring leaf anatomical characteristics: estimation of the number and sizes of stomata and mesophyll cells. *Journal of Experimental Botany*, **45**, 119-127.

Kürschner, W.M. (1997) The anatomical diversity of recent and fossil leaves of the durmast oak (Quercus petraea Lieblein/Q. pseudocastanea Goeppert)—implications for their use as biosensors of palaeoatmospheric CO2 levels. *Review of Palaeobotany and Palynology*, **96**, 1-30.

Li, S., Li, L., Fan, W., Ma, S., Zhang, C., Kim, J. C., ... & Zhou, Y. (2022). LeafNet: A Tool for Segmenting and Quantifying Stomata and Pavement Cells. *The Plant Cell* (in press).

Leslie, A.B., Beaulieu, J., Holman, G., Campbell, C.S., Mei, W., Raubeson, L.R. & Mathews, S. (2018) An overview of extant conifer evolution from the perspective of the fossil record. *American journal of botany*, **105**, 1531-1544.

Marmanis, D., Wegner, J.D., Galliani, S., Schindler, K., Datcu, M. & Stilla, U. (2016) Semantic segmentation of aerial images with an ensemble of CNSS. *ISPRS Annals of the Photogrammetry, Remote Sensing and Spatial Information Sciences, 2016*, **3**, 473-480.

McElwain, J.C., Montañez, I., White, J.D., Wilson, J.P. & Yiotis, C. (2016) Was atmospheric CO_2 capped at 1000 ppm over the past 300 million years? *Palaeogeography, Palaeoclimatology, Palaeoecology*, **441**, 653-658.

McLellan, T. & Endler, J.A. (1998) The relative success of some methods for measuring and describing the shape of complex objects. *Systematic Biology*, **47**, 264-281.

Metcalfe, C. & Chalk, L. (1979) Anatomy of the dicotyledons. Vol I. Systematic anatomy of leaf and stem, with a brief history of the subject. *Anatomy of the dicotyledons. Vol I. Systematic anatomy of leaf and stem, with a brief history of the subject.*,

Möller, B., Poeschl, Y., Plötner, R. & Bürstenbinder, K. (2017) PaCeQuant: A Tool for High-Throughput Quantification of Pavement Cell Shape Characteristics. *Plant Physiology*, **175**, 998-1017.

Mosbrugger, V. & Utescher, T. (1997) The coexistence approach—a method for quantitative reconstructions of Tertiary terrestrial palaeoclimate data using plant fossils. *Palaeogeography, Palaeoclimatology, Palaeoecology*, **134**, 61-86.

Nowak, J., Eng, R.C., Matz, T., Waack, M., Persson, S., Sampathkumar, A. & Nikoloski, Z. (2021) A network-based framework for shape analysis enables accurate characterization of leaf epidermal cells. *Nature Communications*, **12**, 1-13.

Osunkoya, O.O., Boyne, R. & Scharaschkin, T. (2014) Coordination and plasticity in leaf anatomical traits of invasive and native vine species. *American Journal of Botany*, **101**, 1423-1436.

Page, C.N. (2019) New and maintained genera in the taxonomic alliance of *Prumnopitys* s. l.(Podocarpaceae), and circumscription of a new genus: Pectinopitys. *New Zealand Journal of Botany*, **57**, 137-153.

Royer, D. (2001) Stomatal density and stomatal index as indicators of paleoatmospheric CO_2 concentration. *Review of Palaeobotany and Palynology*, **114**, 1-28.

Sánchez-Corrales, Y.E., Hartley, M., Van Rooij, J., Marée, A.F. & Grieneisen, V.A. (2018) Morphometrics of complex cell shapes: lobe contribution elliptic Fourier analysis (LOCO-EFA). *Development*, **145**, dev156778.
Sapala, A., Runions, A. & Smith, R.S. (2019) Mechanics, geometry and genetics of epidermal cell shape regulation: different pieces of the same puzzle. *Current Opinion in Plant Biology*, **47**, 1-8.
Sharma, G. (1972) Environmental modifications of leaf epidermis and morphological features in *Verbena canadensis*. *The Southwestern Naturalist*, 221-228.
Song, W., Li, J., Li, K., Chen, J. & Huang, J. (2020) An automatic method for stomatal pore detection and measurement in microscope images of plant leaf based on a convolutional neural network model. *Forests*, **11**, 954.
Sotiriou, P., Giannoutsou, E., Panteris, E., Galatis, B. & Apostolakos, P. (2018) Local differentiation of cell wall matrix polysaccharides in sinuous pavement cells: its possible involvement in the flexibility of cell shape. *Plant Biology*, **20**, 223-237.
Stark Schilling, D.M. & Mill, R.R. (2011) Cuticle micromorphology of Caribbean and central american species of *Podocarpus* (Podocarpaceae). *International Journal of Plant Sciences*, **172**, 601-631.
Steger, C. (1998) An unbiased detector of curvilinear structures. *IEEE Transactions on pattern analysis and machine intelligence*, **20**, 113-125.
Strimas-Mackey, M.E. (2021) *smoothr: Smooth and tidy spatial features. R package 0.2.1.* .
Thomas, P.W., Woodward, F.I. & Quick, W.P. (2004) Systemic irradiance signalling in tobacco. *New Phytologist*, **161**, 193-198.
Thorsten Wagner, M.H., & xraynaud (2017) *Ridge Detection*. Zenodo.
Van Cotthem, W. (1970) A classification of stomatal types. *Botanical Journal of the Linnean Society*, **63**, 235-246.
Vőfély, R.V., Gallagher, J., Pisano, G.D., Bartlett, M. & Braybrook, S.A. (2019) Of puzzles and pavements: a quantitative exploration of leaf epidermal cell shape. *New Phytol*, **221**, 540-552.
Wilf, P., Zhang, S., Chikkerur, S., Little, S.A., Wing, S.L. & Serre, T. (2016) Computer vision cracks the leaf code. *Proceedings of the National Academy of Sciences*, **113**, 3305-3310.

Chapter 5 : Nature or nurture: Investigating the basis of variation and palaeoecological value of epidermal traits in Podocarpaceae

Introduction

Characteristics of the leaf epidermis are frequently preserved in the fossil record and thus can provide a potential wealth of information on both the fossil species and the palaeoenvironment; however, the basis of many of the relationships between traits, climate and evolutionary history is poorly understood. The links between adaptation and plasticity in macroscopic leaf traits have been studied extensively (Wilf *et al.*, 1998; Rehfeldt *et al.*, 2001; Wright *et al.*, 2004; Franks *et al.*, 2014; Moreira *et al.*, 2014; Yiotis *et al.*, 2017; Mizutani & Kanaoka, 2018, Milligan *et al.*, 2021), resulting in both univariate and multivariate tools for palaeoclimatic estimation (e.g. CLAMP; Wolfe, 1993; Spicer, 2009; Spicer *et al.*, 2020), but the epidermis has received comparatively little attention in this context.

The cuticle of leaves can preserve an imprint of the epidermal cells for tens or even hundreds of millions of years (Vajda *et al.*, 2017), and fragments of cuticle often survive where complete leaves do not (Blomenkemper *et al.*, 2021). Various epidermal traits can be measured from the cuticle, especially size, shape and arrangement of the major epidermal cell types: guard cells, subsidiary cells, trichome cells and epidermal pavement cells (see Chapter 4 of this thesis). Many of these traits have well-studied links with environment and phylogeny in living plants (see Chapter 4 of this thesis; Thomas *et al.*, 2004; Carins Murphy *et al.*, 2014, 2016), and these can be used to glean information from the fossil record. Fossil traits can be used to estimate the palaeoenvironmental conditions directly (physiognomy; e.g. Royer *et al.*, 2007) or to identify the fossil and then apply nearest living relative (NLR) techniques (e.g. Mosbrugger & Utescher, 1997). Both these approaches have advantages and limitations (see Spicer *et al.*, 2020), but understanding the genetic and environmental control of traits is crucial to understand the

limitations of each technique. It may also be possible to use epidermal traits to better understand no-analogue fossils (co-occurring fossils for which the nearest living relatives inhabit different climatic conditions, Jordan, 1997; Brown et. al. 2021). If we can identify differences in functional traits between the fossil and its extant counterpart, we can link these to differences in ecology between the two taxa and quantify these differences in terms of climate.

Identifying functional traits and the mechanisms that underpin them can be challenging because traits can be under the control of environment or genetics ('nature vs nurture'). Standard quantitative genetics approaches divide the variation in a trait or phenotype in a given system into three components: the pure effects of environment (E), in which the plastic response to environment is the same for all genotypes; the pure effects of genotype (G), in which the trait varies according to genotype but shows no plasticity; and the effects of interactions between genotype and environment (G x E), in which there are plastic responses to environment but these responses vary among genotype (Falconer, 1996). These components are typically expressed as proportions of the total variation within the system. Traits under 100% genotypic control will be expressed regardless of growing environment – for this reason, they are particularly useful for taxonomic identification and nearest living relative methods. Some functional traits are under strong genetic control; plants with certain adaptations to aridity (e.g., succulence, small leaves) will still display these traits even when grown in a well-watered environment. Theoretically, traits under 100% environmental control are plastic; stomatal index in *Gingko* has been cited as an example because of its documented correlation with atmospheric CO_2 concentration in extant plants (Beerling *et al.*, 1998; Haworth *et al.*, 2012; McElwain & Steinthorsdottir, 2017), though it is not clear whether this is a true example of a pure environmental effect (Jordan 2011). Environment (E) and genotype by environment (GxE) effects both involve plasticity, but the difference is that E is the plastic response to environment independent of genotypes and G x E reflects the way that the plastic response varies with genotype (e.g. plastic

responses to light intensity that depend on taxonomic identity Thomas *et al.*, 2004; Dunn *et al.*, 2015). Here, we use 'G-traits' and 'E-traits' to refer to traits that have high (c.100%) genotypic and environmental components of variation, respectively.

For palaeoclimatic estimation, E-traits and adaptive G-traits have the greatest utility as proxies, but the categorisation of these traits is highly system-specific: an E-trait in one group of plants may be a G-trait or G x E-trait in another group, or vice-versa. In general, expansion of the system will increase the likelihood that any given trait is under G x E control (Figure 5.1) because no trait is infinitely plastic. This is an important consideration when applying these concepts to the fossil record, because it is nearly impossible to be sure that the fossil falls within the same system that was used to calibrate the proxy (Jordan, 2011).

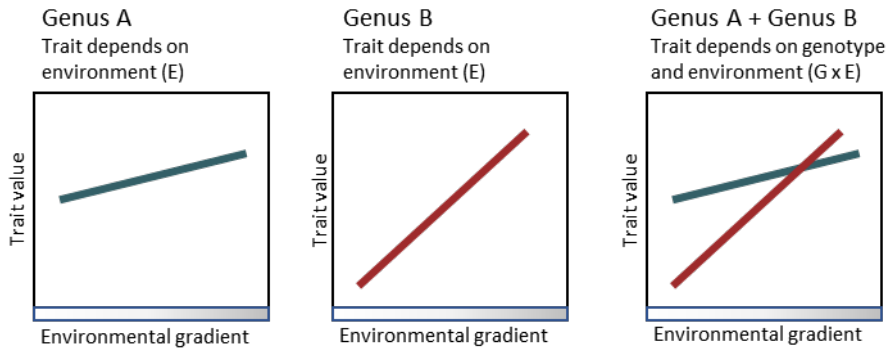

Figure 5.1 Effect of system on trait control. In both Species A and Species B, all variation in this trait is under environmental control; this is an 'E-trait'. However, in the system containing both these species (Species A + Species B), variation is no longer explained by environment; it is explained by the interaction between genotype and environment (G x E). In general, adding taxa to a system will decrease the pure G- and E-components of trait variation, and increase the G x E-component.

Traits with strong G x E components are challenging proxies, as they challenge the assumptions of both NLR approaches and physiognomic approaches (see Spicer et al. 2020). This poses problems for using traits in a palaeoecological setting as it is difficult to be confident that predictions

calibrated on a modern system hold for a palaeontological system. This is particularly fraught for relationships that are calibrated on a single extant species (e.g. *Ginkgo*; Jordan 2011), or where clades have suffered high levels of extinctions. However, if we can identify consistent trait-climate relationships in relatively large and diverse clades, we can be more confident that fossil species are *within*, rather than *adjacent* to these clades, so we can thus be more confident in predictions derived from these models. One clade that is large, diverse and abundant in the fossil record is the Podocarpaceae, making it an ideal group in which to search for good palaeoecological proxies.

The Podocarpaceae is the largest of the 'southern conifer' families, with 17-20 genera and 156 species (Farjon, 2010; Page, 2019). Species of Podocarpaceae (podocarps) inhabit a wide range of environments across the southern hemisphere (and parts of the northern hemisphere), including lowland tropical rainforests, alpine shrubberies, and even seasonally dry regions, although this is not typical for the family (Farjon & Filer, 2013). Podocarps also display a wide range of leaf morphologies, ranging from the appressed, imbricate scale leaves in *Lagarostrobos* to the broad multi-veined leaves of *Nageia*, and this diversity is reflected in their anatomical variation (Stockey & Frevel, 1997; Stockey *et al.*, 1998; Mill & Stark Schilling, 2009; Carpenter *et al.*, 2011; Stark Schilling & Mill, 2011). Podocarps are ubiquitous in the Mid-Mesozoic to Cenozoic palaeobotanical record of the southern hemisphere (Hill & Brodribb, 1999), and their leaf epidermal traits are a key part of studying these fossils (Jordan *et al.*, 2011; Andruchow-Colombo *et al.*, 2019). These traits include characters from both epidermal pavement cells, which can be rectangular, elongated or irregularly shaped, with straight or undulated walls ranging in in size from 500um^2 to over 3000um^2 (this chapter); and stomata, which are generally paracytic or paratetracytic (two lateral subsidiary cells with or without polar subsidiary cells), and in most genera form bands parallel to the leaf axis, although these bands can be irregular or discontinuous. Some traits are taxonomically informative (indicating genetic control; Wells & Hill, 1989), and there is

evidence for the effect of environment (Clugston *et al.*, 2017), but there has not yet been a family-level examination of the extent and relative contribution of each of these components across a broad suite of epidermal traits. This is probably due to the labour-intensive nature of measuring epidermal traits (though see Chapter 4, this thesis) and also because disentangling the genetic and environmental controls on variation can be challenging for slow-growing conifers.

The 'gold standard' for studying genotypic versus environmental control of traits is to undertake multiple common garden experiments, where species or genotypes are cultivated in a range of environmental conditions to distinguish plastic from genotypic responses. Coniferous common garden experiments are uncommon because of the generally slow-growing nature of these plants – there are long-term conifer common gardens in Poland (Wyka *et al.*, 2012) and Canada (Depardieu *et al.*, 2020), but these are usually planted with specific hypotheses in mind and are limited to a few taxa and environmental variables. For studies of conifers, it is not impossible to find natural common garden experiments – by sampling species across their environmental ranges – but in most cases it would be unfeasible to collect fresh material or would require a significant amount of destructive sampling of herbarium specimens. A more common approach for conifers is to use a simplified common garden – where data are collected from plants that have been cultivated in identical or similar environmental conditions (e.g. Fig. 3; Pittermann *et al.*, 2012). This reduces the effect of plasticity so that genotypic control of traits can be isolated.

Here, I analysed variation in the leaf epidermal traits of Podocarpaceae using a simplified common garden approach to identify adaptive, genotypically-controlled traits. To do this, I identified traits that can be reliably measured for an individual (i.e. are constant within a genotype), and compared these traits to the climatic conditions that these species inhabit in their native ranges. I constructed machine learning models to predict suitable climatic conditions from epidermal traits, then assessed the performance of these models to evaluate the potential of these traits to be used as proxies.

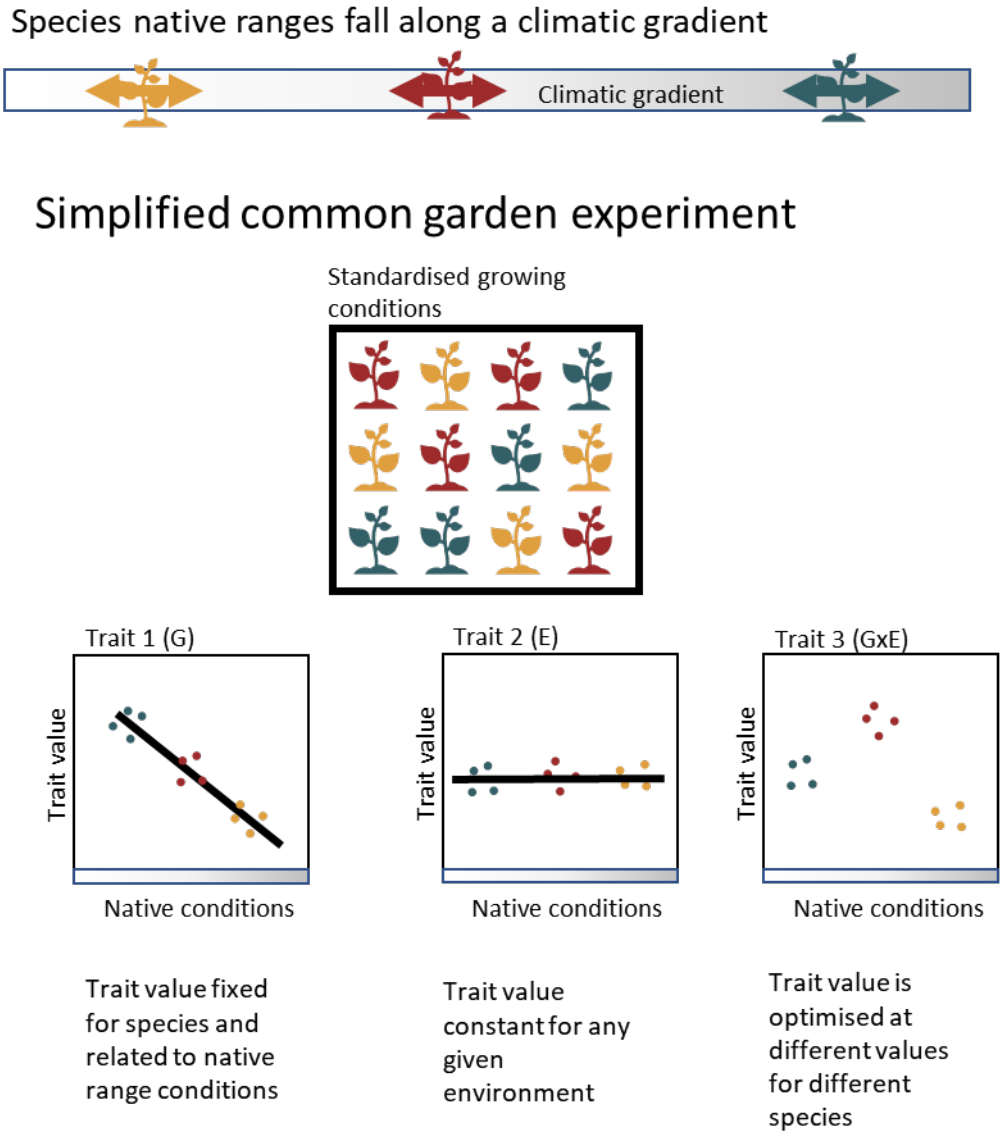

Figure 5.2 Example of trait-climate relationships for a simplified common garden experiment, depending on the dominant control of the trait. Note that in this experimental design, a pure E-trait cannot be distinguished from a trait that is fixed within a system – this is a limitation of the simplified common garden experiment.

Methods

Sample preparation and image capture

We sampled 56 individual greenhouse-grown plants spanning 45 species and seven genera (see Table 5.1). Only genera with dorsiventrally or bifacially flattened leaves were included – taxa with scale-like or awl-like leaves were excluded because I could not obtain a field of view

(approximately 1mm) that did not include the edge of the leaf in these species. Fully expanded adult leaves were collected from healthy plants grown at the University of Tasmania and the Royal Botanic Gardens Edinburgh (Table 5.1). These plants were all growing in shaded, frost-free greenhouses. For species with a wide geographic distribution, I sampled leaves from individuals with multiple provenances (where this was possible).

For large leaves, pieces of approximately 1cm^2 were cut from either side of the midrib in the middle third of the leaf; for smaller leaves, the base, apex and, if practicable, the margins were removed. These samples were soaked in commercial household bleach (50 gL^{-1} sodium hypochlorite and 13 gL^{-1} sodium hydroxide) until the cuticle separated from the mesophyll. Bleach was removed by thoroughly rinsing in water and remaining mesophyll tissue was removed using a fine paintbrush. Sections were stained with 1% crystal violet or safranin solution for 1 minute, then mounted in phenol glycerine jelly. I targeted the surface of the leaf that bore more stomata – usually the abaxial surface – and selected fields of view that contained at least 30 stomata, as suggested by Brown et al (Chapter 4, this thesis). Where stomata were concentrated in distinct regions (particularly where there were <3 pavement cells between each stomatal complex), fields of view were oriented to capture a balance of both stomata and pavement cells (see Figure S1.5 for example). Several fields of view at ×10 magnification (field of view area, 0.56mm^2) were photographed from each section using a Nikon Digital Sight DS-L1 camera (Melville, NY, USA) mounted on a Leica DM 1000 microscope (Nussloch, Germany). The best image (identified as the clearest, without damage or obvious distortion) for each individual plant was selected for analyses.

Table 5.1 Plants sampled in this study. Plants were sampled from the Royal Botanical Gardens, Edinburgh (RBGE) or the University of Tasmania, Hobart (UTAS).

PLANT ID	SPECIES	COLLECTED FROM	ACCESSION #
Acmopyle_pancheri1	*Acmopyle pancheri*	RBGE	19842681
Acmopyle_pancheri2		RBGE	19842747
Acmopyle_pancheri3		UTAS	-
Acmopyle_sahniana1	*Ac. sahniana*	RBGE	20001736
Acmopyle_sahniana2		UTAS	-
Afrocarpus_falcatus1	*Afrocarpus falcatus*	RBGE	20001613
Afrocarpus_falcatus2		UTAS	-
Afrocarpus_gracilior1	*Af. gracilior*	RBGE	19820027
Afrocarpus_mannii1	*Af. mannii*	RBGE	19960587
Dacrycarpus_imbricatus1	*Dacrycarpus imbricatus*	UTAS	-
Dacrycarpus_kinabaluensis1	*D. kinabaluensis*	RBGE	19801226
Falcatifolium_taxoides1	*Falcatifolium taxoides*	UTAS	-
Falcatifolium_taxoides2		UTAS	-
Halocarpus_biformis1	*Halocarpus biformis*	UTAS	-
Halocarpus_kirkii1	*Halocarpus kirkii*	UTAS	-
Nageia_formosensis1	*Nageia formosensis*	UTAS	-
Nageia_nagi1	*N. nagi*	RBGE	19963671
Nageia_nagi2		UTAS	-
Pectinopitys_ferruginea1	*Pectinopitys ferruginea*	RBGE	19842376
Pectinopitys_ladei1	*Pe. ladei*	UTAS	-
Phyllocladus_aspleniifolius1	*Phyllocladus aspleniifolius*	UTAS	-
Phyllocladus_toatoa1	*Ph. toatoa*	UTAS	-
Phyllocladus_trichomanoides1	*Ph. trichomanoides*	UTAS	-
Podocarpus_affinis1	*Podocarpus affinis*	RBGE	20091132
Podocarpus_angustifolius1	*Po. angustifolius*	RBGE	200316
Podocarpus_brassii1	*Po. brassii*	UTAS	-
Podocarpus_chingianus1	*Po. chingianus*	RBGE	19951686
Podocarpus_coriaceus1	*Po. coriaceus*	RBGE	20030490
Podocarpus_costalis1	*Po. costalis*	RBGE	19763956
Podocarpus_dispermus1	*Po. dispermus*	UTAS	-

Podocarpus_dispermus2		RBGE	20110038
Podocarpus_drouynianus1	*Po. drouynianus*	UTAS	-
Podocarpus_forrestii1	*Po. forrestii*	RBGE	19915024
Podocarpus_gnidioides1	*Po. gnidioides*	UTAS	-
Podocarpus_lambertii1	*Po. lambertii*	UTAS	-
Podocarpus_latifolius1	*Po. latifolius*	UTAS	-
Podocarpus_longefoliolatus1	*Po. longefoliolatus*	RBGE	19842738
Podocarpus_lucienii1	*Po. lucienii*	RBGE	20010205
Podocarpus_matudae1	*Po. matudae*	RBGE	19972324
Podocarpus_nakaii1	*Po. nakaii*	RBGE	19763844
Podocarpus_neriifolius1	*Po. neriifolius*	UTAS	-
Podocarpus_neriifolius2		RBGE	19681468
Podocarpus_novae-caledoniae1	*Po. novae-caledoniae*	UTAS	-
Podocarpus_pilgeri1	*Po. pilgeri*	RBGE	20022521
Podocarpus_purdieanus1	*Po. purdieanus*	RBGE	20011344
Podocarpus_sellowii1	*Po. sellowii*	RBGE	20071743
Podocarpus_sylvestris1	*Po. sylvestris*	UTAS	-
Podocarpus_trinitensis1	*Po. trinitensis*	RBGE	20030491
Podocarpus_urbanii1	*Po. urbanii*	RBGE	20011359
Podocarpus_urbanii2		RBGE	20011364
Retrophyllum_minus1	*Retrophyllum minus*	UTAS	-
Retrophyllum_rospigliossii1	*R. rospigliossii*	RBGE	19951953
Retrophyllum_rospigliossii2		UTAS	-
Saxegothaea_conspicua1	*Saxegothaea conspicua*	UTAS	-
Sundacarpus_amarus1	*Sundacarpus amarus*	RBGE	20030752
Sundacarpus_amarus2		UTAS	-

Image processing and feature extraction

Cell outlines were traced using a combination of Ridge Detection (based on the method described by Steger, 1998) in ImageJ and manual tracing. Cell walls were set to 3 pixels (approximately 1 um) wide. Stomata (pore + guard cell pair) and lateral subsidiary cells were manually annotated using the flood fill tool. I then used the EPIDERMALMORPH package (Chapter 4 of this thesis) to

extract 26 measurements from each image (detailed explanations and illustrations given in Chapter 4 of this thesis), then centred and scaled these measurements using a z-transformation.

To align the rotation of images, I used the mean angle of the stomata as a proxy for leaf axis (stomata are arranged parallel to the leaf axis in the Podocarpaceae taxa studied here). The angles of pavement cells and individual stomata are calculated relative to this angle.

Trait reliability

To select only reliable traits, I used the dataset described in Chapter 4 of this thesis, which was collected from a subsample of plants used in this study. I removed all variables that had a within-plant standard deviation greater than 0.2 (i.e., where the standard deviation for that plant exceeded 20% of the total standard deviation for that trait), leaving 26 variables that I included in these analyses.

Environmental variables

I examined the relationships between epidermal traits and five palaeoecological predictors: maximum tree height, mean annual precipitation (MAP), precipitation of the driest month, mean temperature of the warmest quarter, minimum temperature of the coldest month. For the climatic variables, I used the distributional extremes (e.g. the minimum and maximum MAP for a species), which have been shown to be more closely correlated to functional trait values than the mean or median of the climatic niche (Stahl *et al.*, 2014). I included maximum tree height as an environmental variable because of its potential utility for palaeovegetation reconstruction; the vegetation structure of a community is dictated by the height of the plants, so a method of estimating maximum tree height from fossilised cuticle would be extremely valuable for fossil sites where plant form is not preserved. I collated tree height data from Farjon (2010), Eckenwalder (2009) and climate data from the dataset used by Larcombe *et al.* (2018). These climate data are based on the same occurrence records that I used in previous chapters

of this thesis (Brown *et al.*, 2020; Brown *et al.*) and have been cleaned extensively to exclude erroneous, naturalised or cultivated records. For species with uncertain taxonomic status (*Nageia formosensis, Podocarpus forrestii*) I used data for the synonym (*Nageia nagi*) or from the eFlora of China (http://www.efloras.org/). All nine variables used in analysis and their abbreviations are given in Table 5.2.

Table 5.2 Palaeoecological variables of interest.

Variable	Linked to	Minimum	Maximum
Tree height	Shade tolerance & vegetation type	-	max.height
Mean annual precipitation	Drought tolerance	map.min	map.max
Precipitation of the driest month	Drought tolerance	pdryq.min	pdryq.max
Mean temperature of the warmest quarter	Growing season length	meantwmq.min	meantwmq.max
Minimum temperature of the coldest month	Freezing tolerance	mintcm.min	mintcm.max

Statistical analysis

All analyses were performed in R (R Core Team, 2021). I performed correlation checks using the ‘cor’ function and used the ‘princomp’ function for Principal Components Analysis (PCA). I also fitted Random Forest regression models using the ‘caret’ package (Kuhn 2021). I tuned the ‘mtry’ parameter (the number of variables to be sampled at each split of the decision tree) by fitting models with values of mtry between two and 30, assessed by 10-fold cross-validation (three repeats). I used Random Forest regression because this ensemble learning approach is a powerful way of finding non-linear responses to high numbers of predictors (Jordan & Mitchell, 2015).

Results

Correlations between epidermal traits and climate

Unsurprisingly, there are strong correlations between climatic variables (Figure 5.3a). Although several epidermal traits are correlated with each other (e.g. stomatal index and stomatal density, Figure 5.3b, Table S5.1), principal component analysis revealed that 11 principal component axes are required to capture 90% of the variation, with the first two capturing 25% and 19%, respectively (Table S5.2). Individuals of the same genus tended to display similar trait values (Figure 5.4a, c). The first two principal components mainly reflected variation in pavement cell size and shape traits (Figure 5.4b), while the third and fourth mainly reflected variation in stomatal traits (Figure 5.4d).

There were no strong single-trait correlations between epidermal morphology and environment (Figure 5.3c, Table S5.3). There were some weak links – maximum height was correlated with stomatal index (correlation coefficient of -0.41; Table S5.3) and the complexity (undulation) of pavement cells (correlation coefficient of 0.35; Table S5.3). Scatterplots of each trait versus each palaeoecological variable are available in the Supporting Information (Fig S1-9).

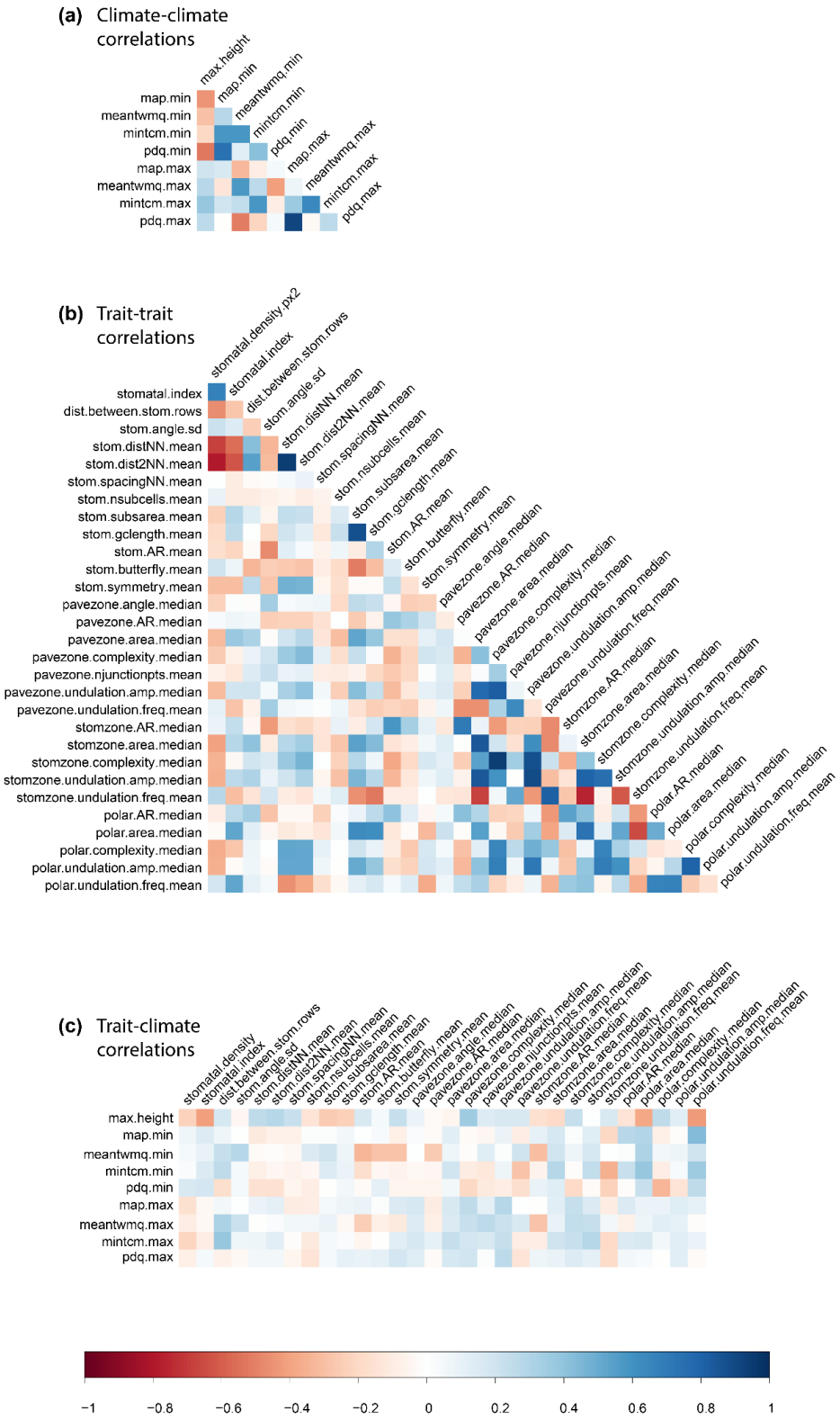

Figure 5.3 Correlations between climatic variables and epidermal traits. The Pearson correlation coefficient between climate-climate variables (a), trait-trait correlations (b) and trait-climate correlations (c). The colour of each tile shows the strength of the correlation, where weak correlations (close to 0) are lighter, and strong correlations are darker. Positive correlations are shown in blue and negative correlations are shown in red.

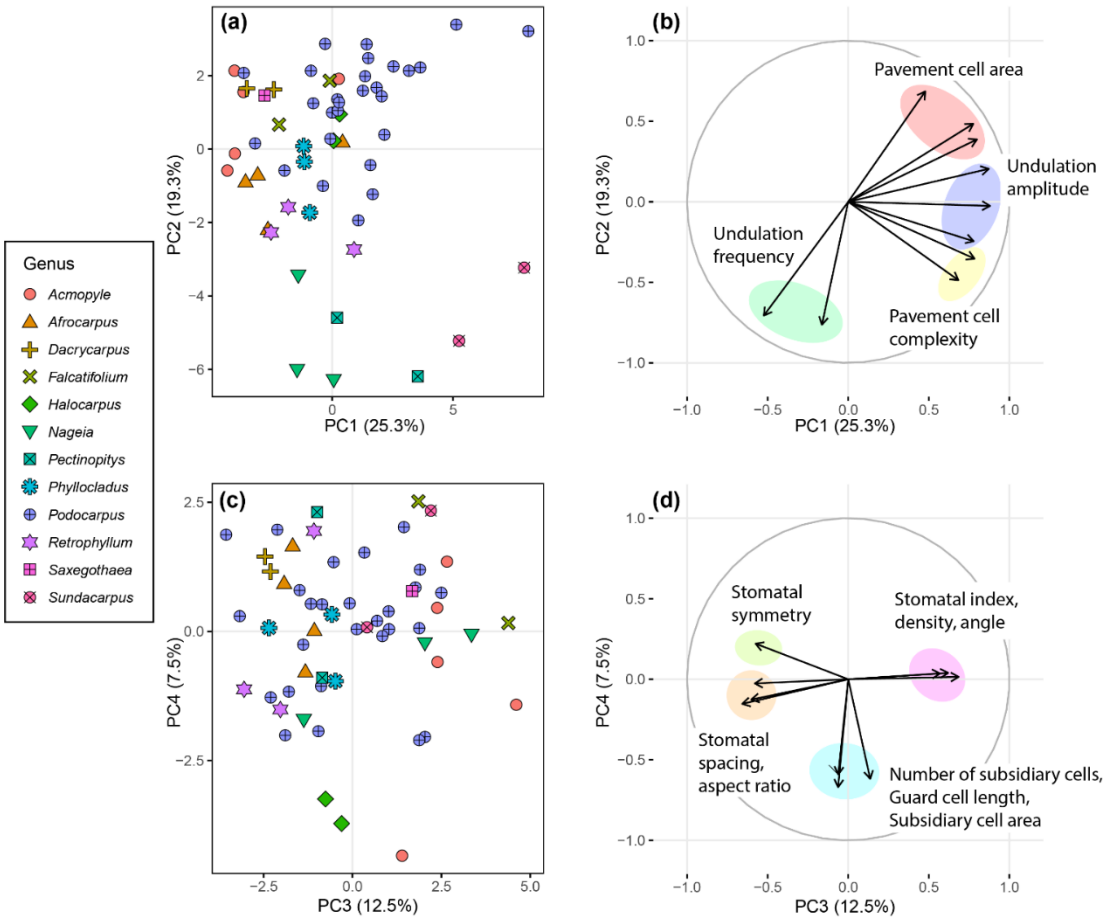

Figure 5.4 Principal components analysis of epidermal traits. The first two principal components (a,b) mainly reflect variation in pavement cell size and shape traits (b), the third (c-d) in stomatal distribution (density, index, distance to first and second nearest neighbours) and shape (aspect ratio, symmetry), while the fourth (c-d) in stomatal complex size (guard cell length, subsidiary cell area) and number of subsidiary cells. Plants from the same genus tended to display similar trait values (a, c). Only the first ten contributing variables for each plot (b,d) are shown.

Random forest analyses

It was not possible to accurately predict the value of any environmental trait (including maximum tree height) from epidermal characters (Table 5.3). The best predictive model was for the lower limit of mean temperature of the warmest quarter (meantwmq.min), which had an r^2 value of 0.34.

Table 5.3 Results of Random Forest regression models fitted to each environmental variable, along with the best mtry parameter (the best number of variables to sample at each split of the decision tree), the r^2 values and the most important variables in the best model.

Environmental variable	Best mtry	r^2	Most important variables
max.height	4	0.30	polar.area.median, polar.undulation.freq.mean, pavezone.complexity.median,
map.min	28	0.19	polar.undulation.freq.mean, stom.angle.sd, stom.gclength.mean
map.max	28	0.21	pavezone.undulation.amp.median, polar.AR.median, pavezone.njunctionpts.mean
meantwmq.min	4	0.34	stom.nsubcells.mean, stomzone.AR.median, stom.AR.mean
meantwmq.max	5	0.26	dist.between.stom.rows, stom.nsubcells.mean, stom.AR.mean
mintcm.min	23	0.23	polar.undulation.freq.mean, stom.spacingNN.mean, stom.symmetry.mean
mintcm.max	9	0.25	pavezone.njunctionpts.mean, dist.between.stom.rows pavezone.angle.median
pdq.min	5	0.22	dist.between.stom.rows, polar.complexity.median, pavezone.complexity.median
pdq.max	14	0.30	pavezone.undulation.amp.median, polar.AR.median, stom.butterfly.mean,

Discussion

Most variation in epidermal traits appears to be related to taxonomic identity, rather than adaptation to the environmental characteristics I studied here. Although there were some weak correlations between traits and distribution, they could not be used to reliably predict the distributional limits of species. The variation that I observed was greater than one would expect for traits

that are under environmental control (where I would expect to see convergence on optimum trait values; Figure 5.1). Thus, it seems likely that most variation in epidermal traits in this family has a high G x E component, so calibrating epidermal physiognomic proxies will require characterisation of both the genotypic and plastic components of variation. Epidermal traits are routinely used to identify fossil podocarps (e.g. Hill & Carpenter, 1991; Mill & Stark Schilling, 2009; Stark Schilling & Mill, 2011), and indeed I found that individuals from the same genus tended to have similar traits (Figure 5.4), so there is likely to be a strong taxonomic or phylogenetic signal in these traits.

Our restriction of sampling to plants that were grown in greenhouses severely limited the sample size and capacity to directly test for phylogenetic and plastic environmental signal in our results. However, related species have similar traits, suggesting that species are constrained by their evolutionary history. It is widely accepted that morphology and ecology tend to be phylogenetically conserved in podocarps (Brodribb & Hill, 1999; Hill & Brodribb, 1999; Brodribb & Hill, 2004), so although it is outside the scope of this thesis, it seems likely that future research into the taxonomic significance of epidermal traits, using a wider range of plants and employing e.g. phylogenetic generalised linear mixed models (Pearse *et al.*, 2014) may prove fruitful.

Although this study was limited by the availability of suitable plants, our results show significant variation in the epidermal traits of species that inhabit similar native environments (Figs S5.1-9). This means that while additional data collection may improve the statistical significance of some of the trends we observed, it is unlikely to reveal useful predictive relationships based on adaptive genotypic variation alone. It may not be possible to use epidermal traits to predict the *climatic ranges* of species, but many physiognomic methods use plastic responses to reconstruct the environment – multiple common garden trials (or ‘natural’ equivalents) may yet identify traits that are useful for physiognomy. However, the apparent phylogenetic signal that I observed highlights the importance of incorporating the effects of both evolutionary history and plasticity when calibrating physiognomic proxies.

I found a relationship between maximum tree height, pavement cell undulation (pavezone.complexity.median and stomzone.complexity.median) and stomatal index (Figure 5.3c, S1b,q,w). It is well-documented that the epidermal cells of many plants are more undulated in shaded conditions (Bruschi *et al.*, 2000; Thomas *et al.*, 2004) and this response appears to be plastic, exemplified in the differences between sun and shade leaves of the same individual (Bruschi *et al.*, 2000). However, our result – that taller trees (more likely to be canopy emergents in Podocarpaceae; Farjon, 2010) have more undulated cells – needs careful consideration in this context. One potential explanation is that in taller trees, increased undulation is a plastic response to being grown in shaded conditions (i.e. in a greenhouse), as has been demonstrated to occur in saplings of boreal conifers (Claveau *et al.*, 2002). In this dataset, the tallest species (which also possessed the most undulated cells) was *Sundacarpus amarus* (Figure 5.4a); wild-collected specimens of this species have similarly extreme epidermal undulation (Stockey & Frevel, 1997), so it seems unlikely that this is a plastic response to greenhouse conditions. Another possibility is that although taller trees are more likely to be in full sun at maturity, they tend to germinate and grow under the canopy. Coupled with the notoriously slow growth rates of conifers compared to angiosperms (Bond, 1989; Brodribb & Hill, 2004), tall trees may actually spend a good portion of their life in the shade, and thus need to be able to tolerate these conditions. On the other hand, shorter trees and shrubs can either inhabit the understorey of forests (low light levels), or can form the canopy in more open vegetation (high light levels). The shorter species in this study generally fall into the latter category (e.g. *Podocarpus gnidioides*), and some understorey podocarps (*Podocarpus drouynianus*) tend to inhabit open, rather than closed forests, so tree height may even be positively correlated with shade tolerance in the Podocarpaceae, in contrast to other plant groups (e.g. Poorter *et al.*, 2003). This idea is supported by the gross leaf morphology – rainforest podocarps (which tend to be tall trees) possess the broadest leaves, increasing light harvesting capacity in low light conditions (Hill & Brodribb, 2003).

Increased shade tolerance in taller trees could also explain the moderate correlation we observed between tree height and stomatal index (-0.41; Fig S5.3). This relationship is of particular interest in a palaeoproxy context because stomatal index is already used as a proxy for atmospheric carbon dioxide, volcanism (via sulphur dioxide) and altitude (Van Cotthem, 1970; Xie *et al.*, 2009; Haworth *et al.*, 2010b; Hu & Zhou, 2012; Steinthorsdottir *et al.*, 2016; McElwain & Steinthorsdottir, 2017; Wang *et al.*, 2018; Porter *et al.*, 2019). The extreme physiological importance of stomata for moderating gas exchange and water loss means that the optimal stomatal index for a leaf is likely dependent on many climatic factors. Thus, any calibration of stomatal index as a proxy for palaeoenvironmental conditions could be easily perturbed by changes in other factors, and is likely to be extremely system-specific (Jordan, 2011). These results suggest that in the Podocarpaceae, variation in stomatal index is caused by both genotype and environment (i.e. stomatal index is a G x E-trait). Interestingly, I did not find the stomatal size vs stomatal density trade-off that has been reported by many authors (e.g. Franks & Beerling, 2009; Brodribb *et al.*, 2013). In this study, these traits seemed largely decoupled (Fig. 5d), though I note that it is possible that this trade-off operates mostly within species, whereas our results are driven more strongly by between-species variation. I also did not account for amphistomy, so did not compare size to the total number of stomata – this may be another reason that I did not observe a trade-off between size and abundance of stomata.

It is not impossible to use G x E-traits to calibrate physiognomic methods, but it is vital that the effect of phylogenetic history is considered when using these characters (Little *et al.*, 2010; Hinojosa *et al.*, 2011). Although consistent, family-wide epidermal proxies of climatic tolerances remain elusive, or results do not rule out the use of epidermal traits for palaeoclimatic estimation. The development of new high-throughput methods to quantify the epidermis (e.g. Brown et al., *this thesis*) means that large studies of epidermal traits are much more feasible, and are limited by the availability of source material, rather than labour-intensive measurement of

traits. We anticipate that future research into the genetic and environmental basis of epidermal variation may yet produce viable palaeoclimatic proxies.

Conclusion

It is no small task to disentangle the complex multivariate relationships between morphology, environment, and phylogenetic history. Conifers are ubiquitous in the fossil record but are not well suited to common garden experiments, so calibrating physiognomic relationships for palaeoclimatic estimation in a sufficiently broad study system (e.g. a diverse family) is extremely challenging, unless we can identify traits that are directly linked to a species climatic range. Here, we found no evidence for such traits; it is likely that phylogenetic and plastic control of variation predominates over any adaptive signal. Future studies into epidermal trait-climate relationships (particularly in Podocarpaceae) should explicitly incorporate both tests for plasticity and phylogenetic signal (despite the methodological challenges in doing so) and it is vital that any predictions made from epidermal traits are adjusted to account for these factors.

References

(2008) *eFloras*. Available at: http://www.efloras.org/florataxon.aspx?flora_id=2&taxon_id=200005467 (accessed June 6th 2021).

Andruchow-Colombo, A., Escapa, I.H., Carpenter, R.J., Hill, R.S., Iglesias, A., Abarzua, A.M. & Wilf, P. (2019) Oldest record of the scale-leaved clade of Podocarpaceae, early Paleocene of Patagonia, Argentina. *Alcheringa*, **43**, 127-145.

Beerling, D.J., McElwain, J.C. & Osborne, C.P. (1998) Stomatal responses of the 'living fossil' *Ginkgo biloba* L. to changes in atmospheric CO_2 concentrations. *Journal of Experimental Botany*, **49**, 1603-1607.

Blomenkemper, P., Bäumer, R., Backer, M., Abu Hamad, A., Wang, J., Kerp, H. & Bomfleur, B. (2021) Bennettitalean Leaves From the Permian of Equatorial Pangea—The Early Radiation of an Iconic Mesozoic Gymnosperm Group. *Frontiers in Earth Science*, **9**, 162.

Bond, W.J. (1989) The Tortoise and the Hare - Ecology of angiosperm dominance and gymnosperm persistence. *Biological Journal of the Linnean Society*, **36**, 227-249.

Brodribb, T. & Hill, R. (1999) The importance of xylem constraints in the distribution of conifer species. *The New Phytologist*, **143**, 365-372.

Brodribb, T. & Hill, R.S. (2004a) The rise and fall of the Podocarpaceae in Australia—A physiological explanation. *The Evolution of Plant Physiology*, pp. 381-399.

Brodribb, T. & Hill, R.S. (2004b) The rise and fall of the Podocarpaceae in Australia—A physiological explanation. *Evolution of Plant Physiology from Whole Plants to Ecosystems* (ed. by A.H.I. Poole), pp. 379-381. Academic Press, London.

Brodribb, T.J., Jordan, G.J. & Carpenter, R.J. (2013) Unified changes in cell size permit coordinated leaf evolution. *New Phytologist*, **199**, 559-70.

Brown, M.J., Holland, B.R. & Jordan, G.J. (2020) HYPEROVERLAP: Detecting biological overlap in n-dimensional space. *Methods in Ecology and Evolution*, **11**, 513-523.

Brown, M.J., Brodribb, T.J. & Jordan, G.J. (2021) No-analogue associations in the fossil record of southern conifers reveal conservatism in precipitation, but not temperature axes. *Global Ecology and Biogeography*, **30**(12), 2455-2466.

Bruschi, P., Vendramin, G.G., Bussotti, F. & Grossoni, P. (2000) Morphological and molecular differentiation between *Quercus petraea* (Matt.) Liebl. and *Quercus pubescens* Willd.(Fagaceae) in northern and central Italy. *Annals of Botany*, **85**, 325-333.

Carins Murphy, M.R., Jordan, G.J. & Brodribb, T.J. (2014) Acclimation to humidity modifies the link between leaf size and the density of veins and stomata. *Plant, Cell and Environment*, **37**, 124-31.

Carins Murphy, M.R., Jordan, G.J. & Brodribb, T.J. (2016) Cell expansion not cell differentiation predominantly co-ordinates veins and stomata within and among herbs and woody angiosperms grown under sun and shade. *Annals of Botany*, **118**, 1127-1138.

Carpenter, R.J., Jordan, G.J., Mildenhall, D.C. & Lee, D.E. (2011) Leaf fossils of the ancient Tasmanian relict *Microcachrys* (Podocarpaceae) from New Zealand. *American Journal of Botany*, **98**, 1164-72.
Claveau, Y., Messier, C., Comeau, P.G. & Coates, K.D. (2002) Growth and crown morphological responses of boreal conifer seedlings and saplings with contrasting shade tolerance to a gradient of light and height. *Canadian Journal of Forest Research*, **32**, 458-468.
Clugston, J., Jeffree, C., Ahrends, A. & Mill, R. (2017) Do environmental factors affect the taxonomic reliability of leaf cuticular micromorphological characters? A case study in Podocarpaceae. *Edinburgh Journal of Botany*, **74**, 299-343.
Depardieu, C., Girardin, M.P., Nadeau, S., Lenz, P., Bousquet, J. & Isabel, N. (2020) Adaptive genetic variation to drought in a widely distributed conifer suggests a potential for increasing forest resilience in a drying climate. *New Phytologist*, **227**, 427-439.
Dunn, R.E., Le, T.Y.T. & Stromberg, C.A.E. (2015) Light Environment and Epidermal Cell Morphology in Grasses. *International Journal of Plant Sciences*, **176**, 832-847.
Eckenwalder, J.E. (2009) *Conifers of the world: the complete reference*. Timber Press, Portland, Oregon.
Falconer, D.S. (1996) *Introduction to quantitative genetics*. Pearson Education UK, GB.
Farjon, A. (2010) *A Handbook of the World's Conifers*. Brill, Leiden/Boston.
Farjon, A. & Filer, D. (2013) *An atlas of the world's conifers: an analysis of their distribution, biogeography, diversity and conservation status*. Brill, Leiden/Boston.
Franks, P.J. & Beerling, D.J. (2009) Maximum leaf conductance driven by CO2 effects on stomatal size and density over geologic time. *Proceedings of the National Academy of Sciences*, **106**, 10343-10347.
Franks, S.J., Weber, J.J. & Aitken, S.N. (2014) Evolutionary and plastic responses to climate change in terrestrial plant populations. *Evol Appl*, **7**, 123-39.
Haworth, M., Elliott-Kingston, C. & McElwain, J.C. (2012) Co-ordination of physiological and morphological responses of stomata to elevated [CO2] in vascular plants. *Oecologia*, **171**, 71-82.
Haworth, M., Gallagher, A., Elliott‐Kingston, C., Raschi, A., Marandola, D. & McElwain, J.C. (2010) Stomatal index responses of Agrostis canina to CO2 and sulphur dioxide: implications for palaeo‐[CO2] using the stomatal proxy. *New Phytologist*, **188**, 845-855.
Hill, R. & Carpenter, R. (1991) Evolution of Acmopyle and Dacrycarpus (Podocarpaceae) foliage as inferred from macrofossils in south-eastern Australia. *Australian Systematic Botany*, **4**, 449-479.
Hill, R.S. & Brodribb, T.J. (1999) Turner Review No. 2 - Southern conifers in time and space. *Australian Journal of Botany*, **47**, 639-696.
Hill, R.S. & Brodribb, T.J. (2003) Evolution of conifer foliage in the Southern Hemisphere. In: *Acta Horticulturae*, pp. 53-58
Hinojosa, L.F., Pérez, F., Gaxiola, A. & Sandoval, I. (2011) Historical and phylogenetic constraints on the incidence of entire leaf margins:

insights from a new South American model. *Global Ecology and Biogeography*, **20**, 380-390.
Hu, J.-J. & Zhou, Z.-K. (2012) 201 The relationship between atmospheric pCO_2 and stomatal frequency in Quercus pannosa and its application to paleoelevation reconstruction. *Japanese Journal of Palynology*, **58**, 91-92.
Jordan, G.J. (1997) Contrasts between the climatic ranges of fossil and extant taxa: Causes and consequences for palaeoclimatic estimates. *Australian Journal of Botany*, **45**, 465-474.
Jordan, G.J. (2011) A critical framework for the assessment of biological palaeoproxies: predicting past climate and levels of atmospheric CO(2) from fossil leaves. *New Phytologist*, **192**, 29-44.
Jordan, G.J., Carpenter, R.J., Bannister, J.M., Lee, D.E., Mildenhall, D.C. & Hill, R.S. (2011) High conifer diversity in Oligo-Miocene New Zealand. *Australian Systematic Botany*, **24**, 121-136.
Jordan, M.I. & Mitchell, T.M. (2015) Machine learning: Trends, perspectives, and prospects. *Science*, **349**, 255-60.
Larcombe, M.J., Jordan, G.J., Bryant, D. & Higgins, S.I. (2018) The dimensionality of niche space allows bounded and unbounded processes to jointly influence diversification. *Nature Communications*, **9**, 4258.
Little, S.A., Kembel, S.W. & Wilf, P. (2010) Paleotemperature proxies from leaf fossils reinterpreted in light of evolutionary history. *PLoS One*, **5**, e15161.
McElwain, J.C. & Steinthorsdottir, M. (2017) Paleoecology, Ploidy, Paleoatmospheric Composition, and Developmental Biology: A Review of the Multiple Uses of Fossil Stomata. *Plant Physiology*, **174**, 650-664.
Mill, R.R. & Stark Schilling, D.M. (2009) Cuticle micromorphology of *Saxegothaea* (Podocarpaceae). *Botanical Journal of the Linnean Society*, **159**, 58-67.
Milligan, J. N., Flynn, A. G., Wagner, J. D., Kouwenberg, L. L., Barclay, R. S., Byars, B. W., ... & Peppe, D. J. (2021). Quantifying the effect of shade on cuticle morphology and carbon isotopes of sycamores: present and past. *American Journal of Botany*, **108**(12), 2435-2451.
Mizutani, M. & Kanaoka, M.M. (2018) Environmental sensing and morphological plasticity in plants. *Seminars in cell & developmental biology*, **83**, 69-77.
Moreira, A.S.F.P., Queiroz, A.C.L., de Vasconcelos Barros, F., Goulart, M.F. & de Lemos-Filho, J.P. (2014) Do leaf traits in two *Dalbergia* species present differential plasticity in relation to light according to their habitat of origin? *Australian journal of botany*, **61**, 592-599.
Mosbrugger, V. & Utescher, T. (1997) The coexistence approach—a method for quantitative reconstructions of Tertiary terrestrial palaeoclimate data using plant fossils. *Palaeogeography, Palaeoclimatology, Palaeoecology*, **134**, 61-86.
Page, C.N. (2019) New and maintained genera in the taxonomic alliance of *Prumnopitys* s. l.(Podocarpaceae), and circumscription of a new genus: Pectinopitys. *New Zealand Journal of Botany*, **57**, 137-153.

Pearse, W.D., Cavender-Bares, J., Puvis, A. & Helmus, M.R. (2014) Metrics and models of community phylogenetics. In *Modern Phylogenetic Comparative Methods and their Application in Evolutionary Biology—Concepts and Practice* (pp. 451-464) Springer-Verlag, Berlin, Heidelberg.

Pittermann, J., Stuart, S.A., Dawson, T.E. & Moreau, A. (2012) Cenozoic climate change shaped the evolutionary ecophysiology of the Cupressaceae conifers. *Proceedings of the National Academy of Sciences*, **109**, 9647-52.

Poorter, L., Bongers, F., Sterck, F.J. & Wöll, H. (2003) Architecture of 53 rain forest tree species differing in adult stature and shade tolerance. *Ecology*, **84**, 602-608.

Porter, A.S., Evans-Fitz.Gerald, C., Yiotis, C., Montañez, I.P. & McElwain, J.C. (2019) Testing the accuracy of new paleoatmospheric CO_2 proxies based on plant stable carbon isotopic composition and stomatal traits in a range of simulated paleoatmospheric O_2:CO_2 ratios. *Geochimica et Cosmochimica Acta*, **259**, 69-90.

Rehfeldt, G.E., Wykoff, W.R. & Ying, C.C. (2001) Physiologic plasticity, evolution, and impacts of a changing climate on *Pinus contorta*. *Climatic Change*, **50**, 355-376.

Royer, D.L., Sack, L., Wilf, P., Lusk, C.H., Jordan, G.J., Niinemets, U., Wright, I.J., Westoby, M., Cariglino, B., Coley, P.D., Cutter, A.D., Johnson, K.R., Labandeira, C.C., Moles, A.T., Palmer, M.B. & Valladares, F. (2007) Fossil leaf economics quantified: calibration, Eocene case study, and implications. *Paleobiology*, **33**, 574-589.

Spicer, R. (2009) CLAMP, climate leaf analysis multivariate program. *The Open University (http://clamp.ibcas.ac.cn.)*,

Spicer, R.A., Yang, J., Spicer, T.E. & Farnsworth, A. (2020) Woody dicot leaf traits as a palaeoclimate proxy: 100 years of development and application. *Palaeogeography, Palaeoclimatology, Palaeoecology*,

Stahl, U., Reu, B. & Wirth, C. (2014) Predicting species' range limits from functional traits for the tree flora of North America. *Proceedings of the National Academy of Sciences*, **111**, 13739-13744.

Stark Schilling, D.M. & Mill, R.R. (2011) Cuticle micromorphology of Caribbean and Central American species of *Podocarpus* (Podocarpaceae). *International Journal of Plant Sciences*, **172**, 601-631.

Steger, C. (1998) An unbiased detector of curvilinear structures. *IEEE Transactions on pattern analysis and machine intelligence*, **20**, 113-125.

Steinthorsdottir, M., Porter, A.S., Holohan, A., Kunzmann, L., Collinson, M. & McElwain, J.C. (2016) Fossil plant stomata indicate decreasing atmospheric CO2 prior to the Eocene–Oligocene boundary. *Climate of the Past*, **12**, 439-454.

Stockey, R.A. & Frevel, B.J. (1997) Cuticle micromorphology of *Prumnopitys philippi* (Podocarpaceae). *International Journal of Plant Sciences*, **158**, 198-221.

Stockey, R.A., Frevel, B.J. & Woltz, P. (1998) Cuticle micromorphology of *Podocarpus,* subgenus Podocarpus, section Scytopodium

(Podocarpaceae) of Madagascar and South Africa. *International Journal of Plant Sciences*, **159**, 923-940.
Thomas, P.W., Woodward, F.I. & Quick, W.P. (2004) Systemic irradiance signalling in tobacco. *New Phytologist*, **161**, 193-198.
Vajda, V., Pucetaite, M., McLoughlin, S., Engdahl, A., Heimdal, J. & Uvdal, P. (2017) Molecular signatures of fossil leaves provide unexpected new evidence for extinct plant relationships. *Nature ecology & evolution*, **1**, 1093-1099.
Van Cotthem, W. (1970) A classification of stomatal types. *Botanical Journal of the Linnean Society*, **63**, 235-246.
Wang, Y., Ito, A., Huang, Y.-J., Fukushima, T., Wakamatsu, N. & Momohara, A. (2018) Reconstruction of altitudinal transportation range of leaves based on stomatal evidence: an example of the Early Pleistocene *Fagus* leaf fossils from central Japan. *Palaeogeography, Palaeoclimatology, Palaeoecology*, **505**, 317-325.
Wells, P.M. & Hill, R.S. (1989) Leaf morphology of the imbricate-leaved Podocarpaceae. *Australian systematic botany*, **2**, 369-386.
Wilf, P., Wing, S. L., Greenwood, D. R., & Greenwood, C. L. (1998). Using fossil leaves as paleoprecipitation indicators: an Eocene example. *Geology*, **26**(3), 203-206.
Wolfe, J.A. (1993) *A method of obtaining climatic parameters from leaf assemblages*. US Government Printing Office, Washington DC.
Wright, I. J., Reich, P. B., Westoby, M., Ackerly, D. D., Baruch, Z., Bongers, F., ... & Villar, R. (2004). The worldwide leaf economics spectrum. *Nature*, **428**(6985), 821-827.
Wyka, T.P., Oleksyn, J., Żytkowiak, R., Karolewski, P., Jagodziński, A. & Reich, P.B. (2012) Responses of leaf structure and photosynthetic properties to intra-canopy light gradients: a common garden test with four broadleaf deciduous angiosperm and seven evergreen conifer tree species. *Oecologia*, **170**, 11-24.
Xie, S., Sun, B., Yan, D. & Du, B. (2009) Altitudinal variation in *Ginkgo* leaf characters: Clues to paleoelevation reconstruction. *Science in China Series D: Earth Sciences*, **52**, 2040-2046.
Yiotis, C., Evans-Fitz.Gerald, C. & McElwain, J.C. (2017) Differences in the photosynthetic plasticity of ferns and *Ginkgo* grown in experimentally controlled low O_2:CO_2 atmospheres may explain their contrasting ecological fate across the Triassic–Jurassic mass extinction boundary. *Annals of Botany*, **119**, 1385-1395.

Chapter 6 General Discussion

Fossil data are extremely useful, but are also complex and sparse, making traditional statistical approaches challenging to apply (Spicer, 1988). Machine learning techniques are powerful tools to analyse these sorts of data and are increasingly being used for palaeoecological studies (Li *et al.*, 2016; Wilf *et al.*, 2016; Berg *et al.*, 2019; Wei *et al.*, 2021). However, machine learning algorithms are not a panacea and cannot be applied indiscriminately, nor do they remove the need for careful consideration of assumptions. Moreover, the sheer diversity of machine learning algorithms (including methods for classification, regression, unsupervised learning and image processing; Ayodele, 2010) means that identifying the appropriate method for a particular problem can be difficult.

The aim of this thesis was to explore the potential for novel applications of machine learning algorithms in palaeoecology, using southern conifers as a study system. Southern conifers are overrepresented in the fossil record, show exceptional preservation of the epidermis via the cuticle, and are generally assumed to be ecologically conservative (Jin *et al.*, 2021), making them ideal for palaeoecological studies. However, their utility is complicated by the presence of no-analogue fossils – instances where the bioclimatic envelopes of fossil species are not the same as those of their nearest relatives, leading to incongruous associations.

In particular, I investigated no-analogue fossils – how to quantify them, what aspects of the bioclimatic envelope have changed, if we can detect these changes via the anatomy, and what no-analogue fossils mean for the future of southern conifers in a changing climate. I addressed this aim in two sections that correspond to the two major classes of palaeoecological estimation: nearest living relative methods and physiognomy.

What can no-analogue pairs tell us about the past, present and future ecology of the southern conifers?

No-analogue pairs (pairs of fossil taxa for which the nearest living relatives occupy non-overlapping climates) indicate that species bioclimatic ranges are not constant over geological timescales, violating the key assumption of nearest living relative approaches (Jordan, 1997; Mosbrugger & Utescher, 1997). Thus, it is imperative to understand the prevalence and processes that have driven this phenomenon, but quantifying these differences and disentangling the climatic factors that are involved required a novel approach. I developed HYPEROVERLAP (Chapter 2) for this purpose, using support vector machines to detect overlap between multi-dimensional point clouds. This allowed me to analyse the Cenozoic record of southern conifers to identify instances of climatic non-overlap (i.e. no-analogue pairs; Chapter 3). I found that no-analogue pairs are frequent (10% of all pairs) across the southern hemisphere, and involve 27 different taxa (forming 73 unique pairs), suggesting that no-analogue pairs are the result of broad-scale processes. I further analysed these no-analogue pairs to identify which aspects of the bioclimatic range had changed and found that while the thermal niche appears to have changed in many taxa, the precipitation niche has remained stable for the majority of southern conifers over the Cenozoic. This result is important for both the future management of biodiversity and for palaeoclimatic estimation.

The southern conifers are thought to be generally limited in their geographic distributions by water and disturbance, either climatic or otherwise (Brodribb & Hill, 1999; Hill & Brodribb, 1999; Brodribb & Hill, 2004; Sundaram & Leslie). The results from Chapter 3 provide evidence that this has been the case over geological timescales, thus highlighting the threat of current and future aridification (rather than warming) for southern conifers.

Palaeoprecipitation is difficult to estimate using physiognomic methods (Wei *et al.*, 2021), so evidence of stability in the precipitation niche of southern conifers is promising for their use as precipitation indicators in nearest living

relative analyses. This could be further strengthened if we can identify particular traits that are linked to climate, and compare these traits between fossil and extant species.

Is it possible to identify changes in the bioclimatic envelope of southern conifers using epidermal physiognomy?

The use of morphological traits of a fossil for palaeoecological inference is well-established (Wolfe, 1993; Spicer, 2009; Spicer *et al.*, 2020) but much of this work (especially multivariate methods) has focused on gross leaf morphology rather than epidermal traits. Leaf form in conifers is strongly constrained by evolutionary history (Hill & Carpenter, 1991; Hill & Brodribb, 2003) and fossils are often recovered as incomplete fragments (Spicer, 1988; Blomenkemper *et al.*, 2021), so current physiognomic methods are generally unsuitable for conifers. However, conifer fossils frequently preserve the cuticle (and thus the outlines of the epidermal cells); these layers form the interface between plant and environment and show significant variation in cell shape, size and arrangement (which is routinely used for identification; Jordan & Hill, 1995; Hill & Paull, 2003; Jordan *et al.*, 2011). Epidermal traits are known to be linked to climate in conifers (Haworth *et al.*, 2010a; Clugston *et al.*, 2017) so it is likely that some features of the epidermis can be used as proxies for the palaeoenvironment. If we can identify these proxies, we can compare the anatomy of fossil and extant species to identify bioclimatic changes between the two, and thus provide further insights into no-analogue associations.

To use epidermal anatomy to investigate the climatic aspects of no-analogue pairs, the following steps are required:

1) Quantify epidermal traits;
2) Link these epidermal traits to climate;
3) Apply these links to the comparative anatomy of fossils versus their extant relatives.

The epidermis has not been studied extensively from a physiognomic perspective, and so current methods of quantifying epidermal traits tend to be specific in terms of traits, taxon and purpose (Stark Schilling & Mill, 2011; Möller *et al.*, 2017; Nowak *et al.*, 2021). To remedy this, I developed EPIDERMALMORPH, an R package that quantifies epidermal traits from images of the leaf cuticle (Chapter 4). This software not only integrates measurement of several existing metrics (e.g. cell size), but also includes several new metrics, and is the first method to automate the description of stomatal arrangement. The software also includes functions to pre-process images, estimate trait reliability and calculate optimum sampling effort for a given group of plants. This software brings together high-throughput measures of cell shape with the holistic approach to epidermal characterisation that is used to identify fossils (e.g. Andruchow-Colombo *et al.*, 2019) and represents a major step towards a unified framework for epidermal cell studies across all fields.

The next step is to link these epidermal traits to climatic variables, and determine whether trait-climate relationships are the result of adaptation (genetic), acclimation (plastic), or some interaction between the two. Conifers are not well suited to reciprocal common garden experiments, and sampling from ‘natural’ common gardens is extremely costly, so we conducted a preliminary study using plants grown in a simple common garden (Chapter 5). This design, while cost-effective and logistically straightforward, limited our scope to finding adaptive proxies – genetically controlled traits that are linked to the environmental conditions of the native range of a species. Thus, our null result highlights the need for further physiognomic calibrations that explicitly include phylogenetic, plastic and adaptive components of trait-climate relationships, before we can apply epidermal physiognomy to the study of no-analogue pairs.

Challenges of using machine learning for palaeoecology

Machine learning methods can vastly outperform traditional algorithms in certain tasks (e.g. Jordan & Mitchell, 2015; Wilf *et al.*, 2016; Jayakody *et al.*, 2017; Berg *et al.*, 2019; Wei *et al.*, 2021), but these approaches are not without caveats and limitations.

For example, HYPEROVERLAP (Chapter 2) outperforms niche modelling approaches (e.g. hypervolume; Blonder *et al.*, 2014; Blonder *et al.*, 2017) when evaluating shared regions of ecospace from point clouds, but will produce erroneous results if the edges of a species' range are not sampled (niche modelling methods can handle this by adding a buffer to each point, but this is problematic for taxa where we can be confident that the species range has been well sampled; Fig. 2.4). Similarly, if images of epidermal cells are not accurately segmented (e.g. if sections of cell walls are missing or cells are erroneously divided by debris) then traits measured from this image will be inaccurate (although many of our metrics in EPIDERMALMORPH use the median rather than the mean value of cells in an image to mitigate this). As with any statistical method, thorough consideration of the underlying assumptions is crucial for the use of machine learning algorithms (Jordan & Mitchell, 2015).

Implementation of machine learning methods is usually more time-consuming than traditional algorithms because of the increased computational requirements (although this is largely being matched by concomitant upgrades to hardware) and the need to tune these models (Jordan & Mitchell, 2015). In some cases (as in Chapter 4), it may be more time-efficient to partially automate a process and manually correct the errors, rather than developing an accurate end-to-end machine learning model. There has been significant progress in developing GUI (rather than scripted) functionality, in particular for image processing (e.g. Arganda-Carreras *et al.*, 2017; Berg *et al.*, 2019), but machine learning continues to be regarded as inaccessible by many scientists.

The bewildering range of machine learning algorithms, each with their own advantages and disadvantages, makes identifying the most appropriate method for any given task difficult. Machine learning is a dynamic and rapidly evolving field of computing, so new algorithms are rapidly appearing in the literature, further bamboozling the novice. However, this diversification is a boon as well as a curse; many recent publications describe machine learning methods that are tailored to particular scientific fields and focus on accessibility as well as accuracy (Ayodele, 2010; Willcock *et al.*, 2018; Sullivan, 2020; Rolf *et al.*, 2021).

Potential for future applications of machine learning in palaeoecology

As we generate increasingly large amounts of data from the fossil record, machine learning techniques will continue to be developed and applied to palaeoecological questions.

Machine learning for physiognomic methods is particularly promising – there has been significant recent work in this area (Li *et al.*, 2016; Wei *et al.*, 2021), although multivariate physiognomy is generally focused on the entire leaf, so the epidermis remains a source of untapped potential. Chapters 4 and 5 of this thesis represent the first steps in developing a new framework for epidermal physiognomy – fully disentangling the genetic and environmental components of variation in epidermal traits in southern conifers is beyond the scope of this thesis but is a promising avenue for future research. In particular, future studies of epidermal traits should use experimental designs that can incorporate both genetic (G) and environmentally (E) controlled variation, as well as the interaction between these two factors (G x E) – either by a reciprocal common garden experiment or by sampling from across species native ranges.

The pixel data generated in these studies also represents an exciting source of training data for future automation – as noted in Chapter 4, image segmentation (i.e. pixel classification) remains a limiting step for high-throughput analysis of the leaf epidermis. Automating this step would allow

us to elevate studies of epidermal traits into the realm of ‘big data’; there are over 3,000 images of cuticle preparations (of the kind suitable for EPIDERMALMORPH) that are already publicly available (e.g. Vőfély *et al.*, 2019), and this number is likely to increase rapidly as open science and publicly available data become a standard part of publishing scientific results. One major repository for these images is the Cuticle Database (Barclay *et al.*, 2007), which provides open access to nearly two thousand images of cuticle preparations. Databases such as these vastly increase the potential sample size for epidermal studies, but because epidermal traits can be environmentally plastic it is vital that appropriate metadata is attached to these entries (as for herbarium specimens).

Machine learning is not only becoming more commonplace in science, but much more accessible – most computers possess hardware capable of performing basic machine learning analyses, and cloud computing platforms facilitate access to supercomputers for many users. Here, I demonstrated the potential for machine learning to be used for palaeoecological studies from multiple perspectives, and published the two new methods that I developed as part of this thesis as R packages so that they can be easily utilised by the scientific community. I believe that creatively applying machine learning to the plant fossil record will continue to provide new insights and contributions to our understanding of plants in the past, present and future.

References

Andruchow-Colombo, A., Escapa, I.H., Carpenter, R.J., Hill, R.S., Iglesias, A., Abarzua, A.M. & Wilf, P. (2019) Oldest record of the scale-leaved clade of Podocarpaceae, early Paleocene of Patagonia, Argentina. *Alcheringa*, **43**, 127-145.

Arganda-Carreras, I., Kaynig, V., Rueden, C., Eliceiri, K.W., Schindelin, J., Cardona, A. & Sebastian Seung, H. (2017) Trainable Weka Segmentation: a machine learning tool for microscopy pixel classification. *Bioinformatics*, **33**, 2424-2426.

Ayodele, T.O. (2010) Types of machine learning algorithms. *New advances in machine learning*, **3**, 19-48.

Barclay, R., McElwain, J., Dilcher, D. & SagEMan, B. (2007) The cuticle database: developing an interactive tool for taxonomic and paleoenvironmental study of the fossil cuticle record. *Courier Forschungsinstitut Senckenberg*, **258**, 39.

Berg, S., Kutra, D., Kroeger, T., Straehle, C.N., Kausler, B.X., Haubold, C., Schiegg, M., Ales, J., Beier, T. & Rudy, M. (2019) Ilastik: interactive machine learning for (bio) image analysis. *Nature Methods*, **16**, 1226-1232.

Blomenkemper, P., Bäumer, R., Backer, M., Abu Hamad, A., Wang, J., Kerp, H. & Bomfleur, B. (2021) Bennettitalean Leaves From the Permian of Equatorial Pangea—The Early Radiation of an Iconic Mesozoic Gymnosperm Group. *Frontiers in Earth Science*, **9**, 162.

Blonder, B., Lamanna, C., Violle, C. & Enquist, B.J. (2014) The n-dimensional hypervolume. *Global Ecology and Biogeography*, **23**, 595-609.

Blonder, B., Morrow, C.B., Maitner, B., Harris, D.J., Lamanna, C., Violle, C., Enquist, B.J. & Kerkhoff, A.J. (2017) New approaches for delineating n-dimensional hypervolumes. *Methods in Ecology and Evolution*, 305-319.

Brodribb, T. & Hill, R. (1999) The importance of xylem constraints in the distribution of conifer species. *The New Phytologist*, **143**, 365-372.

Brodribb, T. & Hill, R.S. (2004) The rise and fall of the Podocarpaceae in Australia—A physiological explanation. *Evolution of Plant Physiology from Whole Plants to Ecosystems* (ed. by A.H.I. Poole), pp. 379-381. Academic Press, London.

Clugston, J., Jeffree, C., Ahrends, A. & Mill, R. (2017) Do environmental factors affect the taxonomic reliability of leaf cuticular micromorphological characters? A case study in Podocarpaceae. *Edinburgh Journal of Botany*, **74**, 299-343.

Haworth, M., Heath, J. & McElwain, J.C. (2010) Differences in the response sensitivity of stomatal index to atmospheric CO2 among four genera of Cupressaceae conifers. *Annals of Botany*, **105**, 411-8.

Hill, R. & Carpenter, R. (1991) Evolution of Acmopyle and Dacrycarpus (Podocarpaceae) foliage as inferred from macrofossils in south-eastern Australia. *Australian Systematic Botany*, **4**, 449-479.

Hill, R.S. & Brodribb, T.J. (1999) Turner Review No. 2 - Southern conifers in time and space. *Australian Journal of Botany*, **47**, 639-696.
Hill, R.S. & Paull, R. (2003) Fitzroya (Cupressaceae) macrofossils from Cenozoic sediments in Tasmania, Australia. *Review of Palaeobotany and Palynology*, **126**, 145-152.
Hill, R.S. & Brodribb, T.J. (2003) Evolution of conifer foliage in the Southern Hemisphere. In: *Acta Horticulturae*, pp. 53-58
Jayakody, H., Liu, S., Whitty, M. & Petrie, P. (2017) Microscope image based fully automated stomata detection and pore measurement method for grapevines. *Plant Methods*, **13**, 94.
Jin, W.T., Gernandt, D.S., Wehenkel, C., Xia, X.M., Wei, X.X. & Wang, X.Q. (2021) Phylogenomic and ecological analyses reveal the spatiotemporal evolution of global pines. *Proceedings of the National Academy of Sciences*, **118**, e2022302118.
Jordan, G.J. (1997) Contrasts between the climatic ranges of fossil and extant taxa: Causes and consequences for palaeoclimatic estimates. *Australian Journal of Botany*, **45**, 465-474.
Jordan, G.J. & Hill, R.S. (1995) Oloigocene leaves of Epacidaceae from Little Rapid River, Tasmania, and the identification of fossil Epacidaceae leaves. *Australian Systematic Botany*, **8**, 71.
Jordan, G.J., Carpenter, R.J., Bannister, J.M., Lee, D.E., Mildenhall, D.C. & Hill, R.S. (2011) High conifer diversity in Oligo-Miocene New Zealand. *Australian Systematic Botany*, **24**, 121-136.
Jordan, M.I. & Mitchell, T.M. (2015) Machine learning: Trends, perspectives, and prospects. *Science*, **349**, 255-60.
Li, S.F., Jacques, F.M.B., Spicer, R.A., Su, T., Spicer, T.E.V., Yang, J. & Zhou, Z.K. (2016) Artificial neural networks reveal a high-resolution climatic signal in leaf physiognomy. *Palaeogeography Palaeoclimatology Palaeoecology*, **442**, 1-11.
Möller, B., Poeschl, Y., Plötner, R. & Bürstenbinder, K. (2017) PaCeQuant: A Tool for High-Throughput Quantification of Pavement Cell Shape Characteristics. *Plant Physiology*, **175**, 998-1017.
Mosbrugger, V. & Utescher, T. (1997) The coexistence approach—a method for quantitative reconstructions of Tertiary terrestrial palaeoclimate data using plant fossils. *Palaeogeography, Palaeoclimatology, Palaeoecology*, **134**, 61-86.
Nowak, J., Eng, R.C., Matz, T., Waack, M., Persson, S., Sampathkumar, A. & Nikoloski, Z. (2021) A network-based framework for shape analysis enables accurate characterization of leaf epidermal cells. *Nature Communications*, **12**, 1-13.
Rolf, E., Proctor, J., Carleton, T., Bolliger, I., Shankar, V., Ishihara, M., Recht, B. & Hsiang, S. (2021) A generalizable and accessible approach to machine learning with global satellite imagery. *Nature Communications*, **12**, 1-11.
Spicer, R. (2009) CLAMP, climate leaf analysis multivariate program. *The Open University (http://clamp.ibcas.ac.cn.)*,
Spicer, R.A. (1988) Quantitative sampling of plant megafossil assemblages. *The Paleontological Society Special Publications*, **3**, 29-51.

Spicer, R.A., Yang, J., Spicer, T.E. & Farnsworth, A. (2020) Woody dicot leaf traits as a palaeoclimate proxy: 100 years of development and application. *Palaeogeography, Palaeoclimatology, Palaeoecology*,
Stark Schilling, D.M. & Mill, R.R. (2011) Cuticle micromorphology of Caribbean and Central American species of *Podocarpus* (Podocarpaceae). *International Journal of Plant Sciences*, **172**, 601-631.
Sullivan, E. (2020) Understanding from machine learning models. *The British Journal for the Philosophy of Science*,
Sundaram, M. & Leslie, A.B. (2021) The influence of climate and palaeoclimate on distributions of global conifer clades depends on geographical range size. *Journal of Biogeography*, **48**, 2286-2297.
Vőfély, R.V., Gallagher, J., Pisano, G.D., Bartlett, M. & Braybrook, S.A. (2019) Of puzzles and pavements: a quantitative exploration of leaf epidermal cell shape. *New Phytol*, **221**, 540-552.
Wei, G., Peng, C., Zhu, Q., Zhou, X. & Yang, B. (2021) Application of machine learning methods for paleoclimatic reconstructions from leaf traits. *International Journal of Climatology*, **41**, E3249-E3262.
Wilf, P., Zhang, S., Chikkerur, S., Little, S.A., Wing, S.L. & Serre, T. (2016) Computer vision cracks the leaf code. *Proceedings of the National Academy of Sciences*, **113**, 3305-3310.
Willcock, S., Martínez-López, J., Hooftman, D.A., Bagstad, K.J., Balbi, S., Marzo, A., Prato, C., Sciandrello, S., Signorello, G. & Voigt, B. (2018) Machine learning for ecosystem services. *Ecosystem services*, **33**, 165-174.
Wolfe, J.A. (1993) *A method of obtaining climatic parameters from leaf assemblages*. US Government Printing Office, Washington DC.

Supporting Information for Chapter 2

Contents

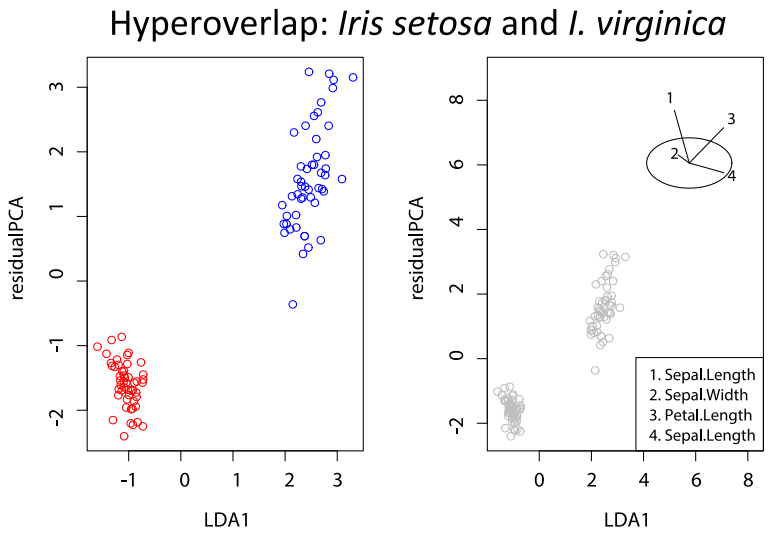

Figure S2.1 An example of the visualisation produced by the `hyperoverlap_lda` function in the HYPEROVERLAP package. Created using two species and five variables of the `iris` dataset (Anderson, 1935).

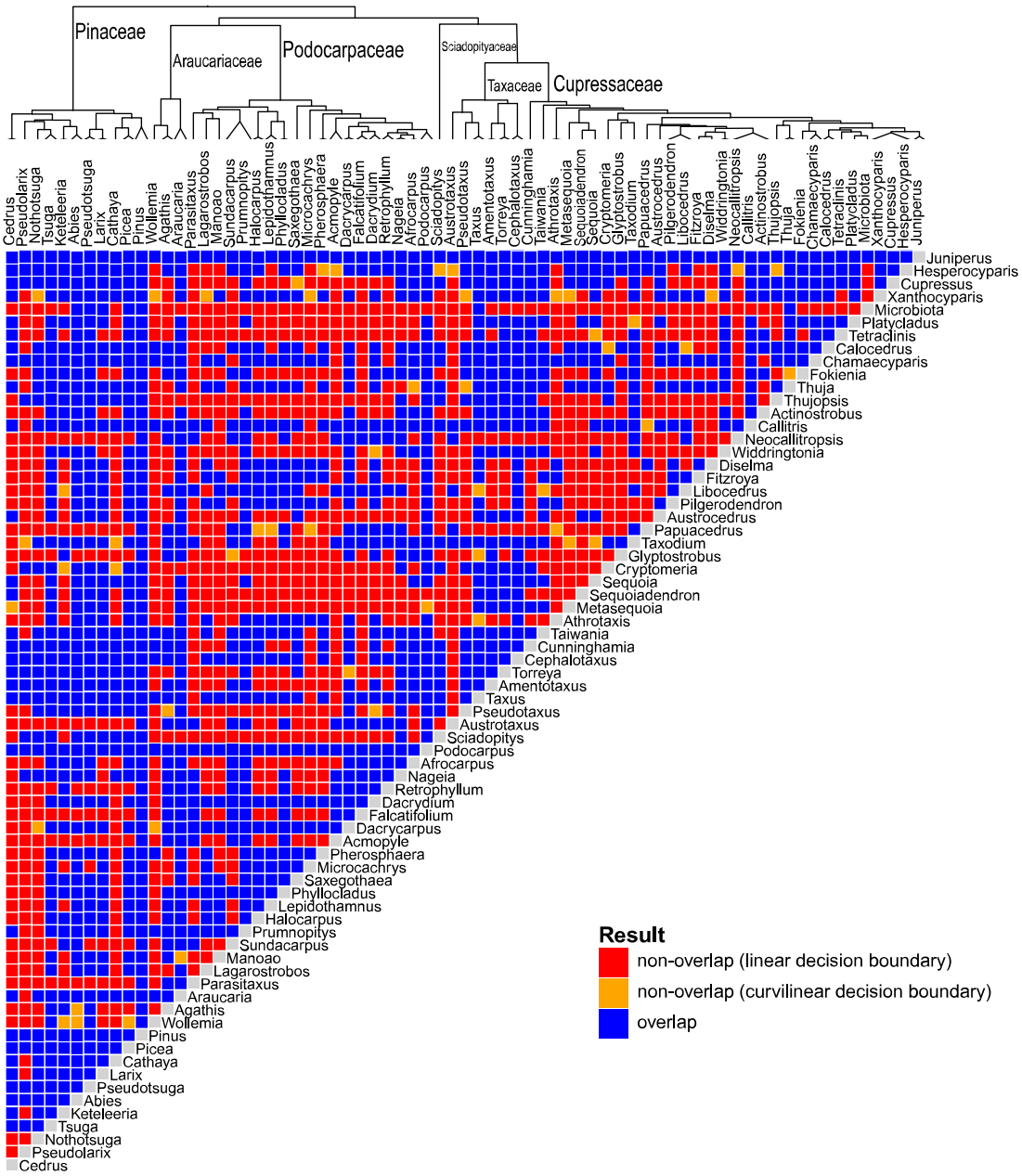

Figure S2.2 Pairwise comparison of climatic distributions of conifer genera (grouped phylogenetically) using HYPEROVERLAP.

Supporting references

Anderson, E. (1935). The irises of the Gaspe Peninsula, *Bulletin of the American Iris Society*, **59**, 2-5.

Supporting Information for Chapter 3

Contents

Table S3.1 and S3.2 For brevity, these tables are available online; https://onlinelibrary.wiley.com/doi/10.1111/geb.13398)

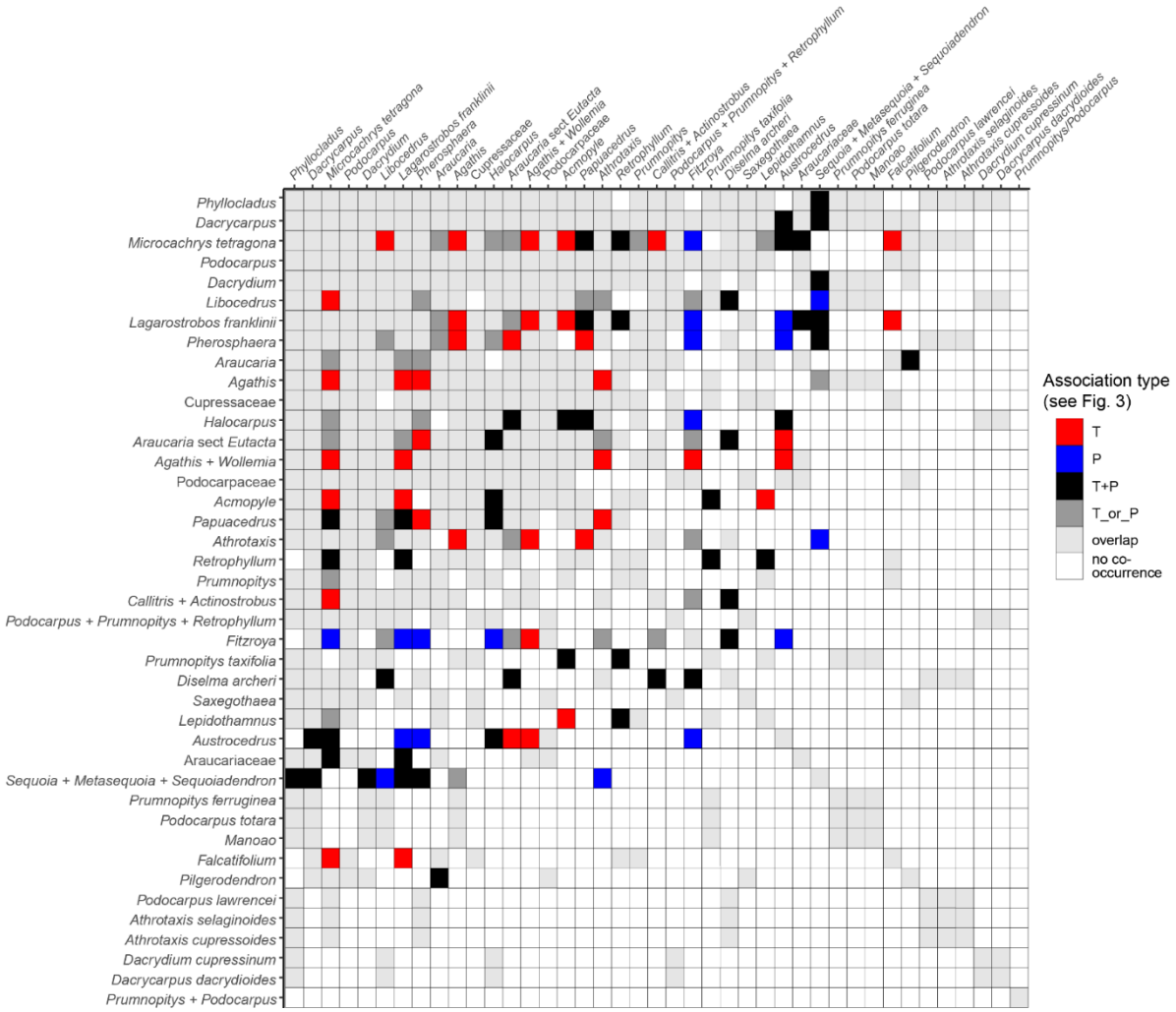

Figure S3.1. Matrix showing no-analogue associations by taxon.

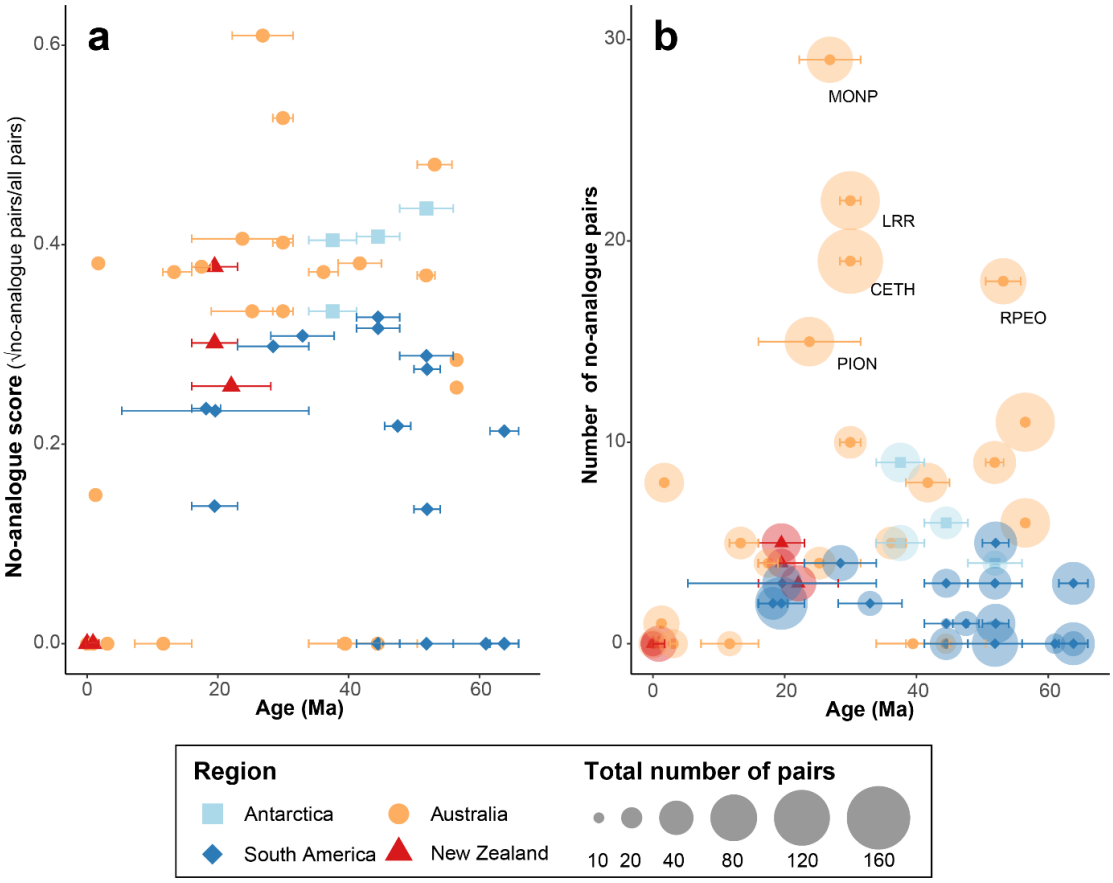

Figure S3.2. No-analogue score (the square root of the number no-analogue pairs divided by the total number of pairs; a) and total number of no-analogue pairs (b) for each site versus age of fossil site.

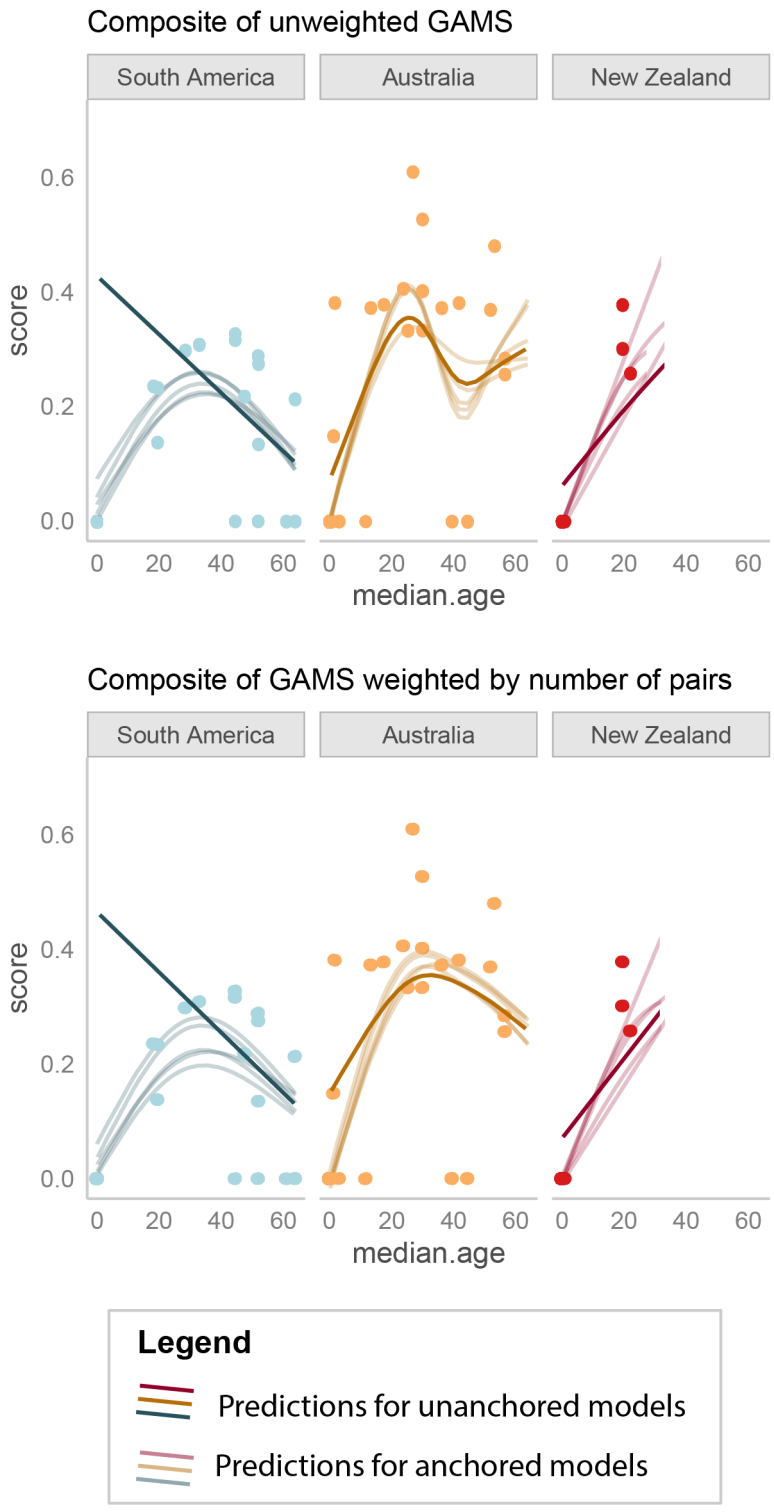

Figure S3.3. Effect of adding anchor points at (0,0) to GAM-fitting datasets. The models fitted without anchor points (dark lines) predict demonstrably incorrect values for recent or extant assemblages, particularly for South American assemblages. Models fitted with either 10, 20, 50, 100 or 1000 points (light lines) all produce very similar predictions. All combinations of parameters produce similar estimates at 20-30Ma.

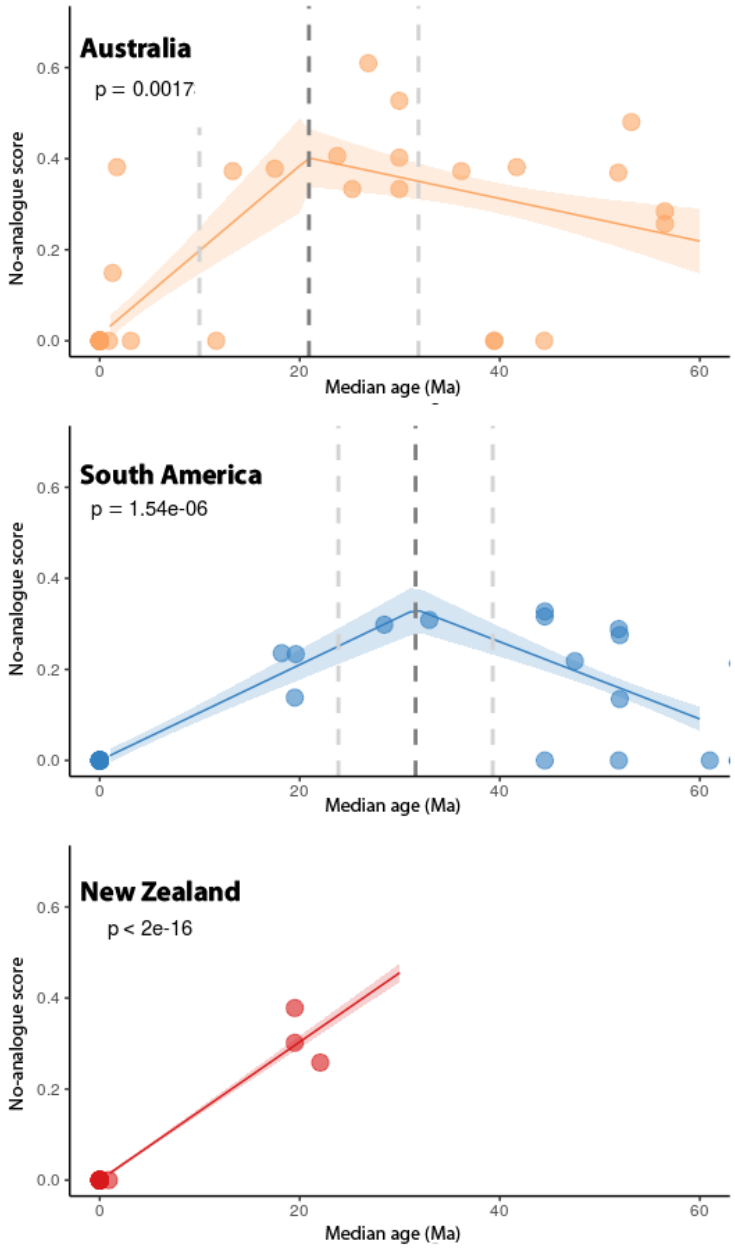

Figure S3.4. Segmented analysis of the no-analogue score for each region. Dotted lines represent the estimated breakpoint (dark) and 95% confidence interval for the location of the breakpoint (light). The estimated slope of each segment is given by a line, and the 95% confidence interval of each section is shaded; p-values shown are for the first segment only.

Supporting references (from Table S3.1)

Archangelsky, S., & Romero, E. J. (1974). Polen de gimnospermas (coníferas) del Cretácico superior y Paleoceno de Patagonia. *Ameghiniana*, **11**(3), 217-236.

Astorga, G. A., Jordan, G. J., & Brodribb, T. (2016). Towards understanding the fossil record better: Insights from recently deposited plant macrofossils in a sclerophyll-dominated subalpine environment. *Review of Palaeobotany and Palynology*, **233**, 1-11.

Atahan, P., Dodson, J. R., & Itzstein‐Davey, F. (2004). A fine‐resolution Pliocene pollen and charcoal record from Yallalie, south‐western Australia. *Journal of Biogeography*, **31**(2), 199-205.

Barreda, V. D. (1997). Palinoestratigrafía de la Formación San Julián en el área de Playa La Mina (provincia de Santa Cruz), Oligoceno de la cuenca Austral. *Ameghiniana*, **34**(3), 283-294.

Barreda, V. D., Cúneo, N. R., Wilf, P., Currano, E. D., Scasso, R. A., & Brinkhuis, H. (2012). Cretaceous/Paleogene floral turnover in Patagonia: drop in diversity, low extinction, and a Classopollis spike. *PLoS One*, **7**(12), e52455.

Barreda, V. D., & Palazzesi, L. (2014). Response of plant diversity to Miocene forcing events: the case of Patagonia. 'Paleobotany and biogeography: a Festschrift for Alan Graham in his 80th year'. *Monographs in Systematic Botany*, **128**. St. Louis, MO: Missouri Botanical Garden Press; p. 1–25.

Barreda, V. D., Zamaloa, M. D. C., Gandolfo, M. A., Jaramillo, C., & Wilf, P. (2020). Early Eocene spore and pollen assemblages from the Laguna del Hunco fossil lake beds, Patagonia, Argentina. *International Journal of Plant Sciences*, **181**(6), 594-615.

Blackburn, D. T., & Sluiter, I. R. K. (1994). The Oligo–Miocene coal floras of southeastern Australia. In 'History of the Australian vegetation. Cretaceous to recent'.(Ed. RS Hill) pp. 328–367.

Carpenter, R. J. (1991). Palaeovegetation and environment at Cethana, Tasmania (Doctoral dissertation, University of Tasmania).

Carpenter R.J. (2012). Proteaceae leaf fossils: Phylogeny, diversity, ecology and austral distributions. *Botanical Review*, **78**, 261-287.

Carpenter, R. J., Hill, R. S., & Jordan, G. J. (1994). Cenozoic vegetation in Tasmania: macrofossil evidence 'History of the Australian vegetation: Cretaceous to Recent', 276.

Carpenter, R. J., & Pole, M. (1995). Eocene plant fossils from the Lefroy and Cowan paleodrainages, Western Australia. *Australian Systematic Botany*, **8**(6), 1107-1154.

Carpenter, R. J., Jordan, G. J., & Hill, R. S. (2007). A toothed Lauraceae leaf from the Early Eocene of Tasmania, Australia. *International Journal of Plant Sciences*, **168**(8), 1191-1198.

Carpenter, R. J., Jordan, G. J., Macphail, M. K., & Hill, R. S. (2012). Near-tropical Early Eocene terrestrial temperatures at the Australo-Antarctic margin, western Tasmania. *Geology*, **40**(3), 267-270.

Carpenter, R. J., Iglesias, A., & Wilf, P. (2018). Early Cenozoic vegetation in Patagonia: new insights from organically preserved plant fossils (Ligorio

Márquez Formation, Argentina). *International Journal of Plant Sciences*, **179**(2), 115-135.
Christophel, D. C., Harris, W. K., & Syber, A. K. (1987). The Eocene flora of the Anglesea locality, Victoria. *Alcheringa*, **11**(4), 303-323.
Clyde, W. C., Wilf, P., Iglesias, A., Slingerland, R. L., Barnum, T., Bijl, P. K., ... & Zamaloa, M. D. C. (2014). New age constraints for the Salamanca Formation and lower Río Chico Group in the western San Jorge Basin, Patagonia, Argentina: implications for Cretaceous-Paleogene extinction recovery and land mammal age correlations. *Bulletin*, **126**(3-4), 289-306.
Dodson, J. R., & Macphail, M. K. (2004). Palynological evidence for aridity events and vegetation change during the Middle Pliocene, a warm period in Southwestern Australia. *Global and Planetary Change*, **41**(3-4), 285-307.
Fasola, A. (1969). Estudio palinológico de la Formación Loreto (Terciario medio), provincia de Magallanes, Chile. *Ameghiniana,* **6**(1), 3-49.
Greenwood, D. R. (1987). Early Tertiary Podocarpaceae-megafossils from the Eocene Anglesea locality, Victoria, Australia. *Australian Journal of Botany*, **35**(2), 111-133.
Hill, R. S. (1984). Tertiary Nothofagus macrofossils from Cethana, Tasmania. *Alcheringa*, **8**(1), 81-86.
Hill, R. S. (1989). New species of *Phyllocladus* (Podocarpaceae) macrofossils from southeastern Australia. *Alcheringa*, **13**(3), 193-208.
Hill, R. S., & Macphail, M. K. (1985). A Fossil Flora From Rafted Plio-Pleistocene Mudstones at Regatta Point, Tasmania. *Australian Journal of Botany*, **33**(5), 497-517.
Hill, R. S., & Bigwood, A. J. (1987). Tertiary gymnosperms from Tasmania: Araucariaceae. *Alcheringa*, **11**(4), 325-335.
Hill, R. S., & Carpenter, R. J. (1991). Evolution of *Acmopyle* and *Dacrycarpus* (Podocarpaceae) foliage as inferred from macrofossils in south-eastern Australia. *Australian Systematic Botany*, **4**(3), 449-479.
Hill, R. S., Jordan, G. J., & Carpenter, R. J. (1993). Taxodiaceous macrofossils from Tertiary and Quaternary sediments in Tasmania. *Australian Systematic Botany*, **6**(3), 237-249.
Hill, R. S., & Merrifield, H. E. (1993). An early tertiary macroflora from West Dale, southwestern Australia. *Alcheringa*, **17**(4), 285-326.
Hill, R. S., & Pole, M. S. (1992). Leaf and shoot morphology of extant *Afrocarpus, Nageia* and *Retrophyllum* (Podocarpaceae) species, and species with similar leaf arrangement, from Tertiary sediments in Australia. *Australian Systematic Botany*, **5**(3), 337-358.
Hill, R. S., Jordan, G. J., Carpenter, R. J., & Paull, R. (2019). *Araucaria* Section Eutacta Macrofossils from the Cenozoic of Southeastern Australia. *International Journal of Plant Sciences*, **180**(8), 902-921.
Jordan, G. J. (1997). Evidence of Pleistocene plant extinction and diversity from Regatta Point, western Tasmania, Australia. *Botanical Journal of the Linnean Society*, **123**(1), 45-71.
Jordan, G. J., Carpenter, R. J., Bannister, J. M., Lee, D. E., Mildenhall, D. C., & Hill, R. S. (2011). High conifer diversity in Oligo-Miocene New Zealand. *Australian Systematic Botany*, **24**(2), 121-136.

Kershaw, A. P., Bretherton, S. C., & van der Kaars, S. (2007). A complete pollen record of the last 230 ka from Lynch's Crater, north-eastern Australia. *Palaeogeography, Palaeoclimatology, Palaeoecology*, **251**(1), 23-45.

Lee, D. E., Bannister, J. M., & Lindqvist, J. K. (2007). Late Oligocene–Early Miocene leaf macrofossils confirm a long history of *Agathis* in New Zealand. *New Zealand Journal of Botany*, **45**(4), 565-578.

Macphail, M., & Cantrill, D. J. (2006). Age and implications of the Forest Bed, Falkland Islands, southwest Atlantic Ocean: evidence from fossil pollen and spores. *Palaeogeography, Palaeoclimatology, Palaeoecology*, **240**(3-4), 602-629.

Macphail, M., Carpenter, R. J., Iglesias, A., & Wilf, P. (2013). First evidence for Wollemi pine-type pollen (*Dilwynites*: Araucariaceae) in South America. *PloS one*, **8**(7), e69281.

McGlone, M. S., Howorth, R., & Pullar, W. A. (1984). Late Pleistocene stratigraphy, vegetation and climate of the Bay of Plenty and Gisborne regions, New Zealand. *New Zealand Journal of Geology and Geophysics*, **27**(3), 327-350.

McGlone, M. S. (2001). The origin of the indigenous grasslands of southeastern South Island in relation to pre-human woody ecosystems. *New Zealand Journal of Ecology*, 1-15.

Melendi, D. L., Scafati, L. H., & Volkheimer, W. (2003). Palynostratigraphy of the Paleogene Huitrera Formation in NW Patagonia, Argentina. *Neues Jahrbuch für Geologie und Paläontologie-Abhandlungen*, 205-273.

Náñez C, Quattrocchio ME, & Ruiz L. 2009. Palinología y micropaleontología de las Formaciones San Julián y Monte León (Oligoceno-Mioceno temprano) en el subsuelo de cabo Curioso, provincia de Santa Cruz, Argentina. *Ameghiniana*, **46**, 669–693.

Paull, R., & Hill, R. S. (2009). *Libocedrus* macrofossils from Tasmania (Australia). *International Journal of Plant Sciences*, **170**(3), 381-399.

Pickett, J. W., Macphail, M. K., Partridge, A. D., & Pole, M. S. (1997). Middle Miocene palaeotopography at Little Bay, near Maroubra, New South Wales. *Australian Journal of Earth Sciences*, **44**(4), 509-518.

Pole, M. (1992). Eocene vegetation from Hasties, north-eastern Tasmania. *Australian Systematic Botany*, **5**(4), 431-475.

Pole, M. (1996). Plant macrofossils from the Foulden Hills Diatomite (Miocene), Central Otago, New Zealand. *Journal of the Royal Society of New Zealand*, **26**(1), 1-39.

Pole, M. (1997). Miocene conifers from the Manuherikia group, New Zealand. *Journal of the Royal Society of New Zealand*, **27**(3), 355-370.

Pole, M. (2007). Early Eocene dispersed cuticles and mangrove to rainforest vegetation at Strahan-Regatta Point, Tasmania. *Palaeontologia Electronica*, **10**(15A), 66.

Pole, M. S., Hill, R. S., Green, N., & Macphail, M. K. (1993). The Oligocene Berwick Quarry flora—rainforest in a drying environment. *Australian Systematic Botany*, **6**(5), 399-427.

Pross, J. (2012). Integrated Ocean Drilling Program Expedition 318 Scientists Persistent near-tropical warmth on the Antarctic continent during the early Eocene epoch. *Nature*, **488**(7409), 73-77.

Romero, E. (1985). Polen de Angiospermas de la formacion Rio Turbio (Eoceno), Provincia de Santa Cruz, Republica Argentina. *Ameghiniana*, **22**(1-2), 43-51.

Rossetto-Harris, G., Wilf, P., Escapa, I. H., & Andruchow-Colombo, A. (2020). Eocene *Araucaria* sect. Eutacta from Patagonia and floristic turnover during the initial isolation of South America. *American Journal of Botany*, **107**(5), 806-832.

Scafati, L., Melendi, D. L., & Volkheimer, W. (2009). A Danian subtropical lacustrine palynobiota from South America (Bororó Formation, San Jorge Basin, Patagonia-Argentina). *Geologica Acta*, **7**(1), 35-62.

Sniderman, J. K. (2011). Early Pleistocene vegetation change in upland south-eastern Australia. *Journal of Biogeography*, **38**(8), 1456-1470.

Taylor, G., Truswell, E. M., McQueen, K. G., & Brown, M. C. (1990). Early Tertiary palaeogeography, landform evolution, and palaeoclimates of the Southern Monaro, NSW, Australia. *Palaeogeography, Palaeoclimatology, Palaeoecology*, **78**(1-2), 109-134.

Torres, T., Méon, H., Otero, R. A., Galleguillos, H., & Pintana, S. (2009, November). Palinoflora y macroflora de la Formación Loreto, Punta Arenas, Región de Magallanes, Chile. 'Congreso Geológico Chileno' (No. 12).

Truswell, E. M., & Macphail, M. K. (2009). Polar forests on the edge of extinction: what does the fossil spore and pollen evidence from East Antarctica say? *Australian Systematic Botany*, **22**(2), 57-106.

Wells, P. M., & Hill, R. S. (1989). Fossil imbricate-leaved Podocarpaceae from Tertiary sediments in Tasmania. *Australian Systematic Botany*, **2**(4), 387-423.

Whang, S. S., & Hill, R. S. (1999). Late Palaeocene Cupressaceae macrofossils at Lake Bungarby, New South Wales. *Australian Systematic Botany*, **12**(2), 241-254.

Wilf, P., Johnson, K. R., Cuneo, N. R., Smith, M. E., Singer, B. S., & Gandolfo, M. A. (2005). Eocene plant diversity at Laguna del Hunco and Río Pichileufú, Patagonia, Argentina. *The American Naturalist*, **165**(6), 634-650.

Wilf, P., Little, S. A., Iglesias, A., del Carmen Zamaloa, M., Gandolfo, M. A., Cúneo, N. R., & Johnson, K. R. (2009). *Papuacedrus* (Cupressaceae) in Eocene Patagonia: a new fossil link to Australasian rainforests. *American Journal of Botany*, **96**(11), 2031-2047.

Wilf, P. (2012). Rainforest conifers of Eocene Patagonia: attached cones and foliage of the extant Southeast Asian and Australasian genus *Dacrycarpus* (Podocarpaceae). *American Journal of Botany*, **99**(3), 562-584.

Wilf, P., Escapa, I. H., Cúneo, N. R., Kooyman, R. M., Johnson, K. R., & Iglesias, A. (2014). First South American *Agathis* (Araucariaceae), Eocene of Patagonia. *American Journal of Botany*, **101**(1), 156-179.

Wilf, P., Donovan, M. P., Cúneo, N. R., & Gandolfo, M. A. (2017). The fossil flip-leaves (*Retrophyllum*, Podocarpaceae) of southern South America. *American Journal of Botany*, **104**(9), 1344-1369.
Zamaloa, M. D. C., & Romero, E. J. (2005). Neogene palynology of Tierra del Fuego, Argentina: conifers. *Alcheringa*, **29**(1), 113-121.
Zetter, R., Hofmann, C. C., Draxler, I., Durango de Cabrera, J., Del MVergel, M., & Vervoorst, F. (1999). A rich middle Eocene microflora at Arroyo de los Mineros, near Cañadón Beta, NE Tierra del Fuego province, Argentina. *Abhandlungen-Geologischen Bundesanstalt*, **56**(1), 439-460.

Supporting Information for Chapter 4

Contents

Supporting Methods – Image preparation for trait reliability

Fully expanded adult leaves were collected from healthy plants grown at the University of Tasmania and the Royal Botanic Gardens Edinburgh (Table S4.1). These plants were all growing in shaded, frost-free greenhouses. For species with a wide geographic distribution, we sampled leaves from individuals with multiple provenances (where this was possible).

For large leaves, pieces of approximately 1cm^2 were cut from either side of the midrib in the middle third of the leaf; for smaller leaves, the base, apex and, if possible, the margins were removed. These samples were soaked in commercial household bleach (50 gL^{-1} sodium hypochlorite and 13 gL^{-1} sodium hydroxide) until the cuticle separated from the mesophyll. Bleach was removed by thoroughly rinsing in water and remaining mesophyll tissue was

removed using a fine paintbrush. Sections were stained with 1% crystal violet or safranin solution for 1 minute, then mounted in phenol glycerine jelly. Several fields of view at ×10 magnification (field of view area, 0.56mm^2) were photographed from each section using a Nikon Digital Sight DS-L1 camera (Melville, NY, USA) mounted on a Leica DM 1000 microscope (Nussloch, Germany). The best 3-5 images (identified as the clearest, without damage or obvious distortion) for each individual plant were selected for analyses.

Table S4.1 Plants sampled for trait reliability analyses. Plants were sampled from the Royal Botanical Gardens, Edinburgh (RBGE) or the University of Tasmania, Hobart (UTAS).

PLANT ID	SPECIES	COLLECTED FROM	ACCESSION #
Acmopyle_pancheri1	*Acmopyle pancheri*	RBGE	19842681
Afrocarpus_falcatus1	*Afrocarpus falcatus*	RBGE	20001613
Afrocarpus_gracilior1	*Afrocarpus gracilior*	RBGE	19820027
Afrocarpus_mannii1	*Afrocarpus mannii*	RBGE	19960587
Falcatifolium_taxoides1	*Falcatifolium taxoides*	UTAS	-
Falcatifolium_taxoides2	*Falcatifolium taxoides*	UTAS	-
Pectinopitys_ladei1	*Pectinopitys ladei*	UTAS	-
Phyllocladus_aspleniifolius1	*Phyllocladus aspleniifolius*	UTAS	-
Phyllocladus_trichomanoides1	*Phyllocladus trichomanoides*	UTAS	-
Podocarpus_brassii1	*Podocarpus brassii*	UTAS	-
Podocarpus_coriaceus1	*Podocarpus coriaceus*	RBGE	20030490
Podocarpus_costalis1	*Podocarpus costalis*	RBGE	19763956
Podocarpus_dispermus1	*Podocarpus dispermus*	UTAS	-
Podocarpus_dispermus2	*Podocarpus dispermus*	RBGE	20110038
Podocarpus_forrestii1	*Podocarpus forrestii*	RBGE	19915024
Podocarpus_lucienii1	*Podocarpus lucienii*	RBGE	20010205
Podocarpus_matudae1	*Podocarpus matudae*	RBGE	19972324
Podocarpus_nakaii1	*Podocarpus nakaii*	RBGE	19763844
Podocarpus_neriifolius1	*Podocarpus neriifolius*	UTAS	-
Podocarpus_neriifolius2	*Podocarpus neriifolius*	RBGE	19681468
Podocarpus_pilgeri1	*Podocarpus pilgeri*	RBGE	20022521
Podocarpus_sellowii1	*Podocarpus sellowii*	RBGE	20071743
Podocarpus_trinitensis1	*Podocarpus trinitensis*	RBGE	20030491
Retrophyllum_rospigliossii1	*Retrophyllum rospigliossii*	RBGE	19951953
Retrophyllum_rospigliossii2	*Retrophyllum rospigliossii*	UTAS	-
Sundacarpus_amarus1	*Sundacarpus amarus*	RBGE	20030752

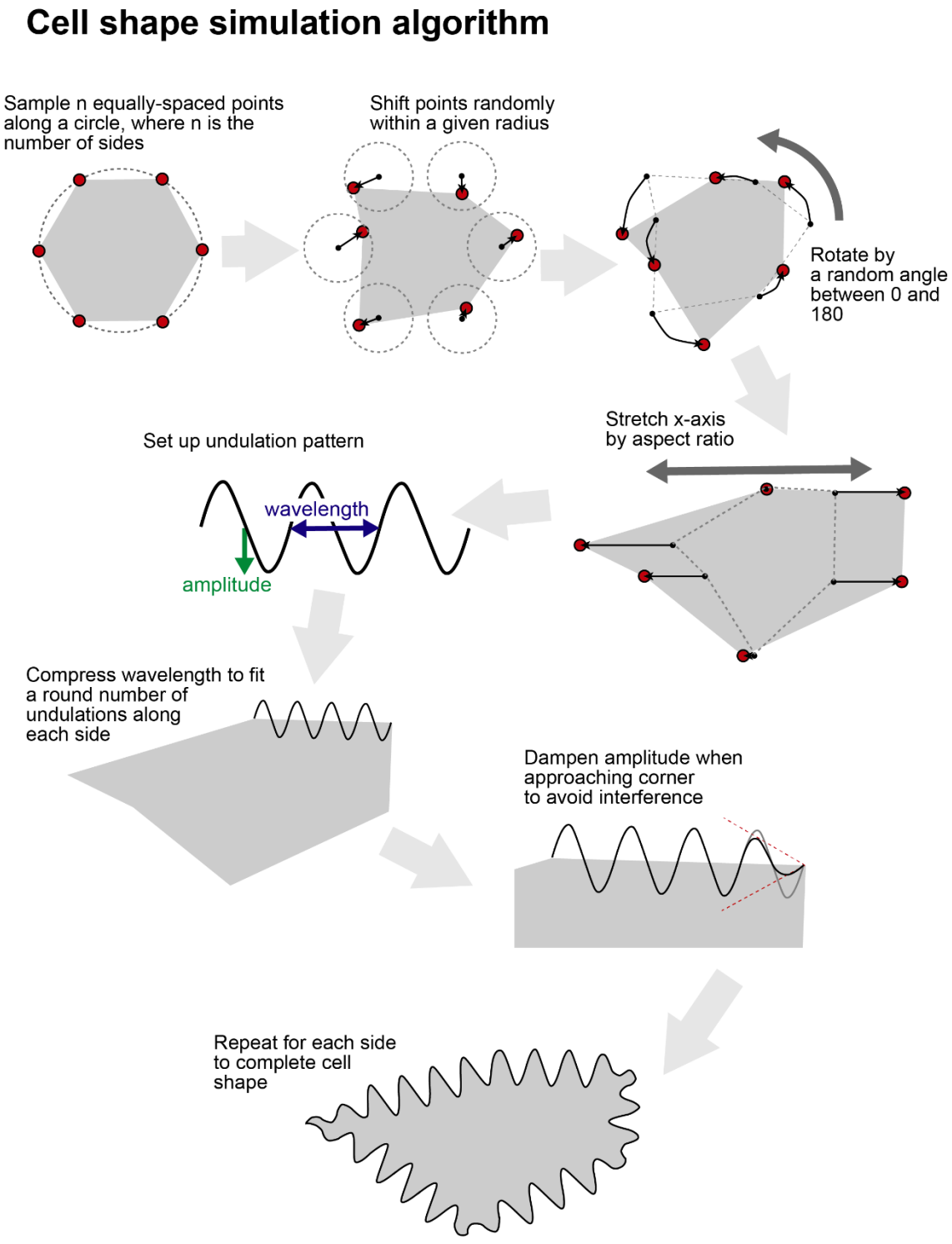

Figure S4.1. Simulated cell generation. We generated cells with 3,4,5 and 6 sides, with aspect ratios of 1,2 and 5. These formed the 'straight-walled' cells. Each of these cells was then undulated with a frequency of 1, 2 and 3, and an amplitude of 0.2, 1 and 2, although for some shapes the maximum amplitude was not reached because of dampening effects.

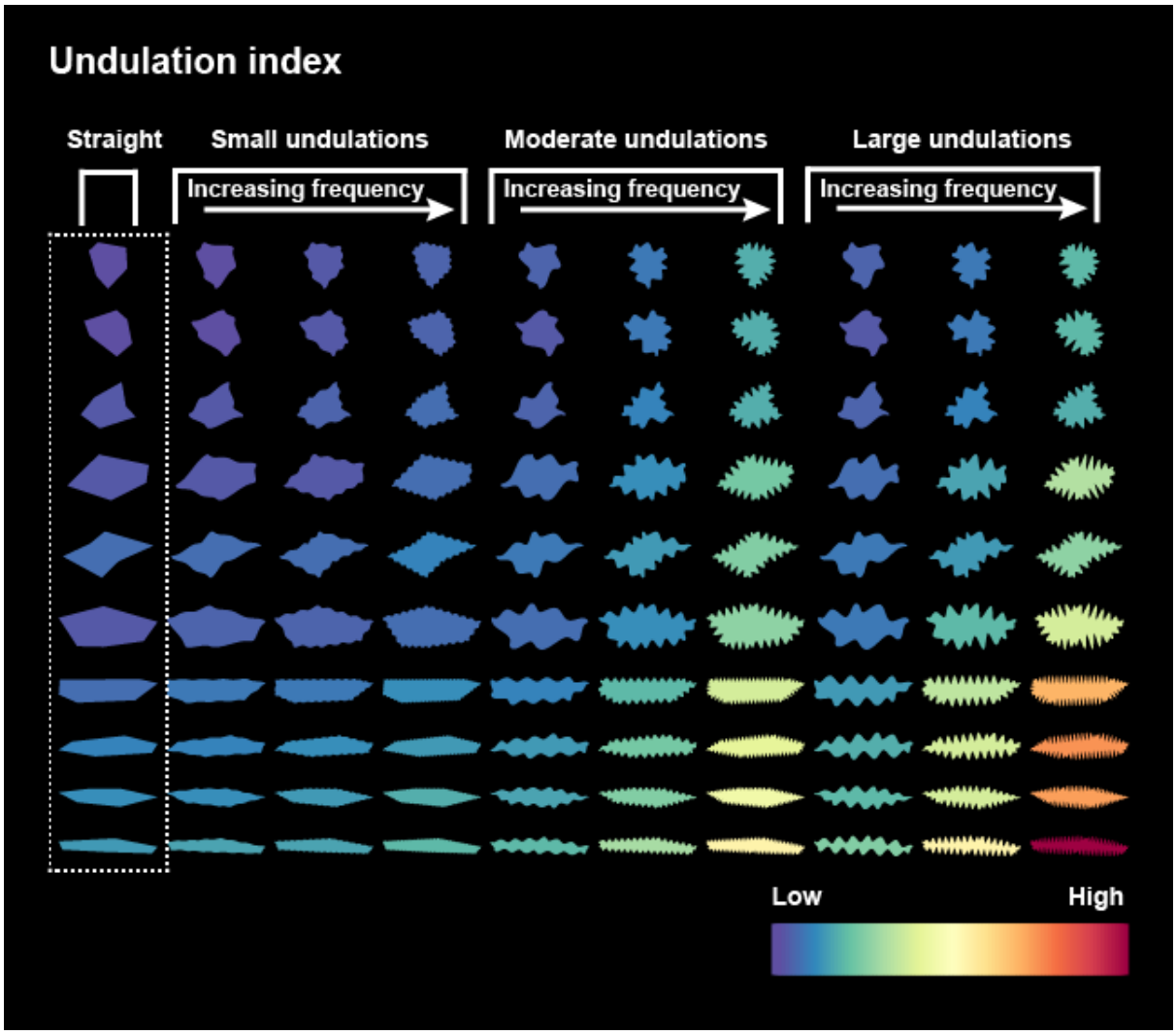

Figure S4.2. Measured values of undulation index (UI; see Table 4.1) on simulated cells. On straight-walled cells (highlighted with white dotted line), UI increases with aspect ratio.

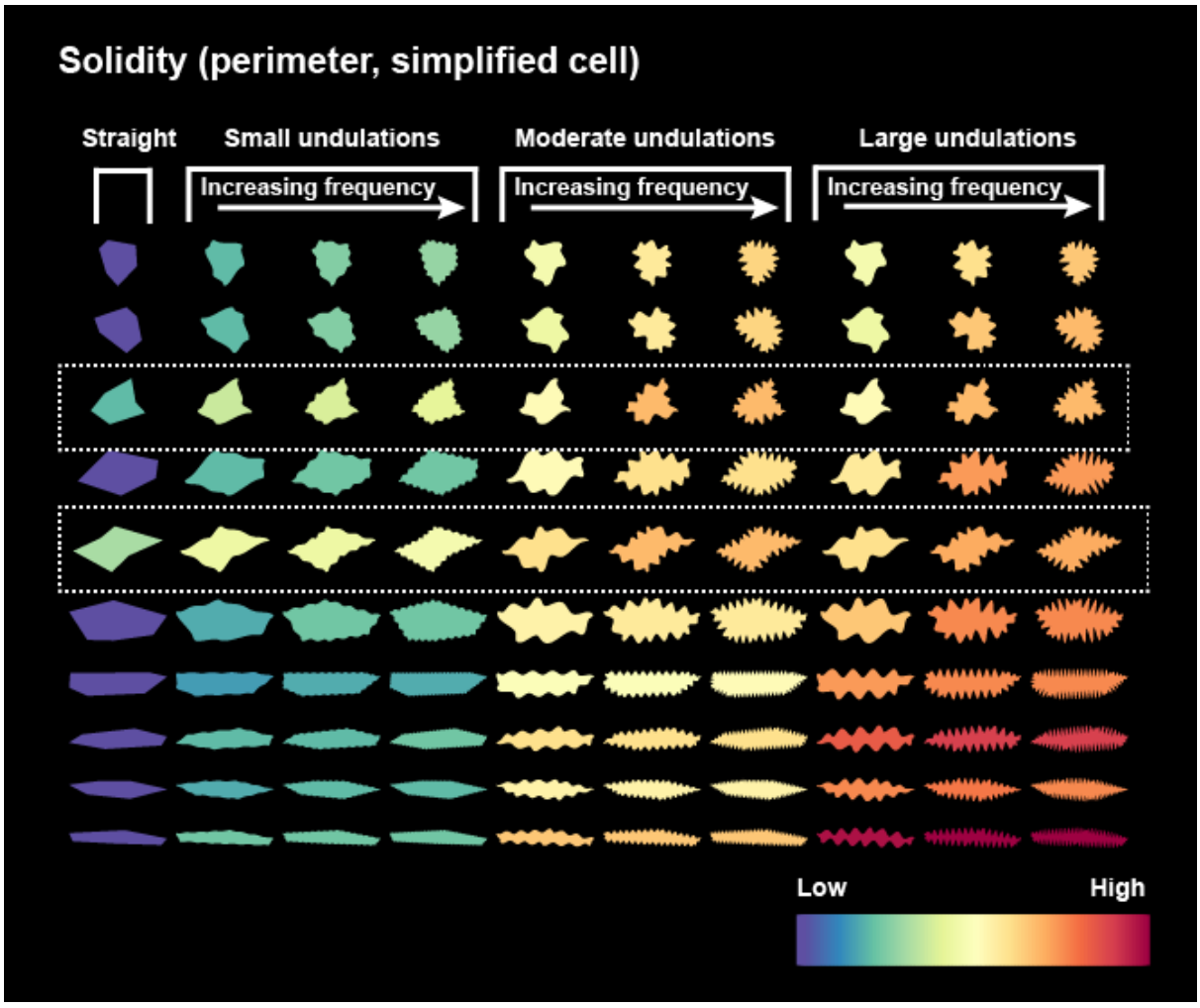

Figure S4.3. Measured values of solidity (see Table 4.1) on simulated cells. Solidity values are inflated for non-convex cells (highlighted with white dotted lines).

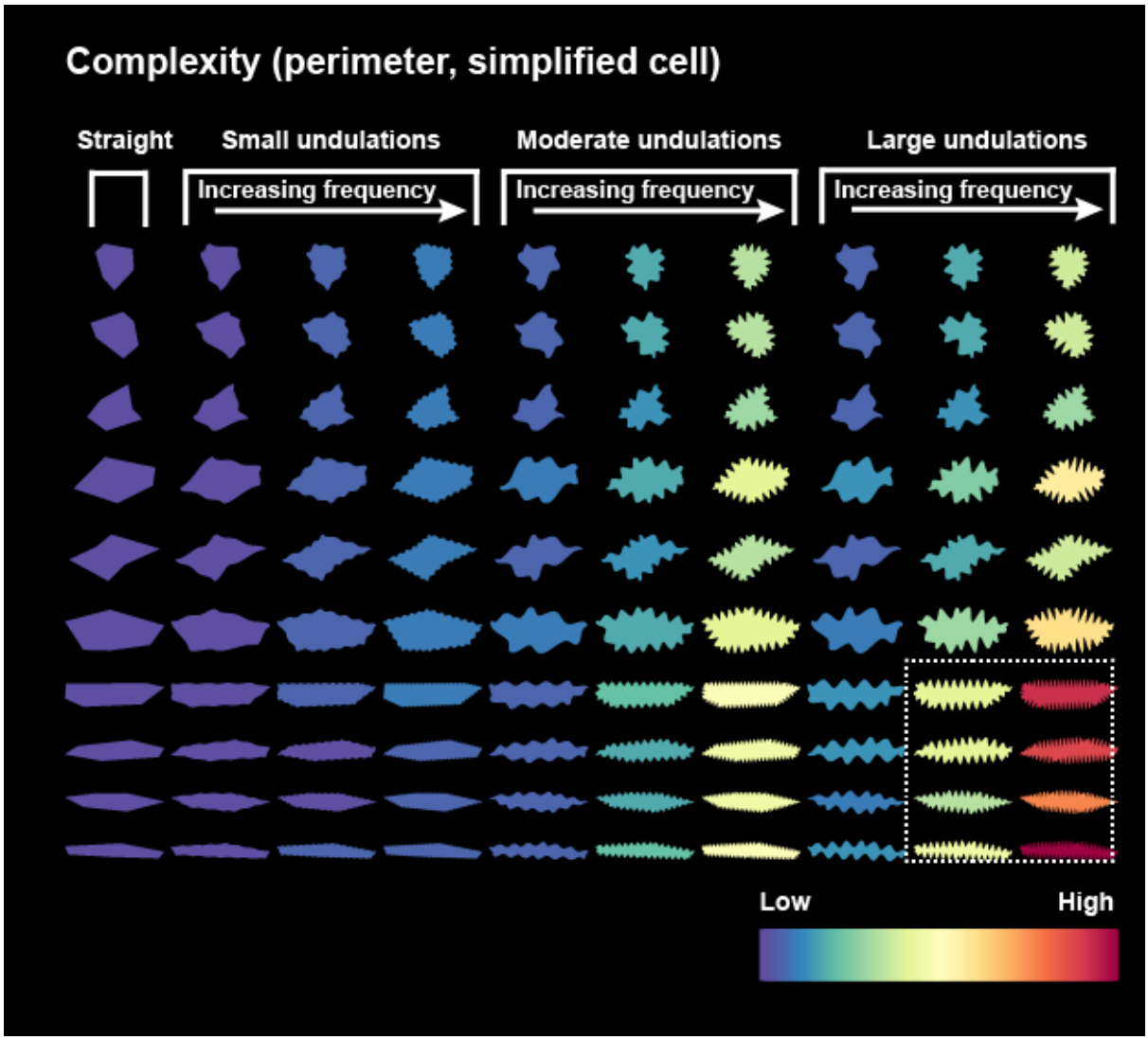

Figure S4.4. Measured values of complexity, a new metric presented here (see Figure 4.2), on simulated cells. Increases with undulation size and with undulation frequency. Note that the highlighted cells have exceptionally high values – this is due to the non-linear relationship between undulated and simple perimeter.

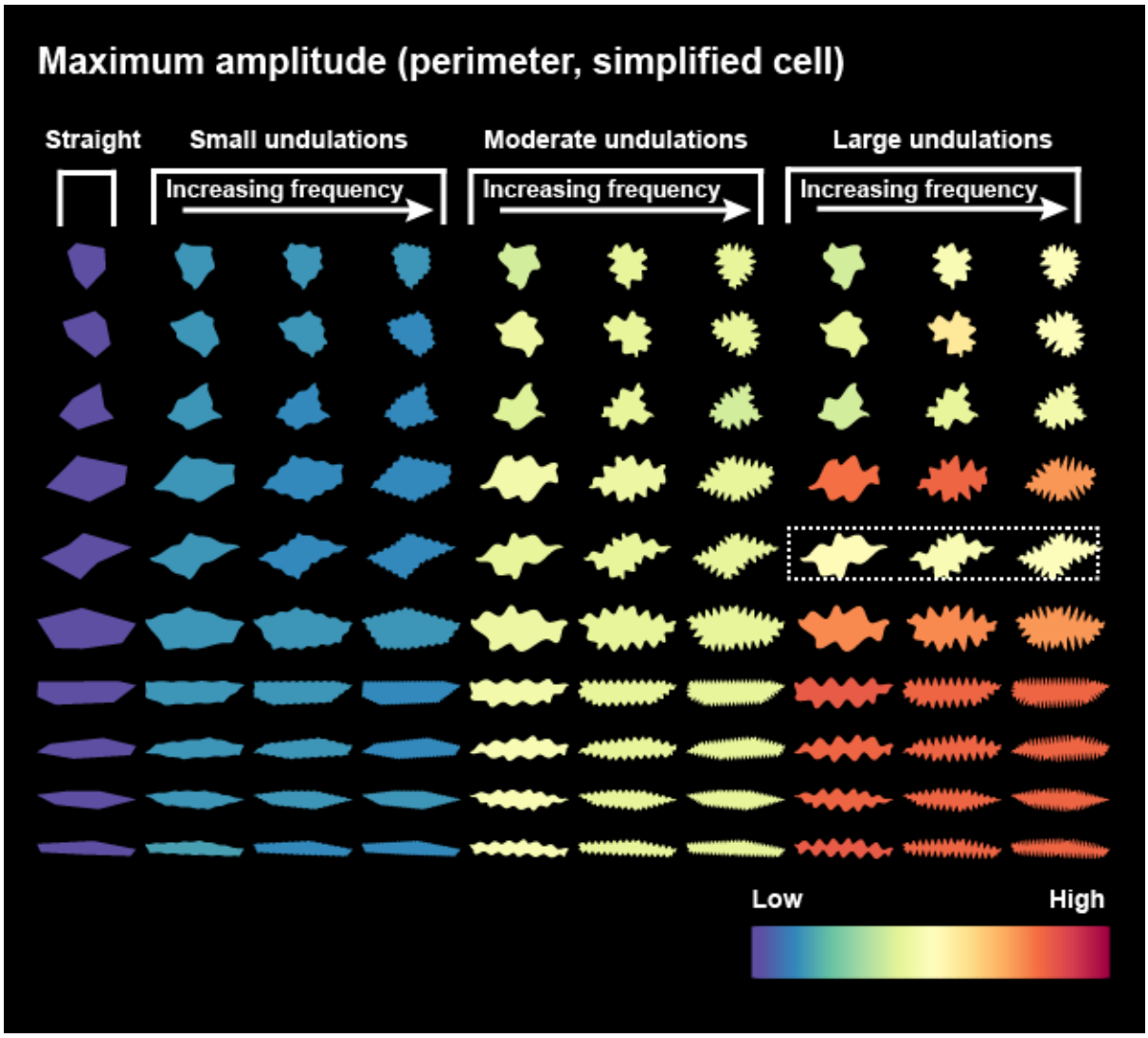

Figure S4.5. Measured values of maximum amplitude, a new metric presented here (see Fig. 4.2), on simulated cells. Increases with undulation size. Note that for some cells (e.g. those highlighted), the shape of the cell precludes the maximum amplitude from being reached – this is a quirk of the cell generation, not of the metric.

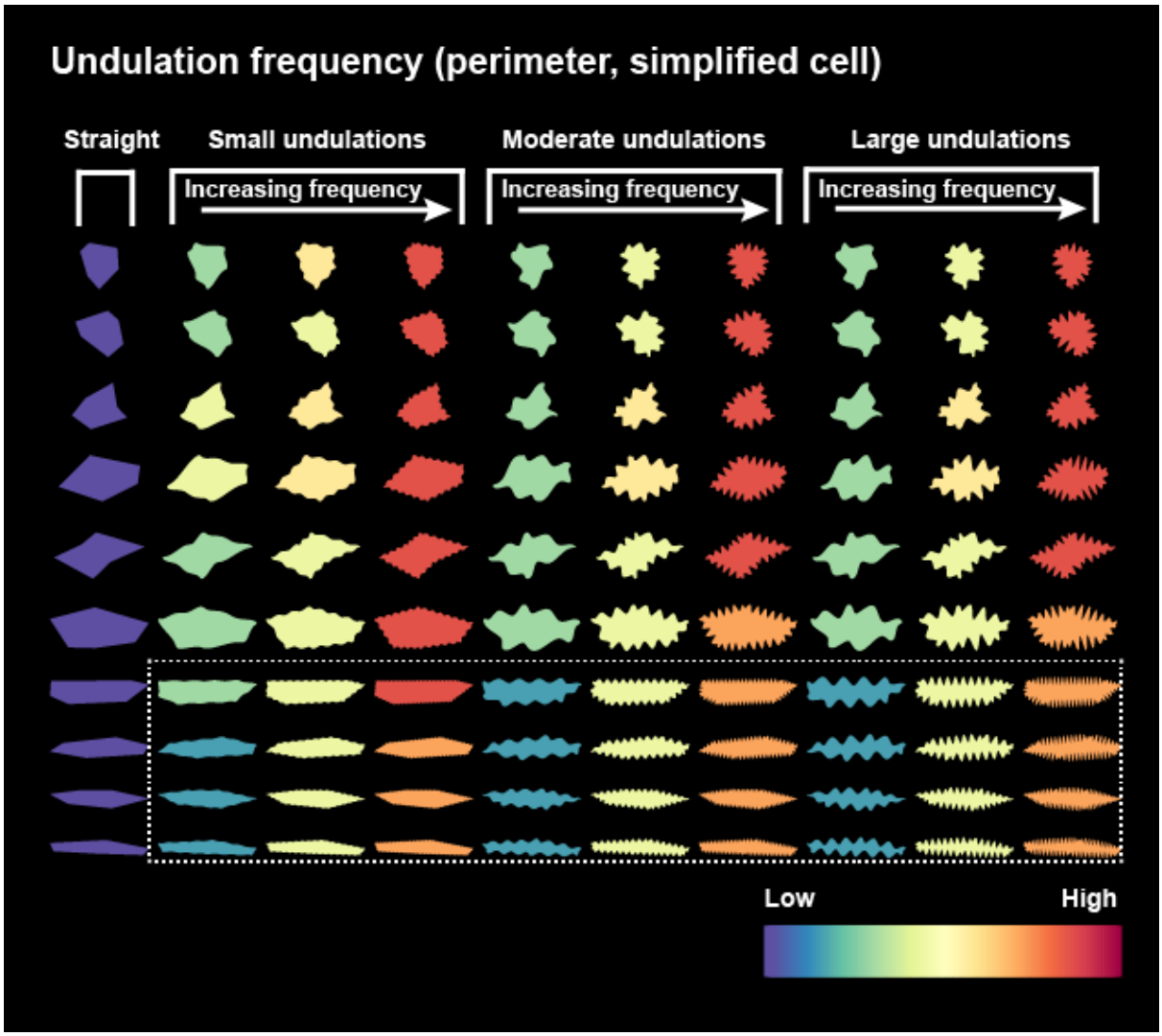

Figure S4.6. Measured values of undulation frequency, a new metric presented here (see Fig. 4.2), on simulated cells. Increases with undulation frequency. Note that for some cells (e.g. those highlighted), the frequency is lower than expected – this is a quirk of the cell generation (specifically the rounding of the wavelength to fit an integer number of undulations along a side), not of the metric.

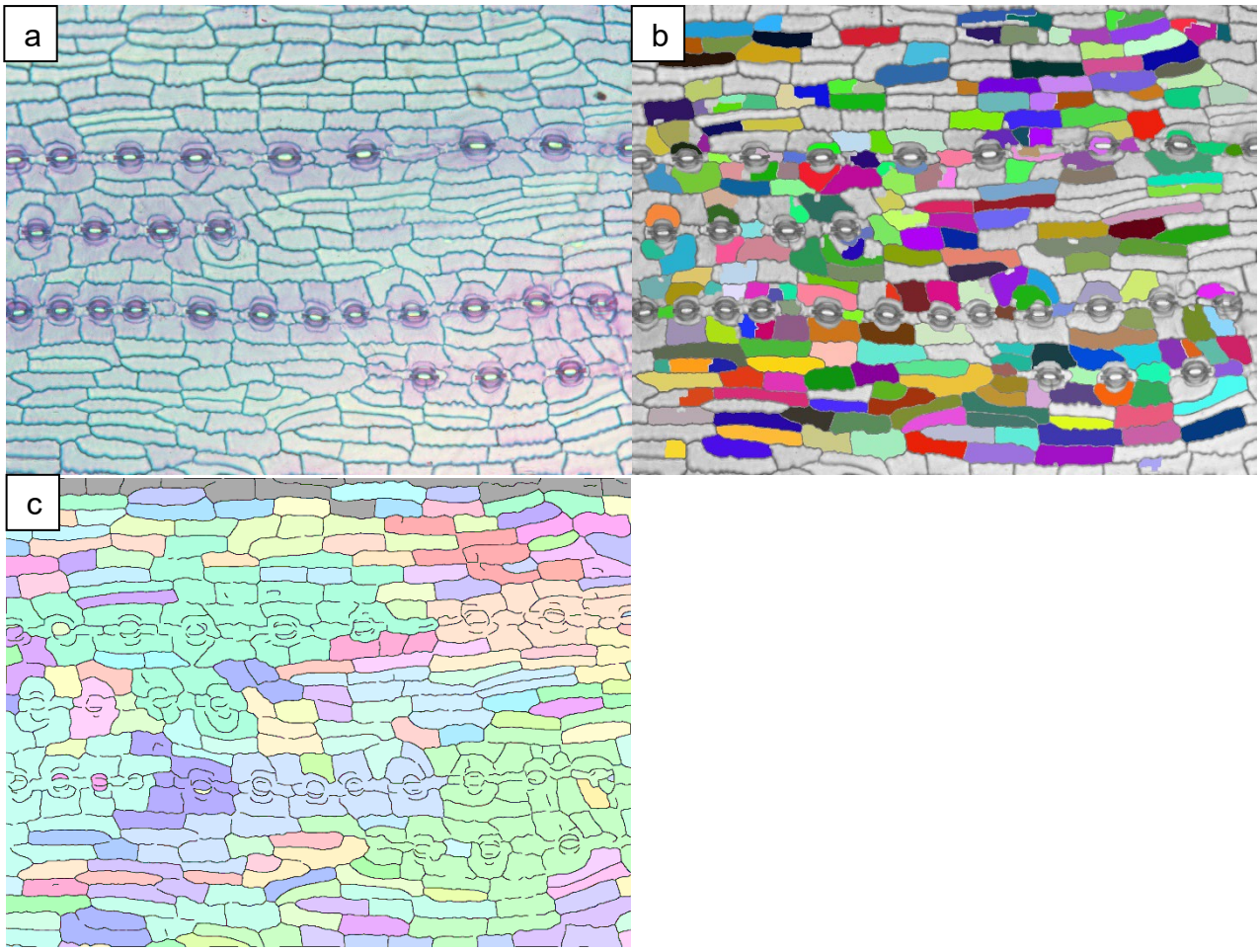

Figure S4.7. Automatic cell segmentation of a high-quality image of *Podocarpus coriaceus*. The raw image (a), PaCeQUant segmentation (b), segmentation after ridge detection (c).

Supporting Information for Chapter 5

Contents

Table S5.1 Correlation matrix between environmental variables

	max.height	map.min	meantwmq.min	mintcm.min	pdq.min
max.height	1	-0.44131	-0.29417	-0.20446	-0.52708
map.min	-0.44131	1	0.274781	0.583954	0.745511
meantwmq.min	-0.29417	0.274781	1	0.590471	0.127852
mintcm.min	-0.20446	0.583954	0.590471	1	0.410408
pdq.min	-0.52708	0.745511	0.127852	0.410408	1
map.max	0.207435	0.169402	-0.32985	-0.10423	0.044274
meantwmq.max	0.279846	-0.13763	0.572236	0.2733	-0.41355
mintcm.max	0.38464	0.190872	0.244657	0.587654	-0.09099
pdq.max	0.26703	-0.00463	-0.51607	-0.2194	0.043227

Table S5.2 Correlation matrix between epidermal traits

	stomatal.density.px2	stomatal.index	dist.between.stom.rows	stom.angle.sd	stom.distNN.mean	stom.dist2NN.mean	stom.spacingNN.mean	stom.nsubcells.mean	stom.subsarea.mean	stom.gclength.mean
stomatal.density.px2	1.00	0.68	-0.47	0.21	-0.68	-0.79	0.00	0.09	-0.23	-0.19
stomatal.index	0.68	1.00	-0.27	0.15	-0.55	-0.62	-0.11	-0.10	0.28	0.26
dist.between.stom.rows	-0.47	-0.27	1.00	-0.25	0.43	0.55	-0.03	-0.11	0.14	0.00
stom.angle.sd	0.21	0.15	-0.25	1.00	-0.34	-0.32	-0.01	-0.08	-0.06	-0.20
stom.distNN.mean	-0.68	-0.55	0.43	-0.34	1.00	0.95	0.04	-0.05	0.24	0.20
stom.dist2NN.mean	-0.79	-0.62	0.55	-0.32	0.95	1.00	0.08	-0.10	0.23	0.12
stom.spacingNN.mean	0.00	-0.11	-0.03	-0.01	0.04	0.08	1.00	-0.06	-0.07	-0.13
stom.nsubcells.mean	0.09	-0.10	-0.11	-0.08	-0.05	-0.10	-0.06	1.00	0.16	0.22
stom.subsarea.mean	-0.23	0.28	0.14	-0.06	0.24	0.23	-0.07	0.16	1.00	0.88
stom.gclength.mean	-0.19	0.26	0.00	-0.20	0.20	0.12	-0.13	0.22	0.88	1.00
stom.AR.mean	-0.17	-0.21	-0.02	-0.48	0.13	0.04	-0.06	0.06	-0.11	0.29
stom.butterfly.mean	0.20	0.07	-0.33	-0.24	-0.27	-0.28	-0.10	-0.19	-0.52	-0.31
stom.symmetry.mean	-0.31	-0.30	0.27	-0.28	0.48	0.46	-0.05	-0.18	-0.03	-0.03
pavezone.angle.median	-0.22	0.01	-0.01	0.35	0.04	0.06	0.07	-0.20	0.25	0.23
pavezone.AR.median	0.03	0.06	0.05	-0.24	-0.22	-0.23	-0.15	0.00	-0.26	-0.06
pavezone.area.median	-0.32	0.38	0.31	-0.02	0.20	0.27	-0.14	-0.31	0.53	0.39
pavezone.complexity.median	-0.26	-0.08	0.08	0.19	0.36	0.44	0.11	-0.18	0.24	0.02
pavezone.njunctionpts.mean	-0.07	-0.12	0.14	0.23	0.08	0.12	-0.09	-0.11	-0.06	-0.20
pavezone.undulation.amp.median	-0.31	0.19	0.21	0.05	0.32	0.41	0.06	-0.25	0.43	0.23
pavezone.undulation.freq.mean	0.10	-0.28	-0.07	0.34	0.05	0.04	0.02	0.06	-0.16	-0.25
stomzone.AR.median	0.08	0.24	-0.05	-0.43	-0.17	-0.20	-0.14	0.09	-0.10	0.19
stomzone.area.median	-0.41	0.28	0.40	-0.10	0.28	0.35	-0.15	-0.28	0.53	0.43
stomzone.complexity.median	-0.34	-0.03	0.19	0.16	0.37	0.46	0.01	-0.23	0.29	0.06

stomzone.undulation.amp.median	-0.36	0.26	0.30	0.09	0.21	0.32	-0.05	-0.30	0.46	0.27
stomzone.undulation.freq.mean	0.27	-0.31	-0.15	0.18	-0.10	-0.13	0.05	0.14	-0.46	-0.52
polar.AR.median	-0.09	0.26	0.34	-0.29	-0.04	-0.03	-0.24	0.03	0.08	0.27
polar.area.median	-0.03	0.52	0.13	-0.05	-0.12	-0.08	-0.13	0.05	0.63	0.61
polar.complexity.median	-0.37	-0.27	0.08	0.01	0.53	0.51	0.10	0.01	0.21	0.10
polar.undulation.amp.median	-0.36	-0.02	0.06	-0.03	0.51	0.51	0.06	0.00	0.50	0.38
polar.undulation.freq.mean	0.19	0.52	0.10	0.04	-0.45	-0.38	-0.17	-0.03	0.11	0.17

(continues over page)

	stom.AR.mean	stom.butterfly.mean	stom.symmetry.mean	pavezone.angle.median	pavezone.AR.median	pavezone.area.median	pavezone.complexity.median	pavezone.njunctionpts.mean	pavezone.undulation.amp.median	pavezone.undulation.freq.mean
stomatal.density.px2	-0.17	0.20	-0.31	-0.22	0.03	-0.32	-0.26	-0.07	-0.31	0.10
stomatal.index	-0.21	0.07	-0.30	0.01	0.06	0.38	-0.08	-0.12	0.19	-0.28
dist.between.stom.rows	-0.02	-0.33	0.27	-0.01	0.05	0.31	0.08	0.14	0.21	-0.07
stom.angle.sd	-0.48	-0.24	-0.28	0.35	-0.24	-0.02	0.19	0.23	0.05	0.34
stom.distNN.mean	0.13	-0.27	0.48	0.04	-0.22	0.20	0.36	0.08	0.32	0.05
stom.dist2NN.mean	0.04	-0.28	0.46	0.06	-0.23	0.27	0.44	0.12	0.41	0.04
stom.spacingNN.mean	-0.06	-0.10	-0.05	0.07	-0.15	-0.14	0.11	-0.09	0.06	0.02
stom.nsubcells.mean	0.06	-0.19	-0.18	-0.20	0.00	-0.31	-0.18	-0.11	-0.25	0.06
stom.subsarea.mean	-0.11	-0.52	-0.03	0.25	-0.26	0.53	0.24	-0.06	0.43	-0.16
stom.gclength.mean	0.29	-0.31	-0.03	0.23	-0.06	0.39	0.02	-0.20	0.23	-0.25
stom.AR.mean	1.00	0.15	0.25	-0.05	0.39	-0.16	-0.34	-0.26	-0.31	-0.22
stom.butterfly.mean	0.15	1.00	-0.15	-0.24	0.32	-0.17	-0.21	-0.21	-0.12	-0.24
stom.symmetry.mean	0.25	-0.15	1.00	-0.23	0.20	0.11	0.19	0.01	0.11	-0.06
pavezone.angle.median	-0.05	-0.24	-0.23	1.00	-0.11	0.18	0.17	0.14	0.15	0.07
pavezone.AR.median	0.39	0.32	0.20	-0.11	1.00	0.02	-0.34	-0.13	-0.23	-0.46
pavezone.area.median	-0.16	-0.17	0.11	0.18	0.02	1.00	0.41	0.02	0.77	-0.46
pavezone.complexity.median	-0.34	-0.21	0.19	0.17	-0.34	0.41	1.00	0.34	0.83	0.31
pavezone.njunctionpts.mean	-0.26	-0.21	0.01	0.14	-0.13	0.02	0.34	1.00	0.07	0.64
pavezone.undulation.amp.median	-0.31	-0.12	0.11	0.15	-0.23	0.77	0.83	0.07	1.00	-0.15
pavezone.undulation.freq.mean	-0.22	-0.24	-0.06	0.07	-0.46	-0.46	0.31	0.64	-0.15	1.00

stomzone.AR.median	0.59	0.33	0.10	-0.12	0.70	0.08	-0.42	-0.23	-0.24	-0.48
stomzone.area.median	-0.15	-0.10	0.06	0.13	0.00	0.85	0.20	-0.15	0.61	-0.48
stomzone.complexity.median	-0.38	-0.20	0.18	0.12	-0.24	0.54	0.95	0.35	0.87	0.22
stomzone.undulation.amp.median	-0.34	-0.13	0.07	0.14	-0.07	0.85	0.60	0.00	0.89	-0.30
stomzone.undulation.freq.mean	-0.10	-0.09	0.00	-0.12	-0.13	-0.67	0.06	0.51	-0.43	0.81
polar.AR.median	0.41	0.12	-0.05	0.05	0.42	0.30	-0.23	-0.21	0.06	-0.44
polar.area.median	-0.13	-0.03	-0.32	0.22	-0.01	0.55	-0.03	-0.25	0.35	-0.40
polar.complexity.median	-0.10	-0.27	0.17	0.04	-0.30	0.12	0.66	0.27	0.48	0.38
polar.undulation.amp.median	-0.18	-0.22	0.18	0.13	-0.33	0.40	0.68	0.07	0.71	0.08
polar.undulation.freq.mean	0.04	0.15	-0.38	0.06	0.24	0.32	-0.22	-0.10	0.07	-0.34

(continues over page)

	stomzone.AR.median	stomzone.area.median	stomzone.complexity.median	stomzone.undulation.amp.median	stomzone.undulation.freq.mean	polar.AR.median	polar.area.median	polar.complexity.median	polar.undulation.amp.median	polar.undulation.freq.mean
stomatal.density.px2	0.08	-0.41	-0.34	-0.36	0.27	-0.09	-0.03	-0.37	-0.36	0.19
stomatal.index	0.24	0.28	-0.03	0.26	-0.31	0.26	0.52	-0.27	-0.02	0.52
dist.between.stom.rows	-0.05	0.40	0.19	0.30	-0.15	0.34	0.13	0.08	0.06	0.10
stom.angle.sd	-0.43	-0.10	0.16	0.09	0.18	-0.29	-0.05	0.01	-0.03	0.04
stom.distNN.mean	-0.17	0.28	0.37	0.21	-0.10	-0.04	-0.12	0.53	0.51	-0.45
stom.dist2NN.mean	-0.20	0.35	0.46	0.32	-0.13	-0.03	-0.08	0.51	0.51	-0.38
stom.spacingNN.mean	-0.14	-0.15	0.01	-0.05	0.05	-0.24	-0.13	0.10	0.06	-0.17
stom.nsubcells.mean	0.09	-0.28	-0.23	-0.30	0.14	0.03	0.05	0.01	0.00	-0.03
stom.subsarea.mean	-0.10	0.53	0.29	0.46	-0.46	0.08	0.63	0.21	0.50	0.11
stom.gclength.mean	0.19	0.43	0.06	0.27	-0.52	0.27	0.61	0.10	0.38	0.17
stom.AR.mean	0.59	-0.15	-0.38	-0.34	-0.10	0.41	-0.13	-0.10	-0.18	0.04
stom.butterfly.mean	0.33	-0.10	-0.20	-0.13	-0.09	0.12	-0.03	-0.27	-0.22	0.15
stom.symmetry.mean	0.10	0.06	0.18	0.07	0.00	-0.05	-0.32	0.17	0.18	-0.38
pavezone.angle.median	-0.12	0.13	0.12	0.14	-0.12	0.05	0.22	0.04	0.13	0.06
pavezone.AR.median	0.70	0.00	-0.24	-0.07	-0.13	0.42	-0.01	-0.30	-0.33	0.24
pavezone.area.median	0.08	0.85	0.54	0.85	-0.67	0.30	0.55	0.12	0.40	0.32
pavezone.complexity.median	-0.42	0.20	0.95	0.60	0.06	-0.23	-0.03	0.66	0.68	-0.22
pavezone.njunctionpts.mean	-0.23	-0.15	0.35	0.00	0.51	-0.21	-0.25	0.27	0.07	-0.10
pavezone.undulation.amp.median	-0.24	0.61	0.87	0.89	-0.43	0.06	0.35	0.48	0.71	0.07
pavezone.undulation.freq.mean	-0.48	-0.48	0.22	-0.30	0.81	-0.44	-0.40	0.38	0.08	-0.34
stomzone.AR.median	1.00	0.09	-0.36	-0.14	-0.28	0.54	0.16	-0.30	-0.28	0.36
stomzone.area.median	0.09	1.00	0.40	0.81	-0.76	0.42	0.74	0.07	0.40	0.40

stomzone.complexity.median	-0.36	0.40	1.00	0.75	-0.06	-0.09	0.11	0.66	0.70	-0.06
stomzone.undulation.amp.median	-0.14	0.81	0.75	1.00	-0.61	0.21	0.52	0.32	0.60	0.26
stomzone.undulation.freq.mean	-0.28	-0.76	-0.06	-0.61	1.00	-0.43	-0.66	0.20	-0.22	-0.37
polar.AR.median	0.54	0.42	-0.09	0.21	-0.43	1.00	0.50	-0.14	-0.06	0.66
polar.area.median	0.16	0.74	0.11	0.52	-0.66	0.50	1.00	-0.10	0.27	0.67
polar.complexity.median	-0.30	0.07	0.66	0.32	0.20	-0.14	-0.10	1.00	0.80	-0.25
polar.undulation.amp.median	-0.28	0.40	0.70	0.60	-0.22	-0.06	0.27	0.80	1.00	-0.16
polar.undulation.freq.mean	0.36	0.40	-0.06	0.26	-0.37	0.66	0.67	-0.25	-0.16	1.00

Table S5.3 Correlation matrix between epidermal traits and environmental variables

	max.height	map.min	meantwmq.min	mintcm.min	pdq.min	map.max	meantwmq.max	mintcm.max	pdq.max
stomatal.density	-0.23	0.07	0.04	0.02	0.16	-0.17	-0.09	-0.22	-0.09
stomatal.index	-0.41	0.15	0.10	0.16	0.18	-0.03	-0.03	-0.10	0.04
dist.between.stom.rows	0.17	0.07	0.24	0.25	-0.18	0.06	0.31	0.38	-0.07
stom.angle.sd	-0.05	0.00	0.29	0.05	0.04	0.00	0.22	0.06	-0.04
stom.distNN.mean	0.26	-0.11	-0.03	-0.08	-0.15	0.09	-0.01	0.08	0.05
stom.dist2NN.mean	0.28	-0.08	-0.01	-0.05	-0.15	0.11	0.03	0.12	0.05
stom.spacingNN.mean	0.23	-0.08	-0.04	-0.07	-0.05	-0.11	0.05	-0.02	-0.06
stom.nsubcells.mean	-0.14	0.01	0.16	-0.05	-0.09	-0.09	0.05	-0.11	-0.14
stom.subsarea.mean	-0.26	0.01	0.20	0.14	-0.01	0.05	0.08	0.05	0.05
stom.gclength.mean	-0.23	0.06	0.08	0.09	0.06	0.08	-0.03	0.03	0.10
stom.AR.mean	0.16	0.01	-0.34	-0.17	-0.03	0.08	-0.24	-0.06	0.09
stom.butterfly.mean	0.04	0.03	-0.28	-0.04	0.11	0.01	-0.09	-0.01	0.12
stom.symmetry.mean	0.23	-0.09	-0.29	-0.07	-0.06	0.16	-0.11	0.12	0.18
pavezone.angle.median	0.09	0.03	0.00	-0.03	-0.06	0.18	0.14	0.17	0.14
pavezone.AR.median	-0.02	-0.03	-0.26	-0.04	-0.05	-0.10	-0.08	0.10	-0.03
pavezone.area.median	-0.05	0.13	0.06	0.20	0.06	0.16	0.15	0.23	0.17
pavezone.complexity.median	0.35	-0.02	-0.02	-0.10	-0.20	0.26	0.22	0.19	0.20
pavezone.njunctionpts.mean	0.15	-0.05	0.14	-0.13	-0.11	0.12	0.27	0.17	0.02
pavezone.undulation.amp.median	0.17	0.08	0.01	0.07	-0.10	0.28	0.21	0.23	0.26
pavezone.undulation.freq.mean	0.17	-0.10	0.21	-0.28	-0.17	0.01	0.17	-0.09	-0.14
stomzone.AR.median	-0.16	0.10	-0.30	-0.07	0.09	-0.01	-0.28	-0.09	0.07
stomzone.area.median	-0.19	0.17	0.19	0.28	0.13	0.12	0.09	0.20	0.10

stomzone.complexity.median	0.24	0.01	0.08	-0.02	-0.19	0.24	0.25	0.22	0.15
stomzone.undulation.amp.median	0.00	0.14	0.17	0.24	-0.02	0.16	0.23	0.28	0.12
stomzone.undulation.freq.mean	0.17	-0.21	0.01	-0.35	-0.22	-0.10	0.06	-0.20	-0.19
polar.AR.median	-0.14	0.28	0.01	0.23	-0.01	0.16	-0.07	0.16	0.06
polar.area.median	-0.38	0.30	0.30	0.38	0.22	0.09	0.08	0.16	0.04
polar.complexity.median	0.25	-0.09	0.06	-0.09	-0.33	0.08	0.12	0.06	0.00
polar.undulation.amp.median	0.13	-0.01	0.07	0.04	-0.15	0.14	0.11	0.13	0.12
polar.undulation.freq.mean	-0.43	0.43	0.21	0.36	0.26	0.10	-0.01	0.09	-0.02

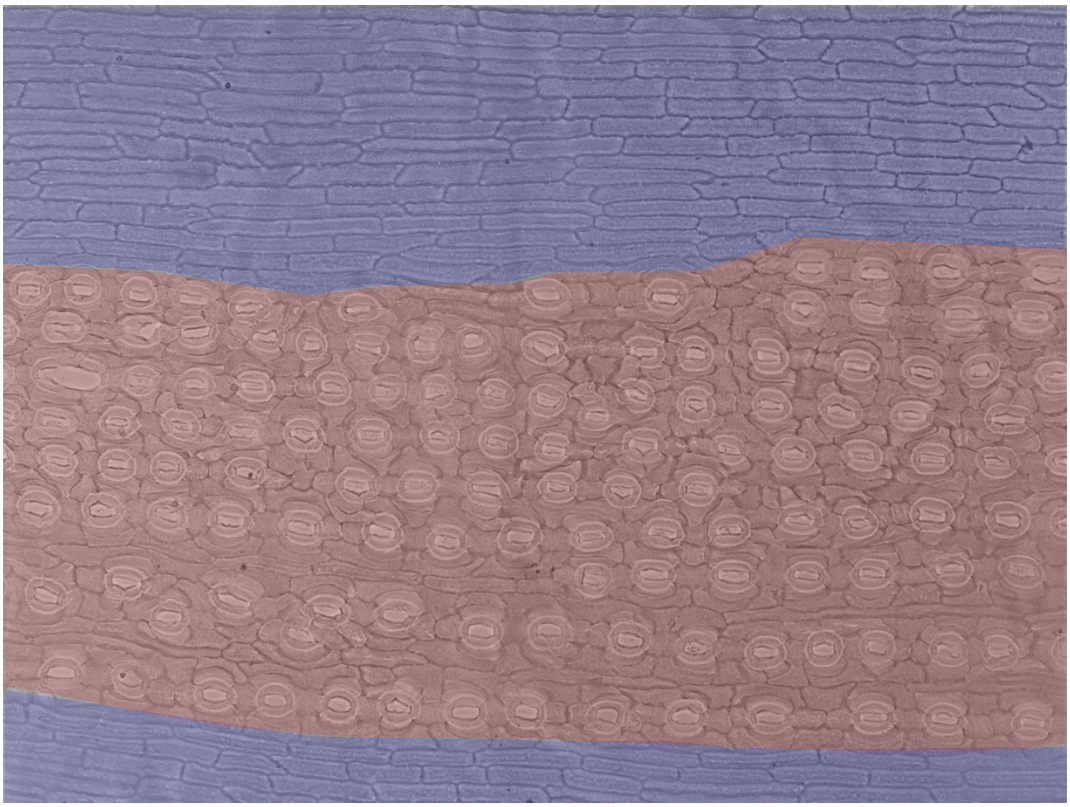

Figure S5.1 Cuticle of *Podocarpus gnidioides*, showing region of concentrated stomata (red) and non-stomatal region (blue).

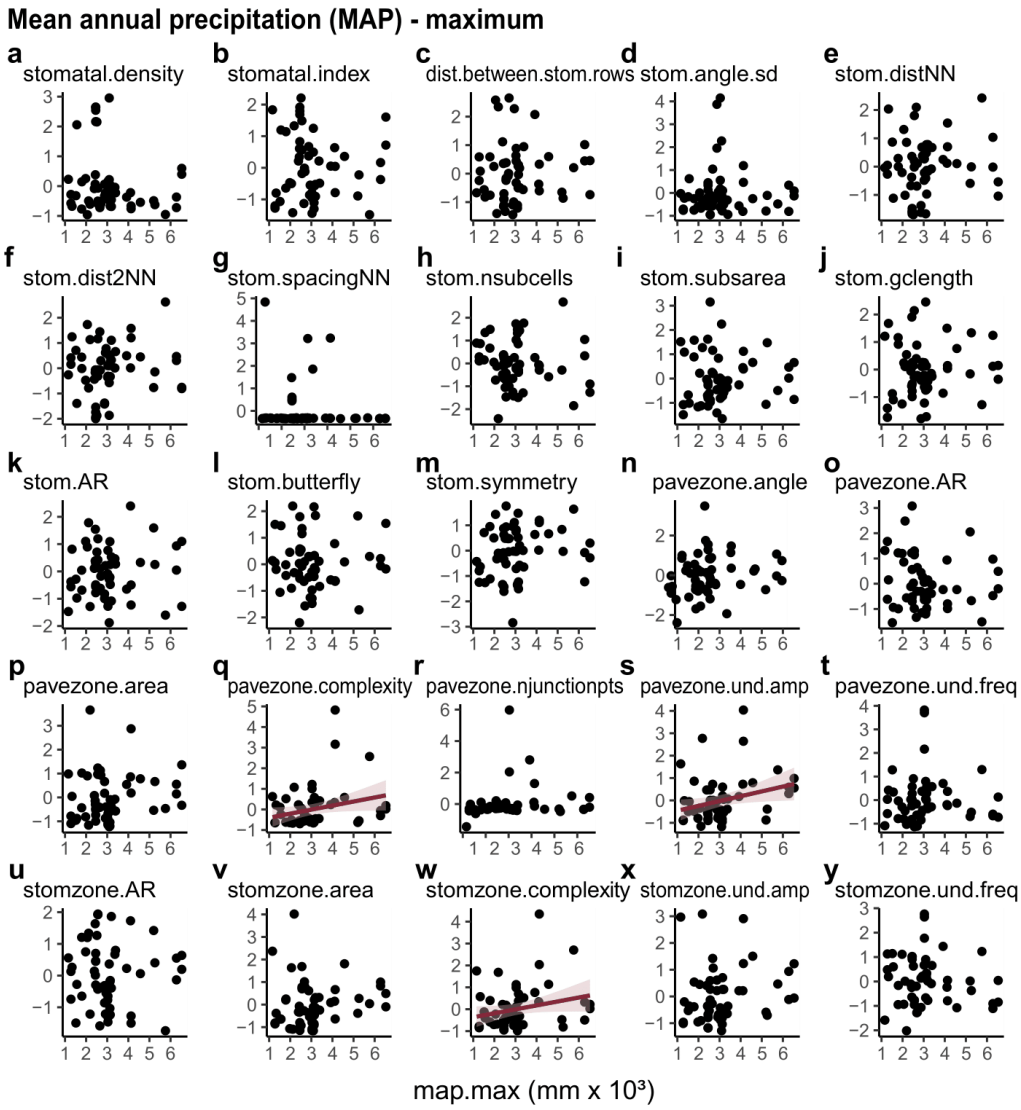

Figure S5.2 Scatterplots between each epidermal trait and mean annual precipitation – maximum. Linear relationships between variables with a correlation coefficient >0.2 are shown.

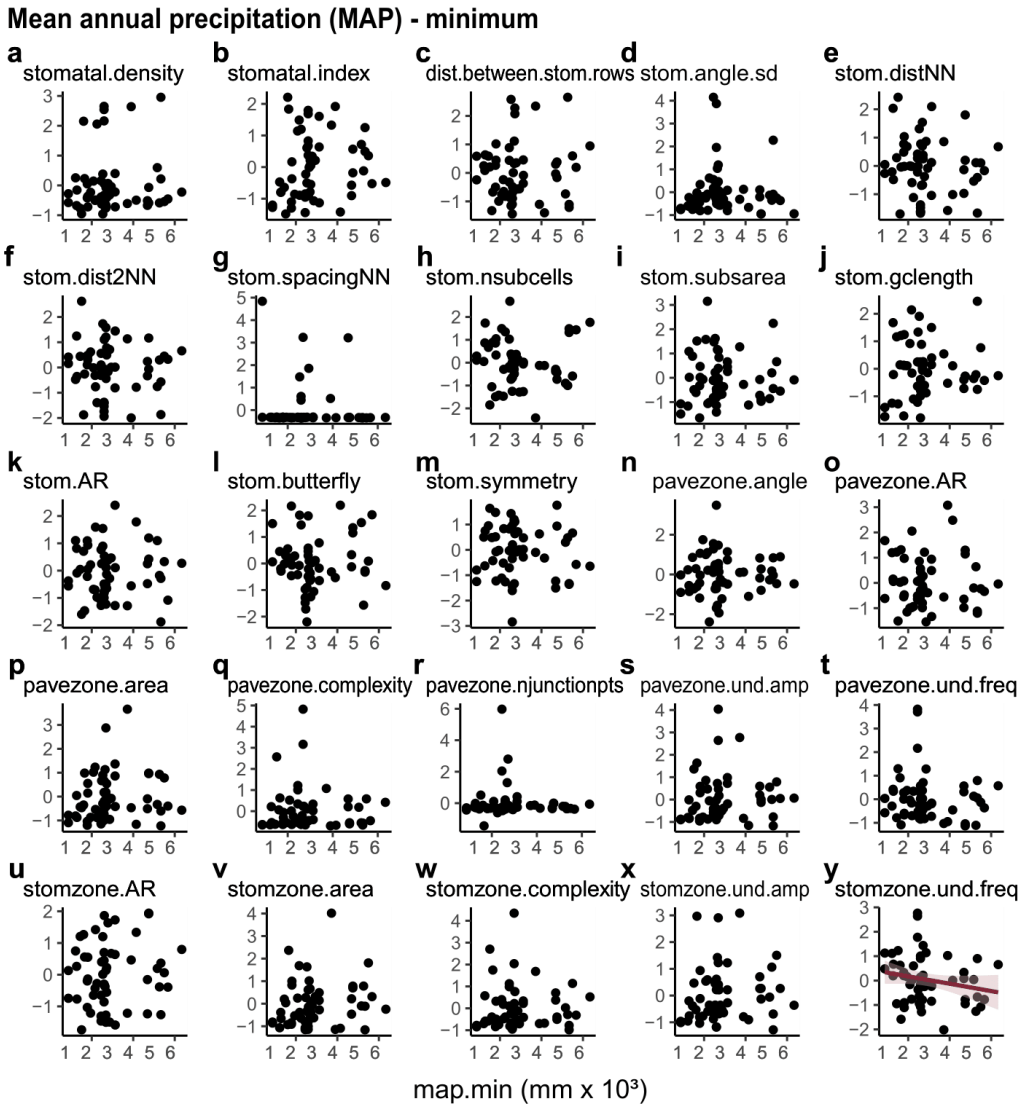

Figure S5.3 Scatterplots between each epidermal trait and mean annual precipitation – minimum. Linear relationships between variables with a correlation coefficient >0.2 are shown.

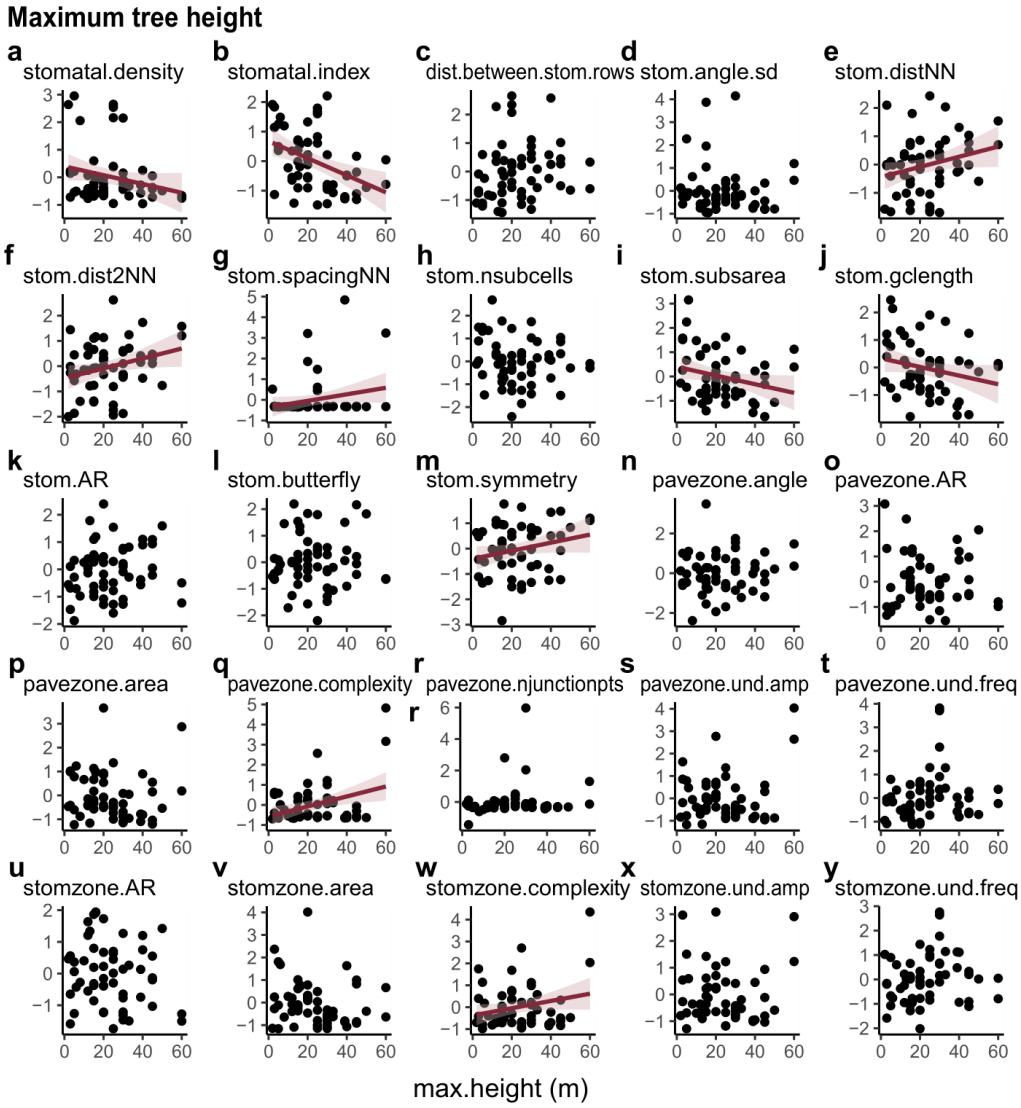

Figure S5.4 Scatterplots between each epidermal trait and maximum tree height. Linear relationships between variables with a correlation coefficient >0.2 are shown.

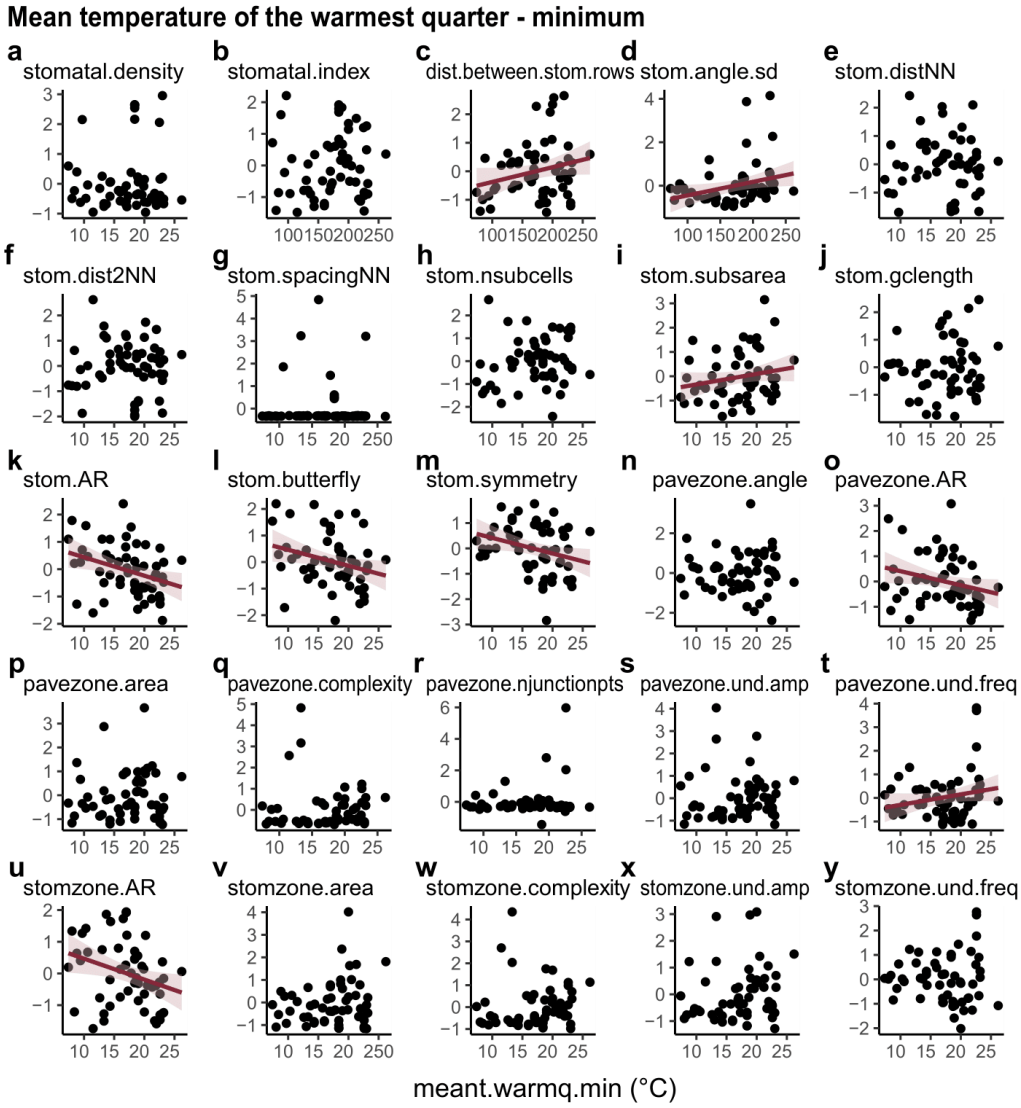

Figure S5.5 Scatterplots between each epidermal trait and mean temperature of the warmest quarter – minimum. Linear relationships between variables with a correlation coefficient >0.2 are shown.

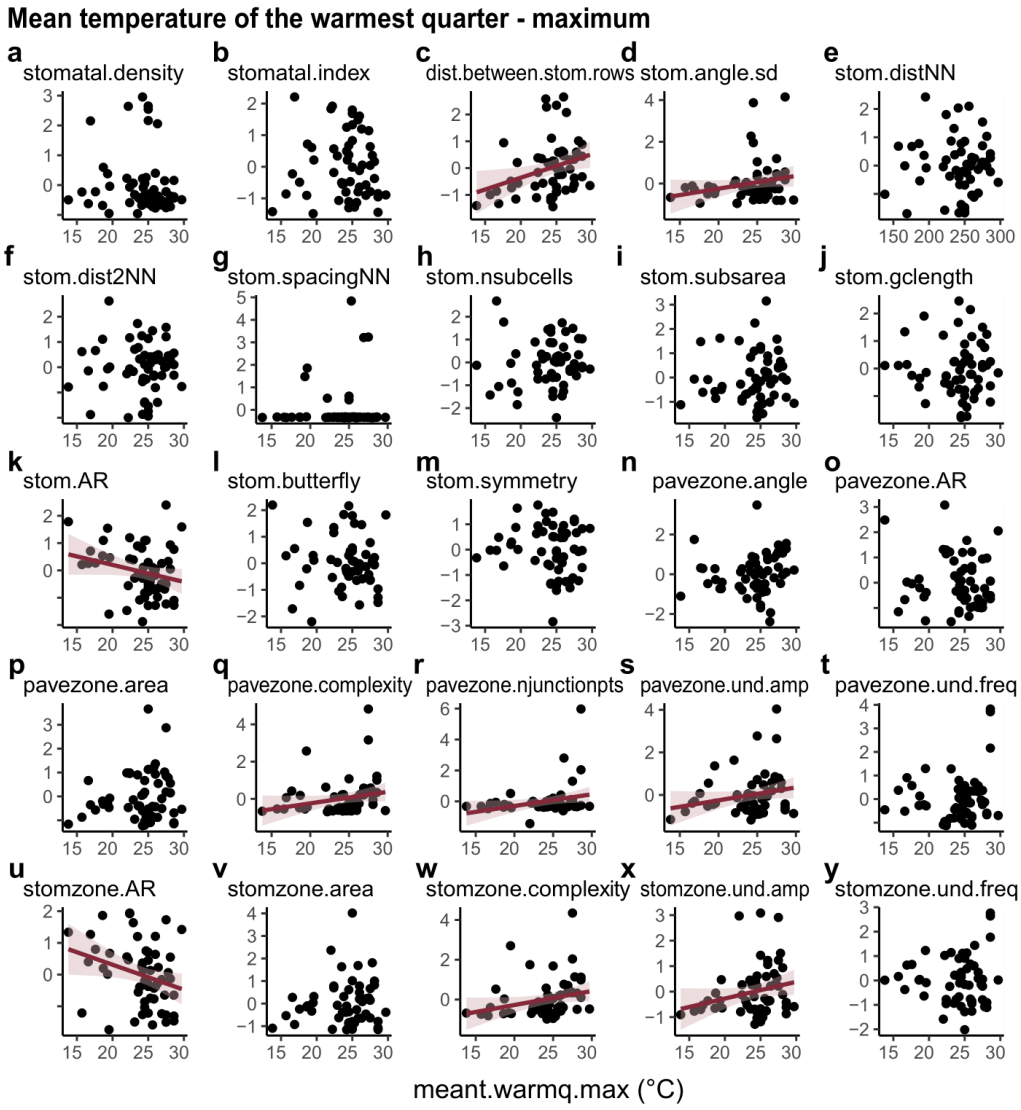

Figure S5.6 Scatterplots between each epidermal trait and mean temperature of the warmest quarter – maximum. Linear relationships between variables with a correlation coefficient >0.2 are shown.

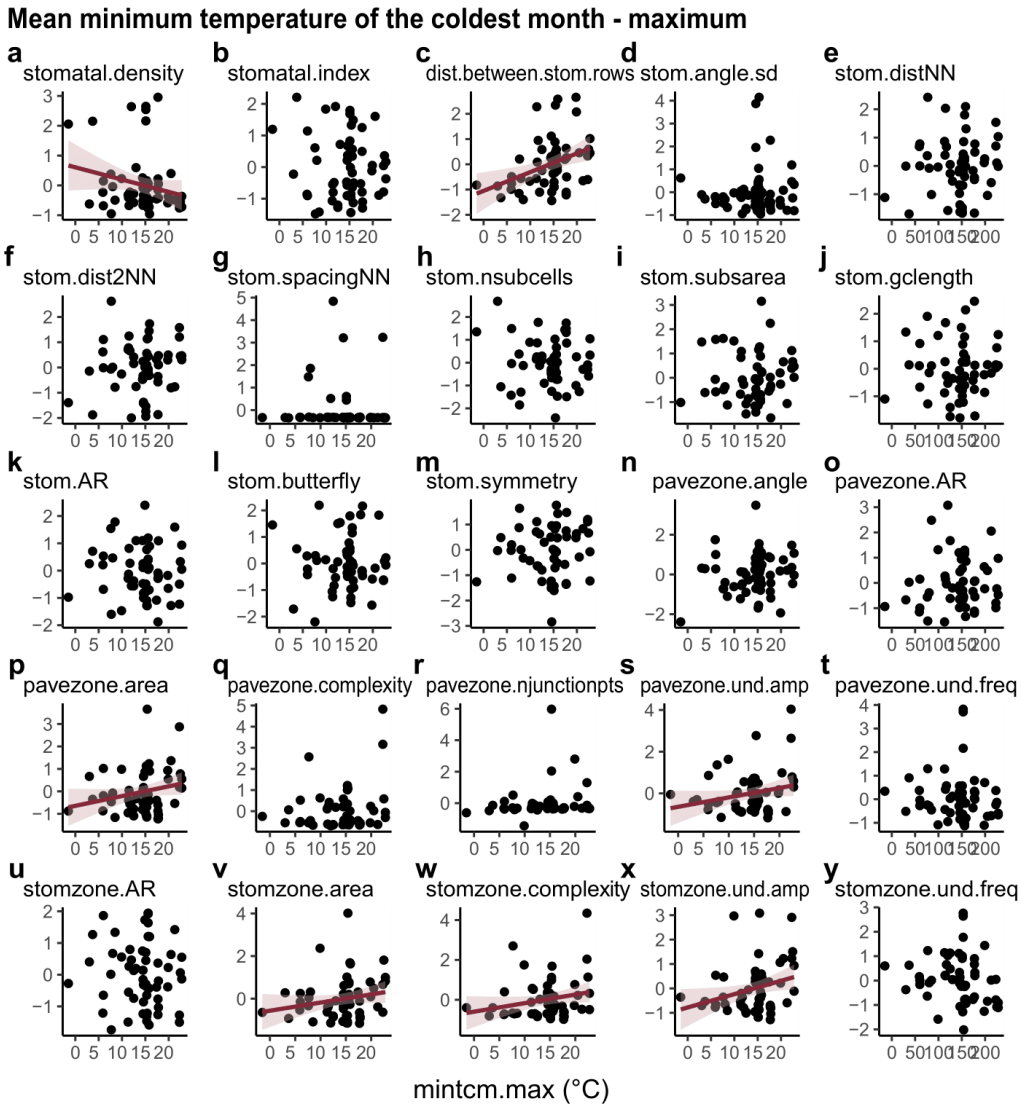

Figure S5.7 Scatterplots between each epidermal trait and minimum temperature of the coldest month - maximum. Linear relationships between variables with a correlation coefficient >0.2 are shown.

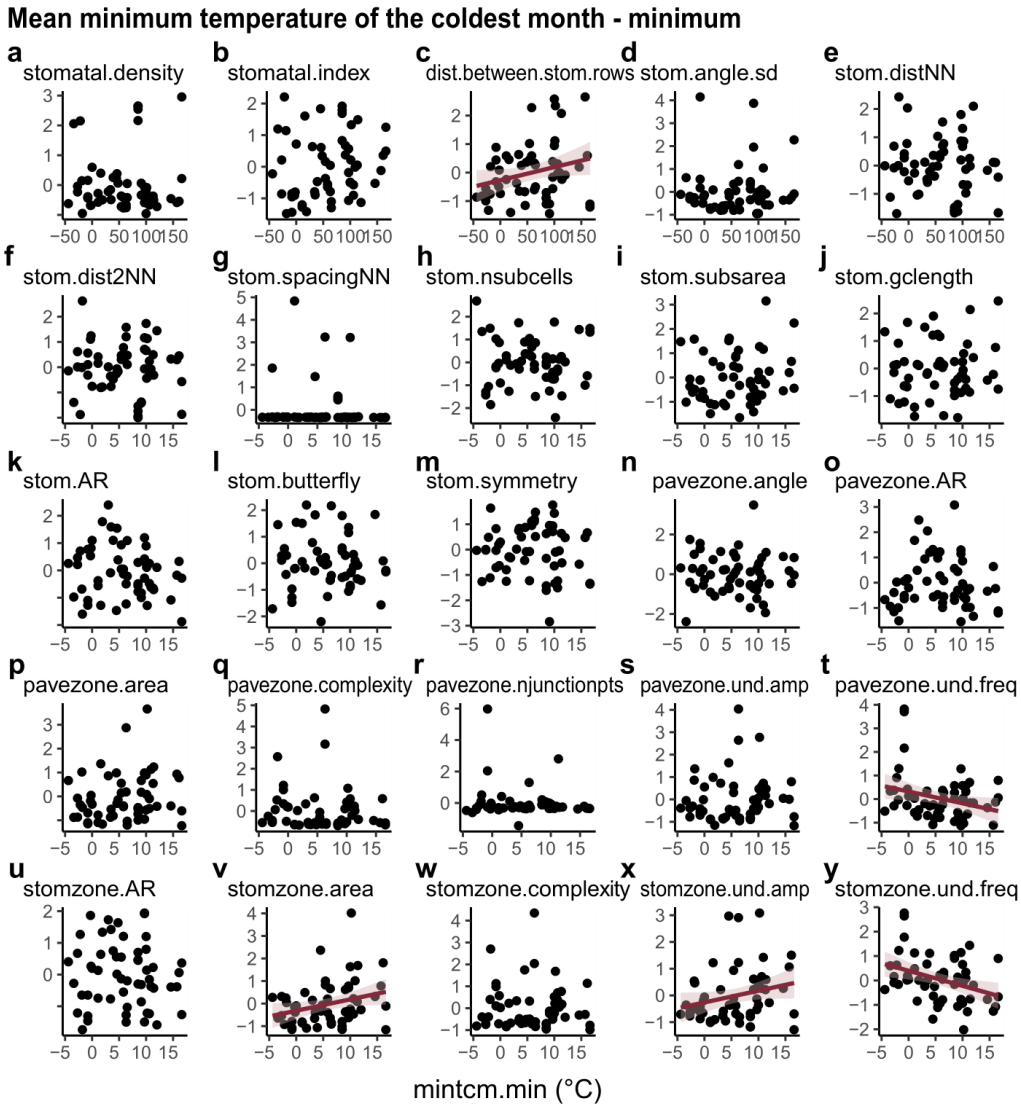

Figure S5.8 Scatterplots between each epidermal trait and minimum temperature of the coldest month – minimum. Linear relationships between variables with a correlation coefficient >0.2 are shown.

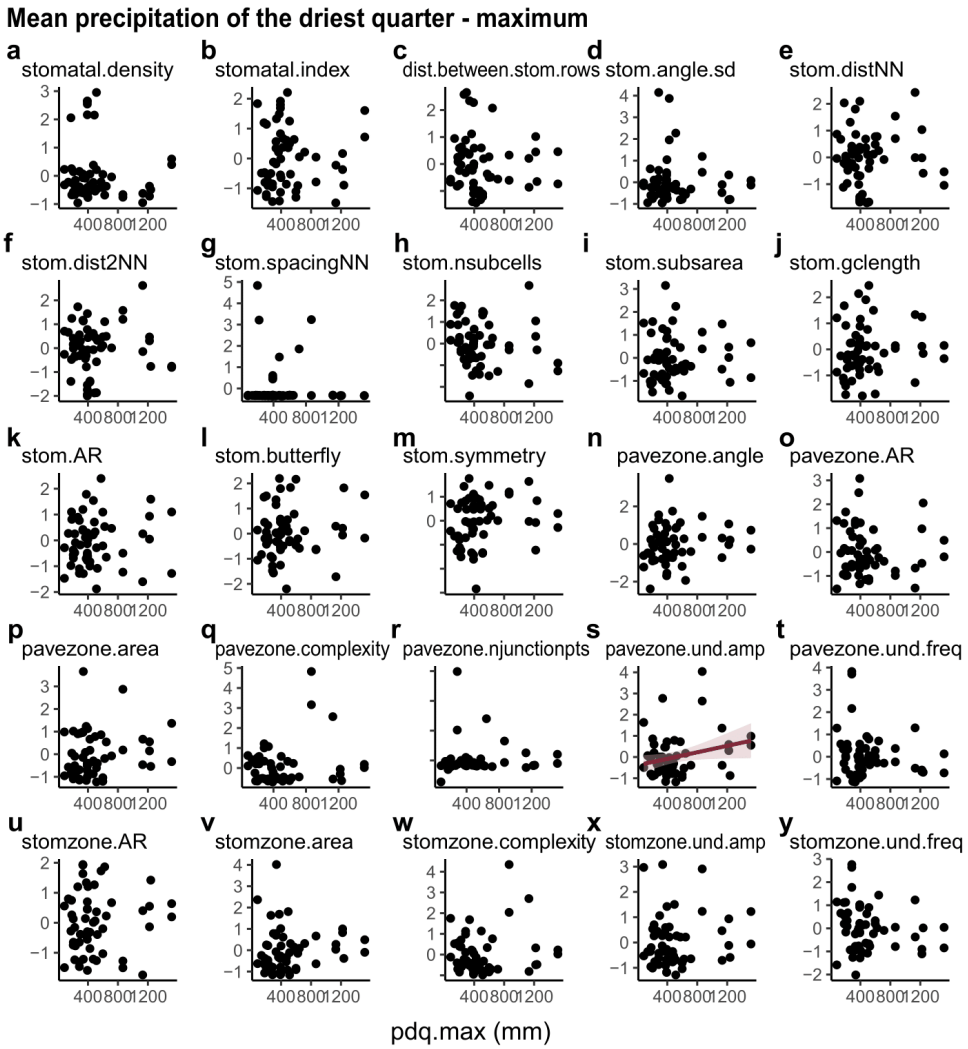

Figure S5.9 Scatterplots between each epidermal trait and precipitation of the driest quarter – maximum. Linear relationships between variables with a correlation coefficient >0.2 are shown.

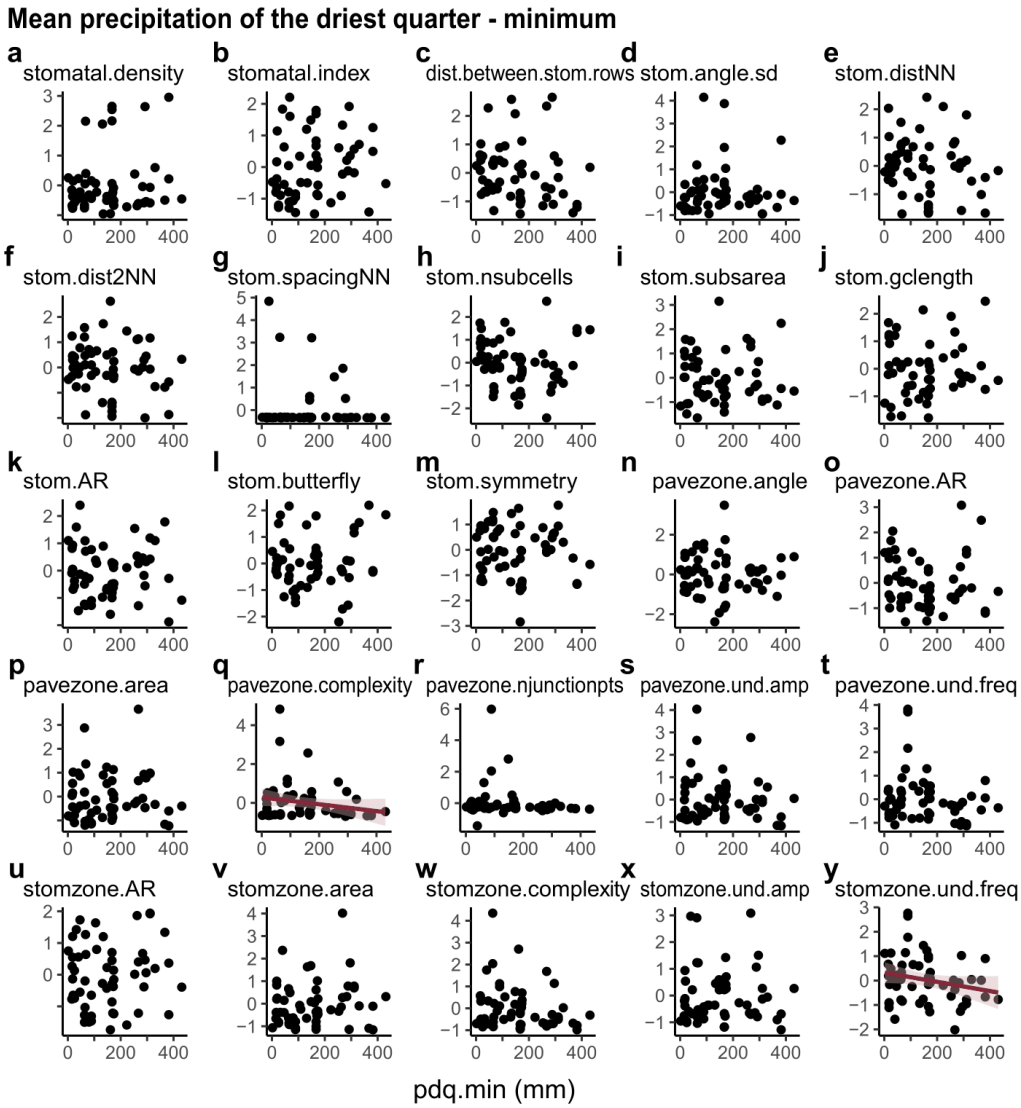

Figure S5.10 Scatterplots between each epidermal trait and precipitation of the driest quarter – minimum. Linear relationships between variables with a correlation coefficient >0.2 are shown.